LYAPUNOV-BASED SWITCHED SYSTEMS CONTROL

By

TENG-HU CHENG

A DISSERTATION PRESENTED TO THE GRADUATE SCHOOL
OF THE UNIVERSITY OF FLORIDA IN PARTIAL FULFILLMENT
OF THE REQUIREMENTS FOR THE DEGREE OF
DOCTOR OF PHILOSOPHY

UNIVERSITY OF FLORIDA

2015

To my parents Chin-Hsiang and Fen-Lan Cheng and my wife Chih-An Chen for their invaluable support

ACKNOWLEDGMENTS

TABLE OF CONTENTS

CHAPTER

LIST OF FIGURES

LIST OF ABBREVIATIONS

DOF   Degree of Freedom

EL   Euler-Lagrange

GPS   Global Positioning System

LMI   Linear Matrix Inequality

MLFs   Multiple Lyapunov Functions

OFB   Output Feedback

RHS   Right Hand Side

ROS   Robot Operating System

UAVs   Unmanned Aerial Vehicles

UUB   Uniformly Ultimately Bounded

Abstract of Dissertation Presented to the Graduate School
of the University of Florida in Partial Fulfillment of the
Requirements for the Degree of Doctor of Philosophy

LYAPUNOV-BASED SWITCHED SYSTEMS CONTROL

By

Teng-Hu Cheng

August 2015

Chair: Warren E. Dixon
Major: Mechanical Engineering

Switched systems theory consists of tools developed for systems containing a combination of continuous and discrete dynamics. The focus in this dissertation is the further development and application of switched systems methods for uncertain nonlinear networked systems. Specifically, control methods are developed in this dissertation when the discontinuities are due to the dynamics or network connections.

In Chapter 2, the discontinuities are due to the dynamics of the system. Specifically, an output feedback (OFB), time-dependent, switched controller is developed for an Euler-Lagrange system with parametric uncertainty and exogenous disturbances. This controller is motivated by the fact that Euler-Lagrange (EL) dynamics model many practical systems with nonlinear dynamics and hybrid behaviors (e.g., a bouncing ball, humanoid robot during walking). In this chapter, a time-dependent switching signal is designed using an average dwell-time scheme based on a multiple Lyapunov functions (MLFs) approach where the switched system achieves semi-global uniformly ultimately bounded (UUB) tracking with arbitrary switching sequences.

In Chapter 3 and 4, the discontinuities in the system are due to the fact that sensing occurs within a network. In Chapter 3, a decentralized switched controller is developed to enable dynamic agents to perform global formation configuration convergence while maintaining network connectivity and avoiding collision within agents and between stationary obstacles using only local feedback under limited and intermittent sensing. In

a multi-agent network system, an individual robot reacts according to information (e.g., relative location) from its neighboring agents. In practice, sensors have limited abilities (e.g., limitation in field-of-view, malfunction) that can lead to intermittent sensing. As a result, constant position feedback for agents may not be available all the time, and these inevitable behaviors might lead to a disconnected network or collisions between agents. Furthermore, these hybrid dynamics motivate the need for switched system analysis. Using a navigation function framework, a decentralized switched controller is developed in Chapter 3 to navigate the agents to the desired positions while ensuring network maintenance and collision avoidance. Simulations are provided to support the development.

In Chapter 4, a decentralized controller that uses event-triggered scheduling is developed for the leader-follower consensus problem under fixed and switching communication topologies. To eliminate continuous inter-agent communication, state estimates of neighboring agents are designed for control feedback and are updated by scheduled communication to reset growing estimate errors. Since the estimate error is associated with a neighbor's control input, when the true state is unknown until the next communication, the state estimate is updated to avoid system instability. The communication event times are based on an event-triggered approach, which considers the interplay between system performance and minimal communication bandwidth and requires no communication for event detection. Since the control strategy produces switched dynamics, analysis is provided to show that Zeno behavior is avoided by developing a positive constant lower bound on the minimum inter-event interval. A Lyapunov-based convergence analysis is also provided to indicate asymptotic convergence of the developed control methodology. Simulation results are provided to demonstrate the effectiveness of the developed control strategy.

In Chapter 5, the decentralized event-triggered control scheme developed in Chapter 4 is extended to a containment control problem, where multiple leaders exist in

11

the networked system and only a subset of followers can communicate to some of the leaders. The estimate-based decentralized controller, requiring only local feedback from neighboring follower agents, is designed for each follower agent so that communication can be intermittent to reduce communication while achieving a global objective. To avoid the Zeno behavior induced from the event-triggered approach, a positive constant lower bound on the inter-event interval is developed. A Lyapunov-based convergence analysis is provided to indicate asymptotic convergence of the developed strategy. Simulation results are provided to demonstrate the effectiveness of the developed control strategy.

CHAPTER 1
INTRODUCTION

1.1   Motivation and Problem Statement

Most natural behaviors can be modeled by continuous dynamics, but in some scenarios continuous dynamics are inadequate to model certain phenomena (e.g., sensor failure, changes of network topologies, state jumps due to a dynamic event), which introduce discontinuities. A switched system involving both continuous and discontinuous dynamics includes a set of subsystems and a switching signal. Each subsystem accommodates continuous dynamics, and the discontinuous events are triggered by the switching signal. In the switched system, only one subsystem can be activated at any time instance, and the transition of activation from one subsystem to another is determined by a switching signal, which is a function of time or system states. The design of a switching signal is as crucial as the controller in terms of stability of the switched system. Even for stable subsystems, an arbitrary switching signal can lead to undesired behavior (e.g., Zeno behavior, instability) [1].

To analyze the stability of a switched system, switched control approaches have been developed, and the selection of these approaches depends on the applications and feasibility of the stability analysis. In general, the development of a common Lyapunov function for the subsystems is favorable because it allows arbitrary switching which requires no constraint on the switching sequence for system stability. However, proving the existence of a common Lyapunov function is not always feasible and that motivates the development of other approaches. The use of multiple Lyapunov functions (MLFs) mitigates the challenges of proving the existence of a common Lyapunov function, but the resulting switching signal is required to satisfy a dwell-time condition for stability. In other words, the minimum time span to remain within an individual subsystem must be enforced.

1.2 Literature Review

Literature reviews for each chapter are presented below.

Euler-Lagrange dynamics are commonly used to model various systems. Some Euler Lagrange systems exhibit discontinuous behavior (e.g., a robot that transitions from a non-contact to contact state in force control applications [2], switching control inputs between pairs of multiple electrodes in Neuromuscular Electrical stimulation [3, 4]). To account for both continuous and discontinuous behavior, hybrid and switched systems methods have been developed. In addition to discontinuous behavior, systems often lack the sensing required for full state feedback, motivating the need for output feedback (OFB) controllers (cf. [5–9]). Researchers have designed OFB controllers for switched systems when measurements are limited, but these controllers have been predominantly designed for linear, switched systems [10–21]. In [10], an OFB controller was designed based on a fuzzy model for a switched linear system to overcome uncertainty in the the system. In [11–18], gain conditions for the OFB controller were obtained by solving a linear matrix inequality (LMI) for a switched linear system. In [19–21], gain conditions were developed for an OFB controller designed for a linear, switched delay system by solving a LMI. However, the extension of these approaches to nonlinear systems are not clear.

OFB controllers for nonlinear systems have received a lot of attention [22–25], but many of these approaches are designed for continuous system without considering discrete events. There are some nonlinear OFB control algorithms for switched systems, but the performance of the approaches are still limited (e.g., resulting in local stability, requiring exact model knowledge) [26–31]. In [26], the average dwell-time scheme for linear systems was extended to nonlinear systems for a supervisory control algorithm. In [27], the average dwell-time concept was extended to nonlinear integral input-to-state stable systems. In [28], full state feedback robust controllers were designed for switched systems to compensate for system uncertainties and disturbances. In [29], an OFB

controller for a switched nonlinear system was designed under the assumption of exact model knowledge. A Takagi–Sugeno (T-S) fuzzy method was used in [30] to address the uncertainties of the switched nonlinear system, but the controller was designed based on a locally linear time-varying system. In [31], an OFB controller was developed for switched nonlinear systems with parametric uncertainty, where a series of local robust OFB controllers was used.

In [32], a robust OFB controller was developed that only requires position measurements for a continuous nonlinear system with parametric uncertainties and bounded disturbances. The contribution in Chapter 2 is to show how the result in [32] can be extended as an OFB controller with a time-dependent switching signal for a switched, nonlinear, Euler-Lagrange system with parametric uncertainties and bounded exogenous disturbances. The switched controller involves the design of a time-varying control gain applied to all subsystems, and it is designed based on multiple Lyapunov functions and ensures that the position tracking error is semi-global uniformly ultimately bounded (UUB).

Multi-agent systems have been investigated in a wide range of applications including: consensus [33, 34], rendezvous [35–37], and formation and flocking of multiple agents [38–41]. For such applications, various decentralized approaches (cf. [42–48]) have been developed to perform cooperative objectives based on information exchange over an underlying network formed by the multi-agent system. However, due to potential disruptions in communication and sensing capabilities of the agents, the exchange of information for feedback control may not be continuous. Uncertainty resulting from intermittent feedback can cause agents to move in a manner that can disconnect the underlying network or lead to collisions between obstacles and agents. Therefore, the development of a decentralized controller that is robust to intermittent feedback while ensuring network connectivity and collision avoidance is well motivated.

Recent research has focused on the preservation of network connectivity [49–54]. In [49] and [50], a potential function framework ensures network connectivity by applying attractive forces to the dynamic agents as they perform cooperative tasks. In [51] and [52], network connectivity of dynamic topologies is preserved during rendezvous and formation control through the use of decentralized graph-theoretic methods. In [53], formation control with connectivity maintenance is achieved by designing a bounded decentralized controller for both static and dynamic interaction topologies. In [54], a navigation function based decentralized controller ensures convergence to a desired configuration and maintenance of network connectivity with collision avoidance to both dynamic and static obstacles for a fixed network topology. The aforementioned results are based on the assumption that continuous feedback through inter-agent communication is available. However, this assumption is conservative and can limit the number of applications, since communication can be interrupted.

Motivated by the potential for intermittent communication, consensus controllers were investigated in [55] and [56], where the discrete dynamics can lead to system instability. These stability issues are resolved through the use of switched controllers. In [57] and [58], synchronization problems were investigated under the possibility of intermittent communication and time-delay networks. However, the control objectives focus on the convergence analysis associated with the minimum communication rate. The control strategies in [55–58] compensate for intermittent feedback, but network connectivity and collision avoidance issues under such a constraint are not addressed.

Since wireless communication may not be always available (either by design or through some fault), on-board sensors (such as cameras) are often used to provide local feedback for agents to perform cooperative tasks. However, due to the complex environment, agents may move out of the field-of-view (cf. [59–61]) of other agents occasionally, resulting in an intermittent and time-varying interaction with other agents. Intermittent sensing problems are considered for formation control problems using

graph-theoretic methods in [62] and [63]. However, network connectivity and collision avoidance are not considered. In [64], a coordination algorithm was designed to stabilize a formation robust to sensing link failures, without considering network connectivity and collision avoidance. A formation problem using sensors with limited field-of-view is developed in [40] by assuming a connected network. In [40] and [59–64], while continuous controllers are utilized to address discrete dynamics to achieve control objectives, collision avoidance and network connectivity maintenance are not considered.

Various hybrid control strategies have been developed to address discontinuities caused by intermittent feedback (cf. [35, 59, 65, 66]). In [67], a Stop-Go based hybrid control approach was developed to maintain network connectivity for a leader-follower containment control problem. In [68], swarm aggregation problems were investigated within fixed and dynamic network topologies for both network connectivity and collision avoidance. However, the dynamic topologies considered in [68] only result from link additions to the network. Similar to the state agreement problem solved in [65], decentralized hybrid controllers developed in [35] and [69] address network connectivity issues for rendezvous problems, but collision avoidance is not considered. Although the results in [35, 59, 65–69] focus on either maintaining network connectivity or obstacle avoidance for multi-agent network system under switching topologies, it is not clear how these methods can be extended to address the more general formation control problem under switching topologies.

Based on our preliminary efforts in [70], formation control problems under intermittent communication/sensing feedback are considered in Chapter 3. Due to the discontinuous dynamics, the aforementioned navigation function based controller designed in [54] is no longer valid. Since the network topology might switch in an unpredictable order within a finite graph set, the design of a hybrid controller for an arbitrary switching system is challenging. Leveraging the Stop-Go policy in [67], a navigation function

17

based decentralized hybrid controller is developed in Chapter 3, which consists of two alternative control inputs and two corresponding switching conditions. The switching between the two controllers depends on two decentralized switching conditions (i.e., decision making requires only information from one-hop neighbors), which are designed such that Zeno behaviors are avoided. Finally, the existence of a common Lyapunov function is established for the designed hybrid controller, and the formation error is proven to converge globally with sufficiently small error (i.e. converges to the neighborhood of the critical points), while maintaining network connectivity and avoiding collision within agents and static obstacles.

To increase efficiency and speed, a group of robots can cooperate to perform a task, wherein the coordination and control of the robots are designed based on neighbors' dynamics and states. To ensure mission completion, the neighbors' dynamics are usually known and their states are communicated continuously (cf. [70–73]). Based on the network architecture, two topologies, centralized and decentralized, have been widely adopted. Centralized communication architectures facilitate global behaviors by networked agents; however, such strategies exacerbate network congestion when compared to decentralized approaches. In a decentralized communication architecture, each agent only communicates with local neighbors (e.g., one-hop neighbors) so that the usage of the communication channel can be minimized, despite the increasing number of agents in the network. Under this network topology, the global objective can still be retained by designing a decentralized controller, using local information for feedback. A network leader can be included in decentralized architectures where only a subset of the agents communicate with and follow the leader (cf. [70–73]). However, most decentralized network control approaches (cf. [74–76]) rely on continuous inter-agent communication for control feedback.

To further reduce bandwidth usage, real-time scheduling methods, also called event-triggered approaches (cf. [77, 78]), can be applied instead of continuous state

feedback. In event-triggered control, the control task is executed when a triggering condition is met, which is typically when the ratio of the norm of some error to the state norm exceeds a predefined threshold. The earliest event-triggered strategies applied to control a multi-agent system are in [79] and [80]. However, the potential bandwidth minimizing advantages are compromised because verifying the event triggering condition requires constant communication. These results were later extended to directed and undirected graphs in [81] and [82], but in these works the triggering condition requires a priori knowledge of the Fiedler value and the final consensus value. These requirements were relaxed in [83] and [84] by designing a new trigger function using the sum of relative states from neighbors. In [85], a time-based triggering function (i.e., a time-dependent threshold) is introduced, and a similar time-varying threshold is applied in [86] for a directed time-varying communication topology. However, the strategies in [79–86] solve the leaderless average consensus problem. The more challenging leader-follower consensus control problem is investigated in [87], but the leader state is assumed to be stationary, which limits applicability; additionally, constant neighbor communication is used to detect the trigger condition, which mitigates the benefits of the event-triggered control strategy.

In practice, unpredictable physical constraints (e.g., random sensor/device failure, obstacles/interference in a complex environment) can cause intermittent communication. When disconnected, the neighbors' states will not be communicated, and the unavailability of the new neighboring states can impact the global objective of the networked system since the decentralized controller is developed and analyzed based on the assumptions of continuous states of the neighboring agents. Since the network disconnection introduces discontinuous dynamics into the system, a switched event-triggered controller for the hybrid system is motivated. However, it is unclear how to directly extend the strategies in the aforementioned results that assume a fixed topology.

In Chapter 4, to eliminate the need of continuous communication and thereby reduce the required communication bandwidth, the neighbors' state estimates are used as a substitute for the neighbor's true states such that obtaining local information for feedback requires less inter-agent communication. Despite the advantages, the estimate error can grow in time, and as shown in the previous literature, the update events are hard to design without continuously communicating the true states. That is, the dynamics of the estimate error is associated with neighbor's true state and neighbor's control input, which are not available until the next communication. Therefore, the update events that minimize the communication bandwidth should be designed under the control constraint while achieving the global objective. To this end, Chapter 4 analyzes the interplay between the control gain and the dynamics of the estimate error to obtain a trigger function that can predict the next required estimate update without using inter-agent communication.

Various applications can be facilitated through the use of a team of collaborative agents. Ideally, communication required for navigation and control of the agents is minimized to maximize the available bandwidth for other mission objectives (e.g., relaying sensing data). Towards this objective, network control approaches have been developed using strategies that only require local communication (e.g., from one and two hop neighbors), and leader/follower strategies where follower agents have partial feedback information [70–73]. For example, the containment control problem considered in this chapter focuses on a decentralized strategy in which a subgroup of agents (i.e., followers) must remain within a finite region spanned by another subgroup (i.e., leaders), where the leader states are only communicated to a subset of followers (i.e., followers that have leader neighbors). However, even for the decentralized containment control problem, most existing solutions (cf. [73, 88–91]) require continuous state feedback to be communicated from neighboring agents for decentralized implementation.

To reduce inter-agent communication, real-time scheduling methods, called event-triggered approaches (cf. [77, 78]), can be applied on an as-needed basis to reduce continuous state feedback. Typically in event-triggered control, the control task is executed when the ratio of a certain error norm to the state norm exceeds a threshold. As a result, when compared to traditional continuous feedback methods, event-triggered execution yields a minimum inter-event interval.

Motivated by the desire to reduce communication traffic and the controller updates, event-triggered results have been developed for multi-agent systems in [79, 81–86]. However, these applications target the same average consensus problem with a leaderless network and require continuous communication with neighboring agents for event detection. Therefore, these event-triggered approaches may not mitigate communication congestion for a large scale network. These results are extended in [92] for a dynamic leader, intermittent communication, and communication-free event detection. However, it is unclear how to directly extend the approaches in [79, 81–86, 92] to the containment control problem. This chapter develops an approach for containment control without continuous communication.

Similar to the development in [92], Chapter 5 develops a decentralized estimator-based event-triggered containment control approach where every follower agent has model-based state estimators dwelling at its neighboring agents as well as itself. These distributed estimators follow the same dynamics as the leader and are synchronized by simultaneous updates at discrete events. Since the follower agents know how far the state estimates are away from its true state, it can communicate its true state to these estimates when necessary, but not vice versa (i.e., neighboring agents have no authority to request updates). This event is generated by a decentralized, estimate-based, event-triggered function. As a result, any follower agent has a decentralized, estimate-based, piecewise continuous controller, which is discontinuous at the event times whenever broadcasting its state to, or receiving estimate updates from, the neighboring agents

21

is required. Therefore, no inter-agent communication is required between any two event times. A lower bounded minimum inter-event interval can be developed, and a convergence analysis shows that the individual agent requires only intermittent communications for asymptotic convergence. Simulation demonstrates asymptotic convergence in the containment control problem with reduced communication between follower agents.

1.3   Contributions

Contributions for each chapter are presented below.

Chapter 2: **Robust output feedback control of uncertain switched Euler-Lagrange systems**: The contribution of this chapter lies in the development of an OFB, time-dependent, switched controller for an Euler-Lagrange system with parametric uncertainty and exogenous disturbances. Since EL system can be used to model most of practical systems with nonlinear dynamics and hybrid behaviors, the developed switched controller has a broad application. Current control strategies for switched nonlinear systems require at least partial knowledge of the system parameters for stabilization, or the system results in local stability. Other than a switched controller extended from the continuous controller developed in [32], the challenge lies in the design of the time-dependent switching signal adopting an average dwell-time scheme developed from the analysis of MLFs approach such that the switched system achieves semi-global uniformly ultimately bounded (UUB) tracking with arbitrary switching sequences.

Chapter 3: **Decentralized formation control with connectivity maintenance and collision avoidance under limited and intermittent sensing**: A decentralized switched controller is developed for dynamic agents to perform global formation con-figuration convergence while maintaining network connectivity and avoiding collision within agents and between stationary obstacles, using only local feedback under lim-ited and intermittent sensing. The control objective of this switched system cannot be

achieved by a continuous controller. The contribution in this chapter lies in the design of a decentralized switched controller based on nonsmooth navigation functions, and the convergence analysis using a common Lyapunov function that yields UUB tracking with an arbitrary switching signal. In other words, the formation error of the entire configuration converges globally with sufficiently small error (i.e. converges to the neighborhood of the critical points) under arbitrary switching topologies.

Chapter 4: **Decentralized Event-Triggered Control for Leader-follower Consensus**: In this chapter, an event-triggered decentralized control scheme for the leader-follower network consensus problem is developed, and the objective is to reduce communication with neighboring agents. The contribution lies in the design of an estimate-based trigger function that requires no interaction with its neighbors during its inter-event interval. The challenge is presented due to the decentralized control structure where direct accesses to the leader's information for some followers are not available. A Lyapunov-based convergence analysis is developed to ensure the developed strategy yields asymptotic network consensus. In addition to the stability analysis, the trigger signal is also proven never to exhibit Zeno behavior.

Chapter 5: **Decentralized Event-Triggered Control of Networked Systems for Containment Contro**l: The event-triggered decentralized control is applied to the containment control problem, where multiple leaders exist in the networked system. The contribution of this chapter lies in reducing the communication frequency between neighboring follower agents and ensuring a global objective when only a subset of followers can intermittently communication to some of the leaders.

CHAPTER 2
ROBUST OUTPUT FEEDBACK CONTROL OF UNCERTAIN SWITCHED EULER-LAGRANGE SYSTEMS

Systems often lack the sensing required for full state feedback, motivating the design of output feedback (OFB) controllers. Some systems also exhibit discontinuous behavior, motivating the development of hybrid and switched systems theory. However, output feedback controllers for switched systems have been typically developed for linear systems. Of the OFB controllers that have been designed for switched nonlinear systems, at least partial knowledge of the system parameters is required, or the system results in local stability. In this chapter, an OFB, time-dependent, switched controller is developed for an Euler-Lagrange system with parametric uncertainty and exogenous disturbances. The time-dependent switching signal is designed using a dwell-time scheme based on multiple Lyapunov functions such that the switched system achieves semi-global uniformly ultimately bounded (UUB) tracking with arbitrary switching sequences.

2.1 Dynamic Model

Consider N distinct Euler-Lagrange subsystems where the dynamics of each subsystem is defined as

$$M_i(q)\ddot{q} + V_{m,i}(q, \dot{q})\dot{q} + G_i(q) + F_i\dot{q} + \tau_{d,i} = \tau_i, \tag{2-1}$$

where $i \in \mathbb{S}$ denotes the ith subsystem, $\mathbb{S} \triangleq \{1, 2, \cdots, N\}$ denotes a finite indexed set of all subsystems, $M_i : \mathbb{R}^n \to \mathbb{R}^{n \times n}$ denotes the inertia matrix, $V_{m,i} : \mathbb{R}^n \times \mathbb{R}^n \to \mathbb{R}^{n \times n}$ denotes the centripetal-Coriolis matrix, $G_i : \mathbb{R}^n \to \mathbb{R}^n$ denotes the gravity vector, $F_i \in \mathbb{R}^{n \times n}$ denotes the constant, diagonal, positive-definite, viscous friction matrix, $\tau_{d,i} : [0, \infty) \to \mathbb{R}^n$ denotes the generalized bounded disturbance, $\tau_i : [0, \infty) \to \mathbb{R}^n$ denotes the control input, and $q, \dot{q}, \ddot{q} \in \mathbb{R}^n$ denote the generalized states. The states q are measurable but $\dot{q}$ and $\ddot{q}$ are not. The functions M_i, $V_{m,i}$, G_i, F_i, and $\tau_{d,i}$ are considered to be unknown.

Property 2.1. [93] The inertia matrix M_i, $\forall i \in \mathbb{S}$, is symmetric, positive definite, and satisfies the following inequality:

$$m_1 \left\| \varsigma \right\|^2 \leq \varsigma^T M_i \varsigma \leq m_2 \left\| \varsigma \right\|^2, \ \forall \varsigma \in \mathbb{R}^n, \ i \in \mathbb{S}, \tag{2–2}$$

where m_1, $m_2 \in \mathbb{R}$ denote two known positive constants, and $\left\| \cdot \right\|$ denotes the Euclidean norm.

Property 2.2. [93] The inertia and the centripetal-Coriolis matrices satisfy the following skew-symmetric relationship

$$\varsigma^T (\frac{1}{2}\dot{M}_i - V_{m,i})\varsigma = 0, \ \forall \varsigma \in \mathbb{R}^n, \ i \in \mathbb{S}. \tag{2–3}$$

Property 2.3. [93] The centripetal-Coriolis matrix satisfies the following relationship

$$V_{m,i}(q, \ \omega)\eta = V_{m,i}(q, \ \eta)\omega, \quad \forall \eta, \ \omega \in \mathbb{R}^n, \ i \in \mathbb{S}. \tag{2–4}$$

Property 2.4. [93] The Euler-Lagrange system from (2–1) can be linearly parametrized as

$$Y\left(q, \ \dot{q}, \ \ddot{q}\right)\theta_i = M_i(q)\ddot{q} + V_{m,i}(q, \ \dot{q})\dot{q} + G_i(q) + F_i\dot{q}, \ i \in \mathbb{S}, \tag{2–5}$$

where $\theta_i \in \mathbb{R}^p$ denotes the vector including all the unknown system constant parameters of ith subsystem, and $Y : \mathbb{R}^n \times \mathbb{R}^n \times \mathbb{R}^n \to \mathbb{R}^{n \times p}$ denotes the regression matrix which is a function of q, $\dot{q}$, and $\ddot{q}$.

By utilizing the desired trajectory, (2–5) can be rewritten as

$$Y_d\left(q_d, \ \dot{q}_d, \ \ddot{q}_d\right)\theta_i =$$
$$M_i(q_d)\ddot{q}_d + V_{m,i}(q_d, \ \dot{q}_d)\dot{q}_d + G_i(q_d) + F_i\dot{q}_d, \tag{2–6}$$

where $i \in \mathbb{S}$, and $Y_d : \mathbb{R}^n \times \mathbb{R}^n \times \mathbb{R}^n \to \mathbb{R}^{n \times p}$ denotes the desired regression matrix as a function of q_d, $\dot{q}_d$, and $\ddot{q}_d$, which denote the desired position, velocity, and acceleration, respectively. By design, q_d, $\dot{q}_d$, $\ddot{q}_d$, and $\dddot{q}_d \in \mathcal{L}_\infty$.

Property 2.5. [93] The centripetal-Coriolis and friction matrices, and the gravity, disturbance, and unknown parameter vectors can be upper bounded as

$$\|V_{m,i}\| \le \xi_{c1,i} \|\dot{q}\| \ \forall q, \ \dot{q} \in \mathbb{R}^n, \ \|F_i\| \le \xi_{f,i},$$

$$\|G_i\| \le \xi_{g,i}, \ \|\tau_{d,i}\| \le \xi_{d,i} \, \forall t \in \mathbb{R}, \ \|\theta_i\| \le \xi_{\theta_1,i}, \ i \in \mathbb{S}, \tag{2–7}$$

where $\xi_{c1,i}, \xi_{f,i}, \xi_{g,i}, \xi_{d,i}, \xi_{\theta_1,i} \in \mathbb{R}$ are positive constants for the ith subsystem.

To facilitate further analysis, the following vector function $\mathsf{Tanh}(\cdot)$ and matrix function $\mathsf{Cosh}(\cdot)$ are defined as

$$\mathsf{Tanh}(\zeta) \triangleq [\tanh(\zeta_1), \dots, \tanh(\zeta_n)]^T, \tag{2–8}$$

and

$$\mathsf{Cosh}(\zeta) \triangleq \mathsf{diag}\{\cosh(\zeta_1), \dots, \cosh(\zeta_n)\},$$

where $\zeta = [\zeta_1, \dots, \zeta_n]^T \in \mathbb{R}^n$, and $\mathsf{diag}\{\cdot\}$ denotes a diagonal matrix. Based on (2–8), the following inequalities hold [32]

$$\frac{1}{2}\tanh^2(\|\zeta\|) \le \ln(\cosh(\|\zeta\|)) \le \sum_{j=1}^{n} \ln(\cosh(\zeta_j)) \le \|\zeta\|^2, \tag{2–9}$$

$$\tanh^2(\|\zeta\|) \le \|\mathsf{Tanh}(\zeta)\|^2 = \mathsf{Tanh}^T(\zeta)\mathsf{Tanh}(\zeta).$$

2.2 Control Development

Robust OFB controllers are developed for each uncertain subsystem under the constraint that the only available measurement for feedback is the position variable q. To quantify the objective, the position tracking error $e \in \mathbb{R}^n$ is defined as

$$e = q_d - q, \tag{2–10}$$

where q_d is the desired trajectory. The difference between the actual system parameters and the estimated parameters for each subsystem is defined as

$$\tilde{\theta}_i \triangleq \theta_i - \hat{\theta}_i, \ i \in \mathbb{S}, \tag{2–11}$$

where $\tilde{\theta}_i \in \mathbb{R}^p$ denotes the parameter estimation error, and $\hat{\theta}_i \in \mathbb{R}^p$ denotes the constant best-guess estimates of θ_i for the ith subsystem. In addition, the estimate error can be upper bounded as

$$\left\| \tilde{\theta}_i \right\| \leq \xi_{\theta_2,i}, \ i \in \mathbb{S}, \tag{2--12}$$

where $\xi_{\theta_2,i} \in \mathbb{R}$ denotes a known positive constant for the ith subsystem.

2.2.1 Robust Output Feedback Tracking Controller

For notational brevity the dependence of all the functions on the states is suppressed hereafter. Based on the subsequent development and stability analysis, the following control input is designed [32]

$$\tau_i = Y_d \hat{\theta}_i - ka\Gamma^{-1}y + \mathsf{Tanh}(e), \ i \in \mathbb{S} \tag{2--13}$$

where $k : [0, \infty) \to \mathbb{R}$ is a positive time-varying, differentiable control gain, $\Gamma : \mathbb{R}^n \to \mathbb{R}^{n \times n}$ is

$$\Gamma \triangleq \mathsf{diag}\left\{ (a - y_1^2)^2, \ (a - y_2^2)^2, \ldots, (a - y_n^2)^2 \right\}, \tag{2--14}$$

where $a \in \mathbb{R}$ is an adjustable positive constant, and $y \in \mathbb{R}^n$ denotes an auxiliary signal for the velocity tracking error defined as [32]

$$y_j \triangleq p_j - ke_j. \tag{2--15}$$

In (2--15), $p_j \in \mathbb{R}$ denotes the solution to [32]

$$
\begin{aligned}
\dot{p}_j = &- \left(a - (p_j - ke_j)^2\right)^2 (p_j - ke_j - \mathsf{tanh}(e_j)) \\
&- k\Big(\mathsf{tanh}(e_j) + a\,(p_j - ke_j)\Big) + \dot{k}e_j
\end{aligned}
\tag{2--16}
$$

where $j \in \{1, 2, \ldots, n\}$ denotes the jth element of the vector variable, and the initial conditions for $p_j(0)$ are selected as

$$-\frac{a}{\sqrt{n}} + k(0)e_j(0) < p_j(0) < \frac{a}{\sqrt{n}} + k(0)e_j(0). \tag{2--17}$$

Provided that the initial condition $p_j(0)$ is selected based on (2–17), then (2–15) can be used to show that

$$|y_j(0)| < \frac{a}{\sqrt{n}},$$

which is independent of the magnitude of $e_j(0)$. Following the development in [32], the continuous time-varying control gain is designed as

$$k \triangleq \frac{1}{m_1} \bigg(k_{n1} \sum_{j=1}^{n} \sum_{k=1}^{p} Y_{djk}^2 \xi_{\theta_1}^2 + k_{n2} \sum_{j=1}^{n} \sum_{k=1}^{p} Y_{djk}^2 \xi_{\theta_2}^2 + 1$$
$$+ k_{n3} \xi_k^2 + k_{n4} a^5 \xi_1^2 + 4a^5 \xi_2^2 + 2a^7 \xi_3^2 + a^7 \xi_4^2 + 4a^9 \xi_5^2$$
$$+ a\xi_6 \bigg), \tag{2–18}$$

where the subscripts of Y_{djk} correspond to the dth row and n^{th} column of the matrix, m_1 was defined in (2–2), ξ_{θ_1}, ξ_{θ_2}, ξ_k, $\xi_{i\in\{1,...,6\}}$ are the maximum control gains over all subsystems defined as

$$\xi_{\theta_1} \triangleq \max_{i\in\mathbb{S}} \left\{ \xi_{\theta_{1,i}} \right\} , \quad \xi_{\theta_2} \triangleq \max_{i\in\mathbb{S}} \left\{ \xi_{\theta_{2,i}} \right\},$$
$$\xi_k \triangleq \max_{i\in\mathbb{S}} \left\{ \xi_{k,i} \right\} \quad , \quad \xi_h \triangleq \max_{i\in\mathbb{S}} \left\{ \xi_{h,i} \right\}, \ h \in \{1, \ldots, 6\},$$

k_{n1}, k_{n2}, k_{n3}, $k_{n4} \in \mathbb{R}$ denote positive constant control gains, $\xi_{\theta_{1,i}}$ was defined in (2–7), $\xi_{\theta_{2,i}}$ was defined in (2–12), $\xi_{k,i} \in \mathbb{R}$ denotes a known positive function defined as

$$\xi_{k,i} \triangleq m_2 \|\ddot{q}_d\| + 3\xi_{c1,i} \|\dot{q}_d\|^2 + \xi_{f,i} \|\dot{q}_d\| + \xi_{g,i}$$
$$+ \xi_{d,i} + \xi_{c1,i} + m_2 a^3,$$

and $\xi_{h,i} \in \mathbb{R}$ denotes some positive constants that upper bound the parameters of the system dynamics and the desired trajectory. To facilitate the subsequent stability analysis, the control gains k_{n1}, k_{n2}, k_{n3}, and k_{n4} are selected based on the sufficient condition

$$\varepsilon < \frac{1}{2}, \qquad k_{n4} > \frac{1}{4(\frac{1}{2} - \varepsilon)}, \tag{2–19}$$

where $\varepsilon \in \mathbb{R}$ denotes a positive constant defined as

$$\varepsilon = \frac{1}{4k_{n1}} + \frac{1}{4k_{n2}} + \frac{1}{4k_{n3}}. \tag{2--20}$$

2.2.2 Error System Development

By taking the time derivative of (2–15) and using (2–16) and (2–17), the open-loop error system for the velocity filter term can be obtained as [32]

$$\dot{y}_j = -(a - y_j^2)^2(y_j - \mathsf{tanh}(e_j)) - k\eta_j, \tag{2--21}$$

where $\eta \in \mathbb{R}^n$ denotes an auxiliary filtered tracking error defined as [32]

$$\eta \triangleq \dot{e} + \mathsf{Tanh}(e) + ay. \tag{2--22}$$

By taking the time derivative of (2–22), pre-multiplying both sides of the resulting equation by M_i, and using (2–1), the open-loop error system is

$$\begin{aligned} M_i\dot{\eta} =& M_i\ddot{q}_d + V_{m,i}\dot{q} + G_i + F_i\dot{q} + \tau_{d,i} - \tau_i \\ &+ M_i\mathsf{Cosh}^{-2}(e)\dot{e} + M_i a\dot{y}, \ i \in \mathbb{S}. \end{aligned} \tag{2--23}$$

After adding and subtracting $Y_d\theta_i$ of (2–6) to (2–23) and utilizing (2–4), (2–10), (2–21), and (2–22), (2–23) can be rewritten as

$$M_i\dot{\eta} = -V_{m,i}\eta + Y_d\theta_i - \tau_i - kaM_i\eta + \chi_i, \ i \in \mathbb{S}, \tag{2--24}$$

where the disturbance term $\chi_i \in \mathbb{R}^n$ is defined as [32]

$$\begin{aligned} \chi_i \triangleq& M_i\mathsf{Cosh}^{-2}(e)(\eta - \mathsf{Tanh}(e) - ay) \\ &- M_i a\Gamma(y - \mathsf{Tanh}(e)) + V_{m,i}(q, \ \dot{q}_d + \mathsf{Tanh}(e) + ay) \\ &\times (\mathsf{Tanh}(e) + ay) + V_{m,i}(q, \ \dot{q}_d)(\mathsf{Tanh}(e) + ay) \\ &- V_{m,i}(q, \ \eta)(\dot{q}_d + \mathsf{Tanh}(e) + ay) + M_i\ddot{q}_d \\ &+ V_{m,i}(q, \ \dot{q}_d)\dot{q}_d + F_i\dot{q} + G_i + \tau_{d,i} - Y_d\theta_i, \end{aligned}$$

29

which can be upper bounded by

$$\|\chi_i\| \leq \left(\sqrt{\sum_{j=1}^{n}\sum_{k=1}^{p}Y_{djk}^2} \right) \xi_{\theta_1,i} + \xi_{1,i}\|x\|$$
$$+ \xi_{2,i}a^2\|y\|^2 + \xi_{6,i}a\|\eta\|\|y\| + \xi_{k,i}$$
$$+ \xi_{3,i}a^2\|y\|^3 + \xi_{4,i}a\|y\|^4 + \xi_{5,i}a\|y\|^5, \tag{2–25}$$

where $a \geq 1$, and $x \in \mathbb{R}^{3n}$ is defined as

$$x \triangleq \begin{bmatrix} \mathsf{Tanh}^T(e) & \eta^T & y^T \end{bmatrix}^T.$$

By substituting (2–13) into (2–24) and using (2–11), the closed-loop error system can be obtained as

$$M_i\dot\eta = -V_{m,i}\eta + Y_d\tilde\theta_i + ka\Gamma^{-1}y - \mathsf{Tanh}(e)$$
$$- kaM_i\eta + \chi_i, \ i \in \mathbb{S}. \tag{2–26}$$

2.3 Stability Analysis of Subsystems

Since the trajectory for a switched system can diverge even when all the subsystems of the switched system are stable [94, Problem A.], the switching signal which determines the switching time instant must be properly developed. However, before designing the switching signal, the stability of each subsystem with its closed-loop error system in (2–26) is first analyzed based on the controller designed in (2–13).

Theorem 2.1. *[32] Given a collection of the subsystem dynamics of the switched system in (2–1), the robust controllers designed for each subsystem in (2–13)-(2–18) with individual control gains satisfying the sufficient conditions described in (2–18) ensures that the position tracking of each subsystem is globally UUB in the sense that*

$$\|e\| \leq \|z\| \leq \bar{d}_i, \quad \forall t \geq T_i(\bar{d}_i, \|z(0)\|), i \in \mathbb{S} \tag{2–27}$$

in the region $\mathbb{D}$ defined as

$$\mathbb{D} \triangleq \left\{ (e,\, \eta,\, y) \in \mathbb{R}^n \times \mathbb{R}^n \times \left(\frac{-a}{\sqrt{n}},\, \frac{a}{\sqrt{n}} \right)^n \right\}, \tag{2–28}$$

where the composite state vector $z \in \mathbb{R}^{3n}$ is defined as

$$z \triangleq \left[e^T\ \eta^T\ y^T \right]^T. \tag{2–29}$$

In (2–27), $\bar{d}_i \in \mathbb{R}$ is a positive constant that defines the radius of a ball containing the position tracking error of ith subsystem as

$$\bar{d}_i > \left(\gamma_1^{-1} \circ \gamma_2 \right) \left(\gamma_{3,i}^{-1}(\varepsilon) \right),\ i \in \mathbb{S},$$

and $T_i(\bar{d}_i, \|z(0)\|) \in \mathbb{R}$ denotes the following positive constant that represents the time duration from the initial time to the time to reach the ball for the ith subsystem as

$$T_i(\bar{d}_i, \|z(0)\|) =$$

$$\begin{cases} 0 & if\ \|z(0)\| \leq (\gamma_2^{-1} \circ \gamma_1)(\bar{d}_i) \\[2mm] \frac{\gamma_2(\|z(0)\|) - \gamma_1((\gamma_2^{-1} \circ \gamma_1)(\bar{d}_i))}{\gamma_{3,i}((\gamma_2^{-1} \circ \gamma_1)(\bar{d}_i)) - \varepsilon} & if\ \|z(0)\| > (\gamma_2^{-1} \circ \gamma_1)(\bar{d}_i), \end{cases}$$

where ε was defined in (2–20), and the strictly increasing functions $\gamma_1,\, \gamma_2,\, \gamma_{3,i} : \mathbb{R} \to \mathbb{R}$ are defined as

$$\gamma_1(\|z\|) \triangleq \lambda_1 \ln \cosh(\|z\|) \tag{2–30}$$

$$\gamma_2(\|z\|) \triangleq \lambda_2 \left\| \left[e^T\ \eta^T \right]^T \right\|^2 + \frac{1}{2} \sum_{j=1}^n \frac{y_j^2}{a - y_j^2} \tag{2–31}$$

$$\gamma_3(\|z\|) \triangleq \left(\frac{1}{2} - \frac{1}{4k_{n4}} \right) \tanh^2(\|z\|), \tag{2–32}$$

where $\lambda_1,\, \lambda_2 \in \mathbb{R}$ are positive constants defined as

$$\lambda_1 \triangleq \min \left\{ \frac{1}{2a},\, \frac{m_1}{2} \right\} \quad \lambda_2 \triangleq \max \left\{ 1,\, \frac{m_2}{2} \right\}.$$

Proof. [32] Let $V_i : \mathbb{R}^{3n} \to \mathbb{R}$ be defined as

$$V_i \triangleq \sum_{j=1}^{n} \ln(\cosh(e_j)) + \frac{1}{2}\eta^T M_i \eta + \frac{1}{2}\sum_{j=1}^{n} \frac{y_j^2}{a - y_j^2}, \ i \in \mathbb{S}. \tag{2-33}$$

Each Lyapunov function in (2–33) is a positive-definite radially unbounded function in the set $\mathbb{D}$. Based on (2–9), the Lyapunov functions in (2–33) can be lower and upper bounded

$$\gamma_1(\|z\|) \le V_i \le \gamma_2(\|z\|), \ i \in \mathbb{S}, \tag{2-34}$$

where z was defined in (2–29), and γ_1 and γ_2 were introduced in (2–30) and (2–31). After taking the time derivative of (2–33) and utilizing (2–3), (2–21), (2–22), and (2–26) the following expression can be obtained

$$\dot{V}_i = -\sum_{j=1}^{n} \tanh^2(e_j) - a\|y\|^2 + \eta^T \left(Y_d \tilde{\theta}_i - kaM_i\eta + \chi_i \right). \tag{2-35}$$

After utilizing (2–2), (2–18), and (2–25), the expression in (2–35) can be upper bounded as

$$\begin{aligned}
\dot{V}_i \le & -\frac{\|\mathsf{Tanh}(e)\|^2}{2} - \frac{1}{2}\|y\|^2 - \frac{1}{2}\|\eta\|^2 \\
& + \frac{1}{4k_{n1}} + \frac{1}{4k_{n2}} + \frac{1}{4k_{n3}} + \frac{1}{4k_{n4}}\|x\|^2 \\
& + \frac{1}{2}\|y\|^2 \left[-1 + \frac{\|y\|^2}{8a^2} + \frac{\|y\|^4}{4a^4} + \frac{\|y\|^6}{2a^6} + \frac{\|y\|^8}{8a^8} \right] \\
& + a\xi_{6,i}(\|y\| - a)\|\eta\|^2 \\
\le & -(\frac{1}{2} - \frac{1}{4k_{n4}})\|x\|^2 + \varepsilon \text{ if } \|y\| < a, \ i \in \mathbb{S}, \ \forall t \ge 0, \tag{2-36}
\end{aligned}$$

where a satisfies $a \ge 1$, and ε was defined in (2–20).

By applying the property in (2–9), (2–36) can be further upper bounded as

$$\dot{V}_i \le -\gamma_3(\|z\|) + \varepsilon \text{ if } \|y\| < a, \ i \in \mathbb{S}, \ \forall t \ge 0, \tag{2-37}$$

where γ_3 was defined in (2–32), and z was defined in (2–29). The expression in (3–30) can be rewritten as [32]

$$\dot{V}_i \leq -\gamma_3\left(\|z\|\right) + \varepsilon, \text{ if } z \in \mathbb{D}, \ \forall t \geq 0. \tag{2–38}$$

From (2–19) and (2–30)-(2–32),

$$\gamma_j(0) = 0, \ j = 1,\ 2. \qquad \gamma_3(0) = 0, \ i \in \mathbb{S}$$

$$\lim_{\|z\| \to \infty} \gamma_j(z) \to \infty, \ j = 1,\ 2$$

$$\lim_{\|z\| \to \infty} \gamma_3(z) = \left(\frac{1}{2} - \frac{1}{4k_{n4}}\right) \quad \varepsilon < \frac{1}{2} - \frac{1}{4k_{n4}}.$$

Therefore, by selecting the initial condition of p according to (2–17), then $p(0)$ with any given $e(0)$ and $\eta(0)$ will satisfy $z(0) \in \mathbb{D}$, so the global UUB tracking result in (2–27) can be ensured for each subsystem. □

2.4   Dwell-Time

To facilitate the application of the dwell-time approach, two quadratic functions γ_2', $\gamma_3' : \mathbb{R} \to \mathbb{R}$ are defined as

$$\gamma_2'(\|z\|) \triangleq \alpha_2 \|z\|^2 \quad \gamma_3'(\|z\|) \triangleq \alpha_3 \|z\|^2, \tag{2–39}$$

where the positive constants $\alpha_2,\ \alpha_3 \in \mathbb{R}$ are selected such that the following two inequalities hold

$$\gamma_2'(\|z\|) \geq \gamma_2(\|z\|), \ z \in \mathbb{D}_{SG} \tag{2–40}$$

$$\gamma_3'(\|z\|) < \gamma_3(\|z\|), \ z \in \mathbb{D}_{SG}, \tag{2–41}$$

where $\mathbb{D}_{SG}$ denotes a domain that contains the largest possible value of z for a given $z\left(0\right)$ and is defined as

$$\mathbb{D}_{SG} \triangleq$$
$$\left\{ z \in \mathbb{R}^{3n} \mid \|z\| \leq \max\left\{ (\gamma_1^{-1} \circ \gamma_2)(\|z(0)\|),\ \bar{d}_{\max} \right\} \right\}, \tag{2–42}$$

where $\bar{d}_{\max} \in \mathbb{R}$ is a known positive constant defined as $\bar{d}_{\max} \triangleq \max\limits_{i \in \mathbb{S}} \{\bar{d}_i\}$ and can be decreased by increasing the control gain defined in (2–20).

To ensure $z \in \mathbb{D}_{SG} \subset \mathbb{D}$ for any given $z(0)$, the adjustable constant a must satisfy the following criterion based on (2–28) and (2–42)

$$\max\left\{\left(\gamma_1^{-1} \circ \gamma_2\right)(\|z(0)\|),\, \bar{d}_{\max}\right\} \leq \frac{a}{\sqrt{n}}. \tag{2–43}$$

By using (2–30) and (2–31), $(\gamma_1^{-1} \circ \gamma_2)(\cdot)$ in (2–43) can be further expressed as

$$(\gamma_1^{-1} \circ \gamma_2)(\cdot) = \cosh^{-1}(\exp(\frac{\gamma_2(\cdot)}{\lambda_1})). \tag{2–44}$$

In addition, by selecting a to be sufficiently large, γ_2 defined in (2–31) can be upper bounded (by using the fact that $\frac{1}{a - y_j^2} \leq \frac{1}{a - \left[\left(\gamma_1^{-1} \circ \gamma_2\right)(\|z(0)\|)\right]^2}$, for $1 \leq j \leq n$) by a quadratic function as

$$\begin{aligned}
\gamma_2(\|z\|) =& \lambda_2 \left\|\left[e^T\ \eta^T\right]^T\right\|^2 + \frac{1}{2}\sum_{j=1}^{n} \frac{y_j^2}{a - y_j^2} \\
\leq& \lambda_2 \left\|\left[e^T\ \eta^T\right]^T\right\|^2 \\
&+ \frac{1}{2(a - \left[\left(\gamma_1^{-1} \circ \gamma_2\right)(\|z(0)\|)\right]^2)}\sum_{j=1}^{n} y_j^2 \\
\leq& \bar{\lambda}_2 \left\|\left[e^T\ \eta^T\ y^T\right]^T\right\|^2 \\
\leq& \bar{\lambda}_2 \|z\|^2, \tag{2–45}
\end{aligned}$$

where $\bar{\lambda}_2 \in \mathbb{R}$ is a positive constant defined as $\bar{\lambda}_2 \triangleq \max\left\{\lambda_2,\, \frac{1}{2(a - \left[\left(\gamma_1^{-1} \circ \gamma_2\right)(\|z(0)\|)\right]^2)}\right\}$ and a satisfies

$$a > \left[\left(\gamma_1^{-1} \circ \gamma_2\right)(\|z(0)\|)\right]^2. \tag{2–46}$$

Based on (2–44) and (2–45), (2–43) can be further upper bounded as

$$\max\left\{\cosh^{-1}(\exp(\frac{\alpha_2 \|z(0)\|^2}{\lambda_1})),\, \bar{d}_{\max}\right\} \leq \frac{a}{\sqrt{n}}, \tag{2–47}$$

34

where based on (2–45) α_2 is selected as $\alpha_2 = \bar{\lambda}_2$, and (2–47) holds provided that a is selected sufficiently large. Therefore, $\mathbb{D}_{SG} \subset \mathbb{D}$ holds if a satisfies (2–46) and (2–47).

The stability of each subsystem is globally UUB in $\mathbb{D}$ from the previous section, but it does not account for the stability when switching between subsystems. To ensure the position tracking error of the switched system is stable, the switching signal must be designed. By applying the similar scheme introduced by [26], the dwell-time can be developed for the switched system with the dynamics in (2–1).

Theorem 2.2. *The system consisting of the subsystems introduced in (2–1) with an appropriately designed dwell-time $\tau^\star$ and robust OFB controllers ensure that the position tracking error is semi-global UUB in the sense that*

$$\|e(t)\| \leq \|z(t)\| \leq r_{SG}, \quad \forall t \geq T_{SG}$$

provided that the dwell-time satisfies

$$\tau_{DT} \geq \tau_{DT}^\star, \tag{2–48}$$

where $\tau_{DT}^\star \triangleq \frac{\ln \mu}{\beta_0 - \beta^\star} \in \mathbb{R}$ is defined as the minimum dwell-time, and r_{SG}, T_{SG}, μ, β_0, $\beta^\star \in \mathbb{R}$ are known positive constants defined in the subsequent analysis.

Proof. To satisfy (2–41) for $z \in \mathbb{D}_{SG}$, α_3 can be selected to be a sufficiently small constant. By utilizing the two auxiliary functions defined in (2–34) and (2–39), (2–38) can be further upper bounded as

$$
\begin{aligned}
\dot{V}_i &\leq -\left(\gamma_3 \circ \gamma_2^{-1} \right)(V_i) + \varepsilon \\
&\leq -\left(\gamma_3' \circ \gamma_2'^{-1} \right)(V_i) + \varepsilon \\
&\leq -\frac{\alpha_3}{\alpha_2} V_i + \varepsilon, \ i \in \mathbb{S},
\end{aligned}
\tag{2–49}
$$

for $z \in \mathbb{D}_{SG}$, $\forall t \geq 0$. Based on (2–49), $\mathbb{D}_{\alpha,i}$ denotes the UUB region of the ith subsystem and is defined as

$$\mathbb{D}_{\alpha,i} \triangleq \left\{ z \in \mathbb{D}_1 \mid V_i \leq \frac{\alpha_2}{\alpha_3}\varepsilon \right\}, \ \forall i \in \mathbb{S},$$

and the union of individual UUB region denoted as $\mathbb{D}_{\bar{\alpha}}$ can be defined as $\mathbb{D}_{\bar{\alpha}} \triangleq \underset{i\in\mathbb{S}}{\cup} \mathbb{D}_{\alpha,i}$, where the area of $\mathbb{D}_{\bar{\alpha}}$ can be reduced by increasing the control gain k.

Let the multiple Lyapunov function candidate $V : \mathbb{R}^{3n} \to \mathbb{R}^n$ be defined as

$$V(z) \triangleq V_{\sigma(t)}(z), \tag{2–50}$$

where $\sigma : [0, \infty) \to \mathbb{S}$ denotes a piecewise constant switching signal that determines the sequence of switching between subsystems. Applying the same concept as [95], it is known from (2–49) that each subsystem is UUB with a decay rate along the Lyapunov function greater than $\frac{\alpha_3}{\alpha_2}$ if $z \in \mathbb{D}_{SG} \setminus \mathbb{D}_{\bar{\alpha}}$.

Let t_1, t_2, ... be the time instants that a switching event occurs, and $m \in \mathbb{N}$ denotes the number of switchings. Then, any switching time sequence with m switches can be expressed as $0 < t_1 < \cdots < t_m < t < t_{m+1}$. Let $\Omega_j \in \mathbb{S}$ denote the value of σ between switches that is defined as

$$\Omega_j \triangleq \sigma(t), \, t \in [t_{j-1}, t_j), \, \forall j \in \mathbb{N}.$$

Using (2–34), (2–40), and (2–49) the maximum value of the Lyapunov function due to switching inside the UUB ball (i.e., $z \in \mathbb{D}_{\bar{\alpha}}$) can be upper bounded as

$$V(z) \leq V_B, \tag{2–51}$$

where $V_B \in \mathbb{R}$ denotes the largest value of the Lyapunov function after switching in the UUB ball and is defined as

$$V_B \triangleq \alpha_2 \left(\gamma_1^{-1} \left(\frac{\alpha_2\varepsilon}{\alpha_3} \right) \right)^2.$$

36

Then, using (2–51) and (2–50), it is straightforward to show

$$V(z) \leq \max\left\{e^{-\beta_{\Omega_m}(t-t_m)}V_{\Omega_m}(z(t_m)),\ V_B\right\}, \tag{2–52}$$

where $\Omega_m \in \mathbb{S}$, $z \in \mathbb{D}_{SG} \cup \mathbb{D}_{\bar\alpha}$, $\forall t \geq 0$, and β_{Ω_m} is the decay rate to the UUB ball for subsystem Ω_m. Based on (2–34), the following inequalities hold

$$V_{\Omega_j}(z) \leq \mu V_{\Omega_l}(z) \quad V_{\Omega_l}(z) \leq \mu V_{\Omega_j}(z),\ j \neq l, \tag{2–53}$$

where $\Omega_j,\ \Omega_l \in \mathbb{S}$ index any two subsystems, and $\mu \in \mathbb{R}$ is a positive constant that denotes the maximum ratio of any two Lyapunov functions of the subsystems and is defined as

$$\mu \triangleq \sup_{t \geq 0}\left\{\frac{\gamma_2(z)}{\gamma_1(z)}\right\},\ z \in \mathbb{D}_{SG} \cup \mathbb{D}_{\bar\alpha}.$$

By using (2–53) and defining $\beta_0 \in \mathbb{R}$ to be a positive constant as $\beta_0 \triangleq \min_{i \in \mathbb{S}}\beta_i$, the expression in (2–52) can be upper bounded as [95]

$$
\begin{aligned}
V(z) &\leq \max\left\{e^{-\beta_0(t-t_m)}V_{\Omega_m}\Big(z(t_m)\Big),\ V_B\right\} \\
&\leq \max\left\{e^{-\beta_0(t-t_m)}\mu V_{\Omega_{m-1}}\Big(z(t_m)\Big),\ V_B\right\} \\
&\leq \max\Big\{e^{-\beta_0(t-t_m)}\mu e^{-\beta_0(t_m-t_{m-1})}V_{\Omega_{m-1}}\Big(z(t_{m-1})\Big) \\
&\qquad\qquad ,\ V_B\Big\} \\
&\leq \cdots \\
&\leq \max\left\{e^{-\beta_0 t}\mu^m V_{\Omega_0}\Big(z(0)\Big),\ V_B\right\} \\
&= \max\left\{e^{-\beta_0 t}\mu^{N_\sigma(t)}V\Big(z(0)\Big),\ V_B\right\},
\end{aligned}
\tag{2–54}
$$

for $z \in \mathbb{D}_{SG} \cup \mathbb{D}_{\bar\alpha}$, $\forall t \geq 0$. In (2–54), $N_\sigma \in \mathbb{R}$ denotes the number of switchings during time interval $[0,\,t)$, $t \in [t_m,\,t_{m+1})$. Moreover, in (2–54) the inequality holds even if the switching sequence is arbitrarily specified provided that the dwell-time condition in (2–48) is satisfied.

By selecting a desired decay rate $\beta^\star \in \mathbb{R}$ for the switched system, where

$$0 < \beta^\star < \beta_0,$$

such that

$$e^{-\beta_0 t} \mu^{N_\sigma(t)} \leq e^{-\beta^\star t}, \; t \in [t_m, \, t_{m+1}), \tag{2--55}$$

the minimum dwell-time $\tau_{DT}^\star$ can be determined based on (2–55), and the number of switchings is finite and can be upper bounded by

$$N_\sigma \leq \frac{t}{\tau_{DT}^\star}, \; t \in [t_m, \, t_{m+1}).$$

Then, (2–54) can be expressed as

$$V(z) \leq \max \left\{ e^{-\beta^\star t} V\left(z(0)\right), \, V_B \right\}. \tag{2--56}$$

Based on (2–56), $r_{SG} \in \mathbb{R}$ denotes the radius of the UUB ball of the switched system and can be determined by using (2–34) as

$$r_{SG} \triangleq \gamma_1^{-1}(V_B).$$

By using (2–56), $T_{SG} \in \mathbb{R}$ denotes the time to reach the UUB ball for any given $z(0)$ and can be determined as

$$T_{SG} \geq \begin{cases} \frac{-\ln \frac{V_B}{V(z(0))}}{\beta^\star}, & \text{if } V\left(z(0)\right) > V_B \\ 0 & , & \text{otherwise.} \end{cases} \tag{2--57}$$

In (2–56), the decay rate $\beta^\star$ can be arbitrarily selected within $(0, \, \beta_0)$, which character-izes the decay rate of the entire switched system. The time to reach the UUB ball for any given $V\left(z(0)\right)$ can be decreased by increasing $\beta^\star$, as indicated in (2–57). However, increases in $\beta^\star$ require a larger dwell-time, as indicated in (2–57). Thus, there is an

interplay between dwell-time and the time to reach the UUB ball. Based on this dwell-time scheme, the position tracking error of the switched system is semi-global UUB with arbitrary switching sequences. □

2.5 Simulation

In this section, a switched system consisting of two subsystems is demonstrated to corroborate the stability analysis. Each subsystem is a two-link, revolute joint robot manipulator [96]. The true system parameters of the two subsystems are given as $\theta_1 = [3.473, \ 0.196, \ 0.242, \ 5.3, \ 1.1]^T$ and $\theta_2 = [3.6, \ 0.4, \ 0.4, \ 3.3, \ 1.1]^T$, respectively. The best-guess system parameters (with about 10% errors) used in the simulations were selected as $\hat{\theta}_1 = [3.7, \ 0.22, \ 0.22, \ 4.8, \ 1]^T$ and $\hat{\theta}_2 = [3.3, \ 0.36, \ 0.44, \ 3, \ 1]^T$, respectively. To validate the tracking performances of the closed-loop system, two simulations with different switching signals are conducted, where the switching signals are piecewise constant signals with 1 second and 3 second periodic durations as depicted in Fig. 2-1 and Fig. 2-2 . Both simulations use the same desired trajectory defined as

$$q_d = \begin{bmatrix} \sin{(t)} \\ \cos{(t)} \end{bmatrix}.$$

The comparisons of the tracking performance of axis 1 and axis 2 are shown in Fig. 2-3 and Fig. 2-4.
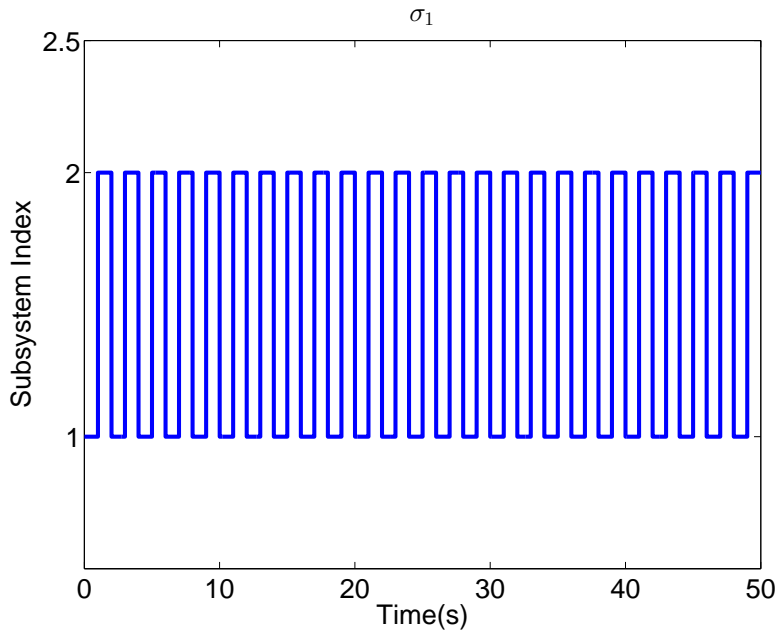
Figure 2-1. The switching signal σ_1 with a periodic duration of 1 second. The vertical axis indicates the subsystem being activated at time t.
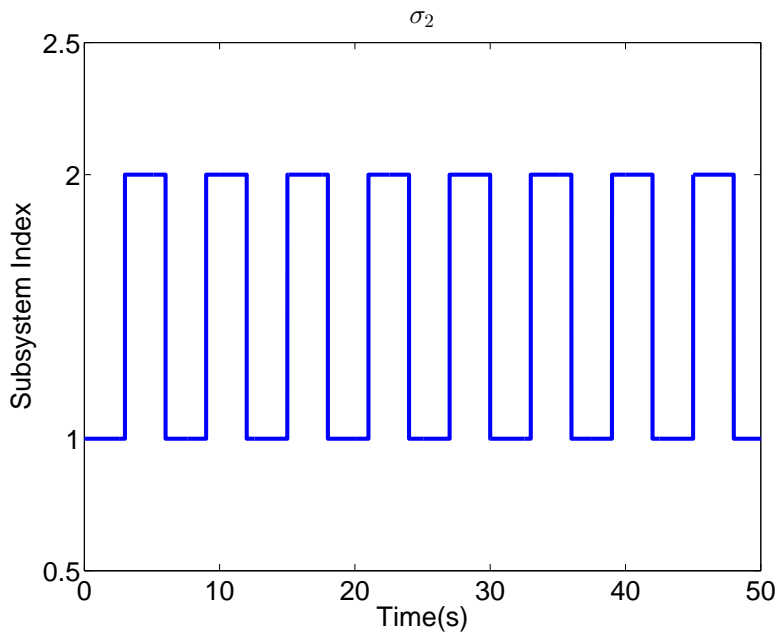
Figure 2-2. The switching signal σ_2 with a periodic duration of 3 seconds. The vertical axis indicates the subsystem being activated at time t.
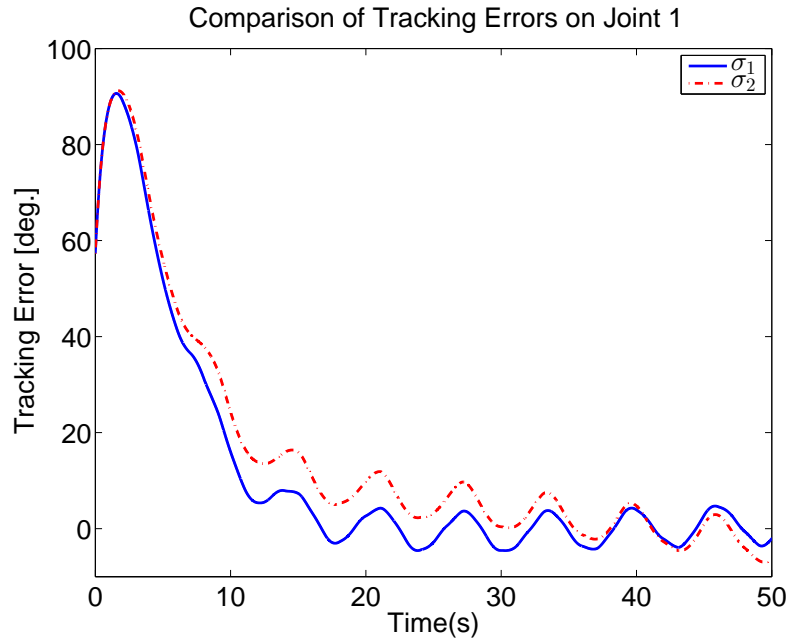
Figure 2-3. Tracking errors of axis 1 using switching signals σ_1 and σ_2.
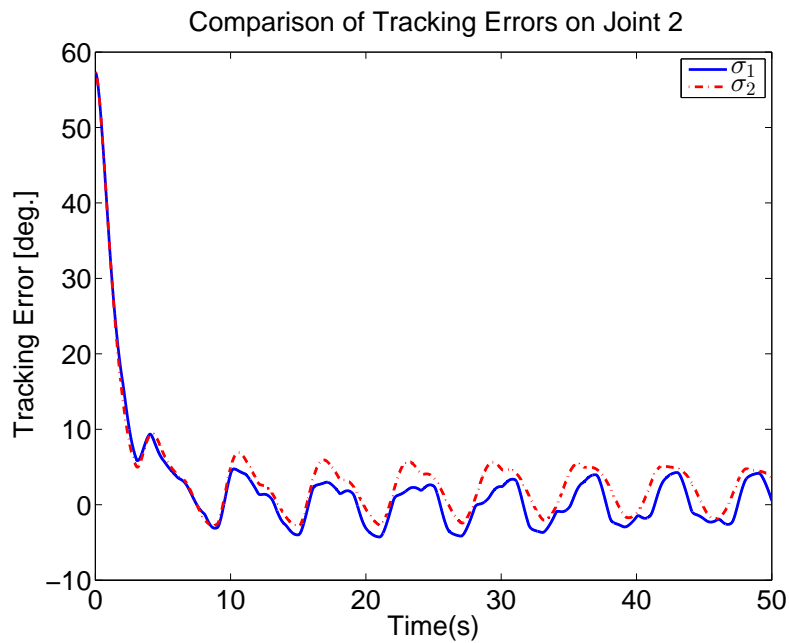
Figure 2-4. Tracking errors of axis 2 using switching signals σ_1 and σ_2.

Fig. 2-5-2-6 show the control inputs on axis 1 and axis 2 of the manipulator using the two switching signals, respectively. Due to the discontinuous dynamics in the

switched system, the control inputs are discontinuous when the system parameters are switched between $\hat{\theta}_1$ and $\hat{\theta}_2$.
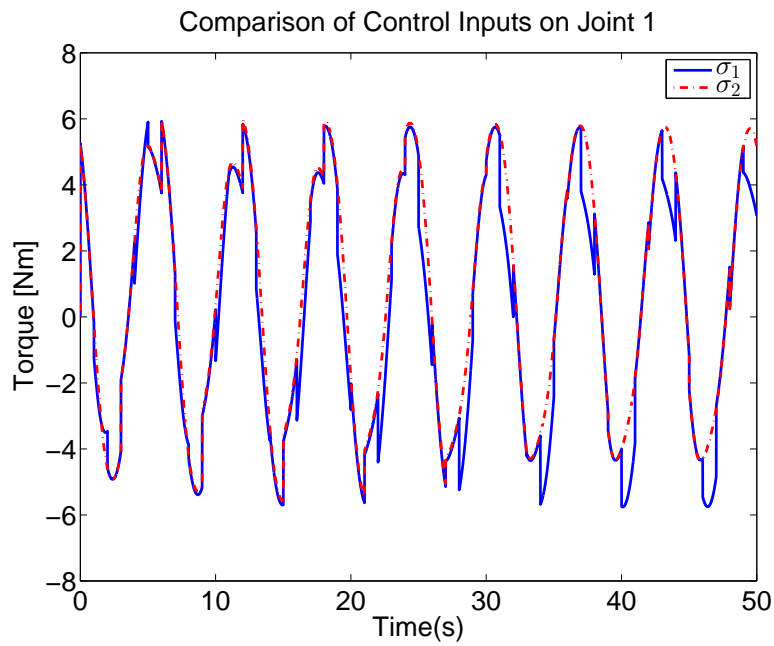
Figure 2-5. Control inputs on axis 1 using switching signals σ_1 and σ_2.
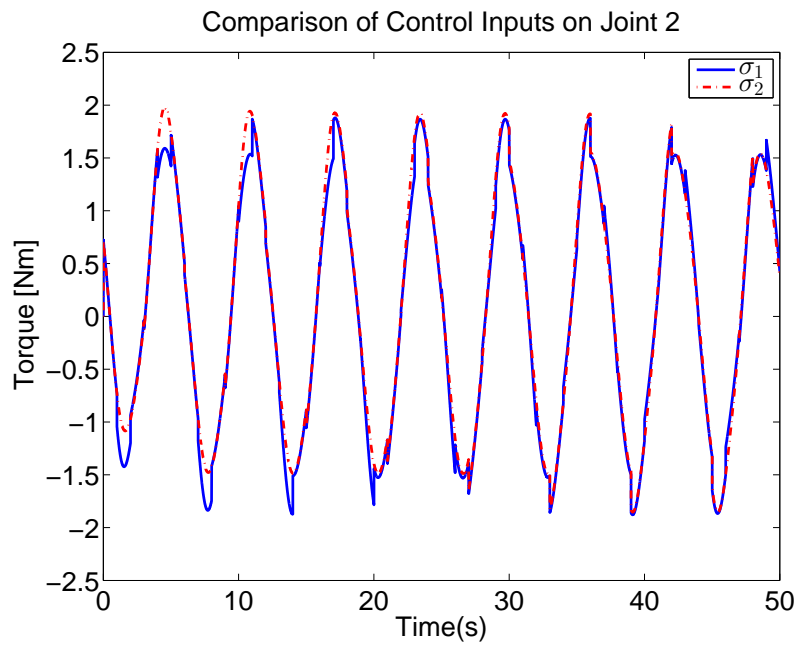
Figure 2-6. Control inputs on axis 2 using switching signals σ_1 and σ_2.

Fig. 2-7 shows the Lyapunov functions using the two switching signals, where the Lyapunov functions are discontinuous at the switching instances.
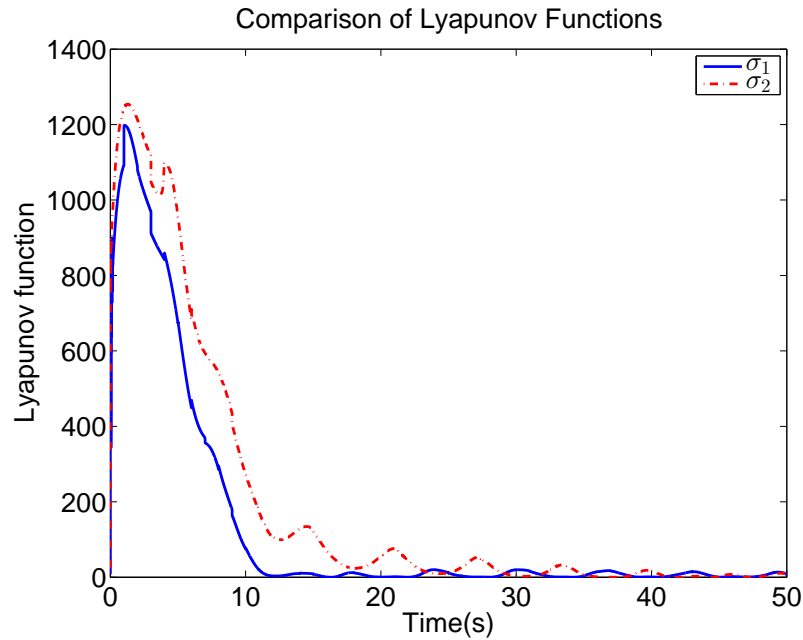
Figure 2-7. Comparison of Lyapunov functions using switching signals σ_1 and σ_2.

2.6   Discussion

The tracking errors of the closed-loop switched systems shown in Fig. 2-3 and Fig. 2-4 are semi-global UUB. Due to the best-guess term $\hat{\theta}_i$ in the control input, the control inputs are piecewise continuous, where the discontinuities of the torques reflect on the discontinuous angular acceleration. To ensure that the velocity tracking errors y are continuous under the discontinuous dynamics, the control gain is designed to be continuous. Moreover, in Fig. 2-7 the Lyapunov functions are piecewise continuous bounded functions, which implies the three signals (i.e., e, η, y) in the Lyapunov function are also bounded. The jumps of the Lyapunov function during switches are shown in Fig. 2-7, where the discontinuities are considered in (2–53). Based on the theory where the worst scenario is considered, the Lyapunov function is assumed to at most increase by same constant ratio after switching, and thus it will take longer to converge. However, the tracking errors of the closed-loop system using σ_1 and σ_2 converge to the ball at

43

almost the same rate, which implies the worst case scenario did not happen. In addition, the UUB balls for the tracking errors are about the same size under the same control gain.

2.7 Conclusion

A robust OFB controller with a time-dependent switching signal is developed for a switched Euler-Lagrange system, which consists of subsystems with parametric uncertainties and additive bounded disturbances. An switching signal is designed based on the dwell-time. A analysis consisting of multiple Lyapunov functions is developed that yields semi-global UUB OFB tracking with arbitrary switching sequences. Simulations are provided to corroborate the developed theorems.

CHAPTER 3
NETWORK CONNECTIVITY AND COLLISION AVOIDANCE UNDER INTERMITTENT FEEDBACK

Multi-agent formation control under the constraint of intermittent feedback is considered in this chapter. The potential for intermittent feedback can result in collisions by mobile agents and partitioning of the network. To address these challenges, a decentralized hybrid controller based on a navigation function framework is developed to achieve desired formation configuration while preserving network connectivity (i.e., agents remain in the feedback zone of formation neighbors) and avoiding collision with dynamic agents and static obstacles. Convergence of the hybrid system is proven by using a common Lyapunov function with nonsmooth analysis, and the designed switching conditions avoid Zeno behavior. A numerical simulation demonstrates the performance of the developed controller.

3.1   Problem Formulation

Consider N dynamic point-mass agents in the finite workspace $\mathcal{F} \subset \mathbb{R}^2$ with motion governed by the following kinematics

$$\dot{q}_i = u_i, \ i = 1, \ldots, N, \tag{3–1}$$

where $q_i \in \mathbb{R}^2$ represents the position of agent i in a two-dimensional space, and $u_i \in \mathbb{R}^2$ denotes the control input of agent $i \in \mathcal{V}$, where $\mathcal{V} \triangleq \{1, 2, \cdots, N\}$ is an index set of all agents in the system. The objective is to maintain network connectivity while also achieving a desired formation. Mathematically, this objective can be quantified as

$$\|q_i - q_j - c_{ij}\| \to 0 \text{ as } t \to \infty, \ \forall j \in \mathcal{N}_i^f, \ \forall i \in \mathcal{V}, \tag{3–2}$$

where $\mathcal{N}_i^f$ is a time-invariant set of preassigned formation neighbors, and $c_{ij} \in \mathbb{R}^2$, satisfying $\|c_{ij}\| < R_s$ and $c_{ij} = -c_{ji}$, describes the desired relative position between agent i and the adjacent agent j. The subsequent development is based on the assumption that each agent has a limited feedback range, which is encoded by a disk centered at

the agent. Position feedback from neighboring agents through communication/sensing is available within the interior of this disk (i.e., feedback zone). However, the feedback might be intermittent (i.e., existing links within the disk region may fail), which implies that two agents might not have continuous state feedback even if they remain within the disk interior.

Since feedback may be intermittent, the time-varying agent set $\mathcal{N}_i^s(t) \subseteq \mathcal{N}_i^f$ is defined as the set of formation neighbors that is in the feedback zone of agent i, $d_{ij} < R_s$, and can provide feedback to agent i, where

$$d_{ij}(t) \triangleq \|q_i(t) - q_j(t)\| \in \mathbb{R}_{\geq 0}$$

denotes the time-varying distance between the two agents, and $R_s \in \mathbb{R}$ is a positive constant denoted as the maximal feedback radius for every agent. As a result, the graph of the network system is an undirected, time-varying graph that can be modeled as $\mathcal{G}(t) \triangleq (\mathcal{V}, \mathcal{E}(t))$, where $\mathcal{E}(t) \triangleq \{(j, i) \in \mathcal{V} \times \mathcal{V} | j \in \mathcal{N}_i^s(t), i \in \mathcal{V}, i \neq j\}$ is a time-varying edge set. To include all the time-varying graphs, a switched graph is defined as G_σ, where $\sigma : [0, \infty) \to \mathcal{P}$ is a switching signal, and $\mathcal{P} \in \{1, 2, \ldots, P\}$ is a finite index set such that $\{G_p : p \in \mathcal{P}\}$ includes all possible graphs $\underset{t \geq 0}{\cup} \mathcal{G}$.

Other than the objective described in (3–2), network connectivity is essential for achieving formation control. However, due to the potential for intermittent feedback, continuous feedback from a formation neighbor is not guaranteed. The loss of feedback considered in this chapter is assumed to be temporary in the sense that the feedback can be recovered after failing for a finite time period (i.e., the feedback is intermittent). Therefore, the necessary condition for network connectivity maintenance is to enforce agents to remain inside the feedback zone of its formation neighbors for all time. In this chapter, network connectivity for intermittent network topologies is defined as follows.

Definition 3.1. Network connectivity is achieved when the distance between formation neighbor j remains within a set bounded as

$$d_{ij}(t) < R_s, \ j \in \mathcal{N}_i^f, \ i \in \mathcal{V}, \ \forall t \geq 0. \tag{3--3}$$

Consider stationary obstacles $o_1, o_2, \ldots, o_m$ in the workspace $\mathcal{F}$, which are represented by a set of m points indexed by $\mathcal{M} = \{1, 2, \ldots, m\}$. To prevent collisions among agents and obstacles, a disk region centered at agent i with radius $\delta_1 < \|c_{ij}\|$ is defined. Any agent or obstacle in this region is considered as a potential collision hazard for agent i, and the time-varying potential collision set $\mathcal{N}_i$ is defined as

$$\mathcal{N}_i(t) \triangleq \{j \in \mathcal{V} \mid d_{ij}(t) \leq \delta_1, \ j \neq i\}. \tag{3--4}$$

In summary, the objective is to asymptotically achieve a formation configuration as in (3--2), while ensuring network connectivity as in (3--3) and collision avoidance between agents and stationary obstacles $o_1, o_2, \ldots, o_m$ as in (3--4).

Assumption 3.1. [74] The communication/sensing link failures between agents happen a finite number of times in a finite time interval, (i.e., the switching signal σ has finite switches in any finite time interval.) Specifically, given any non-overlapping time interval $[t_k, t_{k+1})$, $k = 0, 1, \ldots$, then $0 < \tau < t_{k+1} - t_k < T$, where $\tau \in \mathbb{R}$ is the non-vanishing dwell-time, and $T \in \mathbb{R}$ is a positive constant. The graph G_σ is fixed for $t \in [t_k, t_{k+1})$, $\forall k = 0, 1, 2, \ldots$.

Assumption 3.2. [54] The critical points introduced from the navigation function are all isolated points.

Assumption 3.3. [54] The desired formation neighbor set of agent i is inside its initial feedback zone (i.e., $\mathcal{N}_i^f \subset \mathcal{N}_i^s(t_0)$, for $i \in \mathcal{V}$, where $t_0 \in [0, \infty)$ is the initial time instance), and the neighboring agents are not initially located at any critical points (e.g., agents colliding) indicated in Assumption 3.2.

Assumption 3.4. [54] The desired relative position described by c_{ij} is achievable (i.e., $\delta_1 < \|c_{ij}\| < R_s - \delta_2$, where $\delta_2 \in \mathbb{R}^+$ denotes a buffer distance for maintaining network connectivity, so the relative position would not result in a partition of the graph or cause collision of any two agents), and the agents do not take certain pathological configurations. An example pathological configuration would be one in which all of the agents and goals are co-linear. However, this and other such configurations are assumed to be isolated in the space of all configurations, and are practically resolved by small perturbations.

Assumption 3.5. Agents have continuous feedback of the agent or obstacle position within the distance of δ_1 since the possibility of losing feedback is mitigated when the relative distances become shorter. The radius of collision disk δ_1 is much less than the feedback range R_s (i.e., $\delta_1 \ll R_s$). Agent $i \in \mathcal{V}$ is aware of the relative distance to the agent $j \in \mathcal{N}_i$ or the stationary obstacle $k \in \mathcal{M}$ within its collision disk (i.e., $d_{ij} \leq \delta_1$ or $d_{ik} \leq \delta_1$).

3.2 Control Development

Based on [54], a navigation function $\varphi_i : \mathcal{F} \to [0,\,1]$ for each agent i is designed as,

$$\varphi_i = \frac{\gamma_i}{\left(\gamma_i^k + \beta_i\right)^{\frac{1}{k}}}, \tag{3–5}$$

where $k \in \mathbb{R}$ is an adjustable positive control gain, $\gamma_i : \mathbb{R}^2 \to \mathbb{R}_{\geq 0}$ is a goal function, and $\beta_i : \mathbb{R}_{\geq 0} \to [0,\,1]$ is a constraint function for agent i. Based on the objective in (3–2), the goal function γ_i in (3–5) is designed as

$$\gamma_i(q_i,\,q_j) \triangleq \sum_{j \in \mathcal{N}_i^f} \|q_i - q_j - c_{ij}\|^2. \tag{3–6}$$

The continuous constraint function β_i is defined as

$$\beta_i \triangleq \prod_{j \in \mathcal{N}_i^f} b_{ij} \prod_{k \in \mathcal{N}_i \cup \mathcal{M}_i} B_{ik}, \tag{3–7}$$

which enables collision avoidance and network connectivity maintenance, where $\mathcal{M}_i$ denotes the set of stationary obstacles within the collision region of agent i. To maintain network connectivity, the nonsmooth function $b_{ij} : \mathbb{R}_{\geq 0} \to [0, 1]$ in (3–7) is designed as

$$
b_{ij}(d_{ij}) \triangleq \begin{cases} 1, & d_{ij} < R_s - \delta_2, \\ -\frac{1}{\delta_2^2}(d_{ij} + 2\delta_2 - R_s)^2 + \frac{2}{\delta_2}(d_{ij} + 2\delta_2 - R_s), & R_s - \delta_2 \leq d_{ij} \leq R_s, \\ 0, & d_{ij} > R_s, \end{cases} \tag{3–8}
$$

where b_{ij} is not differentiable at R_s. Specifically, b_{ij} is designed to prevent agent i from leaving the feedback zone of its formation neighbor $j \in \mathcal{N}_i^f$. In (3–7), for $k \in \mathcal{N}_i \cup \mathcal{M}_i$, $B_{ik} : \mathbb{R} \to [0, 1]$ is defined as

$$
B_{ik}(d_{ik}) \triangleq \begin{cases} -\frac{1}{\delta_1^2}d_{ik}^2 + \frac{2}{\delta_1}d_{ik}, & 0 \leq d_{ik} \leq \delta_1, \\ 1, & d_{ik} > \delta_1. \end{cases}
$$

Therefore, $\beta_i \to 0$ as agent i enters the constraint region, (i.e. as agent i approaches other agents, stationary obstacles, or tries to leave the feedback range of their adjacent agents $j \in \mathcal{N}_i^f$, $\forall t \geq 0$). Based on Assumption 3.4, γ_i and β_i will not be zero at the same time, and the navigation function φ_i reaches its maximum at 1 when $\beta_i = 0$ and its minimum at 0 when $\gamma_i = 0$.

Due to the intermittent feedback, consider the two time-varying sets $\mathcal{V}_f$ and $\mathcal{V}_u$, defined as $\mathcal{V}_f(t) \triangleq \left\{ i \in \mathcal{V} | \mathcal{N}_i^s(t) = \mathcal{N}_i^f \right\}$ and $\mathcal{V}_u \triangleq \mathcal{V} \setminus \mathcal{V}_f$. The set $\mathcal{V}_f$ includes agents that can receive feedback from all of its formation neighbors $j \in \mathcal{N}_i^f$ at $t \in \mathbb{R}_{\geq 0}$. Otherwise, agent i will be in $\mathcal{V}_u$ at some $t \in \mathbb{R}_{\geq 0}$. Using the navigation function in (3–5), the decentralized hybrid controller for agent i is designed as

$$
u_i = \begin{cases} -\Gamma \nabla_{q_i} \varphi_i, & i \in \mathcal{V}_f, \\ 0, & i \in \mathcal{V}_u, \end{cases} \tag{3–9}
$$

where $\Gamma \in \mathbb{R}^+$ is a positive constant gain, and $\nabla_{q_i}(\cdot) \triangleq \frac{\partial}{\partial q_i}(\cdot)$. Based on the switching condition of the hybrid controller designed in (3–9), Zeno behaviors can not exist

provided that Assumption 3.1 holds. That is, u_i has to stay at least T period at one of the control policies in (3–9) before switching to the other one, which implies infinite switchings in finite time is impossible.

3.3 Connectivity Analysis

Lemma 3.1. *If the initial graph of the multi-agent system is connected, i.e.,*

$$d_{ij}(t_0) < R_s, \ \forall j \in \mathcal{N}_i^f, \ \forall i \in \mathcal{V},$$

then the controller in (3–9) ensures agent i and j remain connected for all time.

Proof. Consider an agent $i \in \mathcal{V}$ located at $q_i \in \mathcal{F}$, where the relative distances d_{ij} between its formation neighbors are approaching the feedback range limit R_s, which implies $\prod_{j \in \mathcal{N}_i^f} b_{ij} \to 0$, then three cases must be considered. The first two cases are for agents in $\mathcal{V}_f$ while the third case is for agents in $\mathcal{V}_u$.

Case 1. As agent $j \in \mathcal{N}_i^f$ approaches the boundary of the feedback region (i.e., $\|q_i - q_j\|$ approaches R_s from the left) of agent $i \in \mathcal{V}_f$, then β_i tends to zero. The gradient of φ_i is

$$\nabla_{q_i} \varphi_i = \frac{k \beta_i \nabla_{q_i} \gamma_i - \gamma_i \nabla_{q_i} \beta_i}{k(\gamma_i^k + \beta_i)^{\frac{1}{k}+1}}. \tag{3–10}$$

Consider

$$\nabla_{q_i} \beta_i = \prod_{k \in \mathcal{N}_i \cup \mathcal{M}_i} B_{ik} \sum_{h \in \mathcal{N}_i^f} (\nabla_{q_i} b_{ih}) \prod_{l \in \mathcal{N}_i^f, l \neq h} b_{il} + \prod_{j \in \mathcal{N}_i^f} b_{ij} \sum_{h \in \mathcal{N}_i \cup \mathcal{M}_i} (\nabla_{q_i} B_{ih}) \prod_{l \in \mathcal{N}_i \cup \mathcal{M}_i, l \neq h} B_{il}.$$

Provided only agent j is near the boundary (i.e., $\|q_i - q_j\| \to R_s^-$), $\nabla_{q_i} \beta_i$ has only one dominant term:

$$\nabla_{q_i} \beta_i = (\nabla_{q_i} b_{ij}) \prod_{l \in \mathcal{N}_i^f, l \neq j} b_{il} \prod_{k \in \mathcal{N}_i \cup \mathcal{M}_i} B_{ik} + O(b_{ij}),$$

where $O\left(\cdot\right)$ is the Big O notation[1] , which vanishes as $\|q_i - q_j\|$ approaches R_s. The other term in the numerator of $\nabla_{q_i}\varphi_i$ in (3–10) is $k\beta_i \nabla_{q_i}\gamma_i = O\left(b_{ij}\right)$. Hence, $\nabla_{q_i}\varphi_i$ in (3–10) can be expressed as

$$\nabla_{q_i}\varphi_i = \frac{-\gamma_i\left(\nabla_{q_i}b_{ij}\right)\prod\limits_{l\in\mathcal{N}_i^f, l\neq j}b_{il}\prod\limits_{k\in\mathcal{N}_i\cup\mathcal{M}_i}B_{ik} + O\left(b_{ij}\right)}{k(\gamma_i^k + \beta_i)^{\frac{1}{k}+1}}. \tag{3–11}$$

Note that the gradient of b_{ij} w.r.t. q_i can be written as

$$\nabla_{q_i}b_{ij} = \begin{cases} 0, & d_{ij} < R_s - \delta_2 \text{ or } d_{ij} > R_s, \\ -\frac{2(d_{ij}+\delta_2-R_s)(q_i-q_j)}{\delta_2^2 d_{ij}}, & R_s - \delta_2 \leq d_{ij} < R_s, \end{cases} \tag{3–12}$$

where γ_i, b_{il}, B_{ik}, k, δ_2, and R_s are positive constants. Thus, using (3–11) and (3–12), the velocity of agent i (i.e., $\dot{q}_i = -\Gamma\nabla_{q_i}\varphi_i$) points in the direction of $q_j - q_i$, which forces agent i to move toward agent j.

Case 2. Suppose several agents j_1, j_2, $\ldots$, $j_s \in \mathcal{N}_i^f$ are near the boundary of the feedback region of agent $i \in \mathcal{V}_f$. That is, d_{ij_m} is near R_s for each $m = 1, 2, \ldots, s$. For this case, $\nabla_{q_i}\varphi_i = \dfrac{-\gamma_i\sum\limits_{m}\prod\limits_{l\in\mathcal{N}_i^f, l\neq j_m}b_{il}\prod\limits_{k\in\mathcal{N}_i\cup\mathcal{M}_i}B_{ik}\left(\nabla_{q_i}b_{ij_m}\right)}{k(\gamma_i^k+\beta_i)^{\frac{1}{k}+1}} + O\left(\prod\limits_{m}b_{ij_m}\right)$. The first term in $\nabla_{q_i}\varphi_i$ tends to zero; however, since the b_{ij_m} terms are quadratic near R_s, the order of the zero contributed by the first term is one degree less than $O\left(\prod\limits_{m}b_{ij_m}\right)$, so the first term dominates as each $d_{ij_m} \to R_s$. Hence $\dot{q}_i = -\Gamma\nabla_{q_i}\varphi_i$ is approximately a linear combination of the vectors $q_{j_1} - q_i, q_{j_2} - q_i, \ldots, q_{j_s} - q_i$, where the largest contribution comes from those j_m closest to the feedback boundary. Thus, node i moves almost toward j_m resulting in a largest decrease in d_{ij_m}, so network connectivity can be maintained.

---

[1] Here the standard notation $f = O(g)$ as $x \to a$ is being used. By this it is meant that $|f(x)| < C|g(x)|$ for some constant C when x is sufficiently close to a. When $f = O(g)$ and $h = O(g)$ (with possibly different constants) the sum $f + h = O(g)$. It is understood that different constants might be used, but in each case the growth or decay behavior is characterized by g as x gets close to a.

Case 3. Consider a agent $i \in \mathcal{V}_u$ (or more than one agent in the set of $\mathcal{V}_u$). The controller will be $u_i = 0$ based on (3–9). Since both agent i and its neighbor $j \in \mathcal{N}_i^f$ are in the undirected graph, agent j can't receive feedback from agent i, so $j \in \mathcal{V}_u$, thus $u_j = 0$. Since both i, j agents have no control input, the distance between them remains the same (cf. the STOP model in [67]).

By Assumption 3.3, $\mathcal{N}_i^f \subset \mathcal{N}_i^s(t_0)$, $i \in \mathcal{V}$. Furthermore, from *Case 1-Case 3*, the decentralized hybrid control policy in (3–9) ensures the distances between agent $i \in \mathcal{V}$ and its formation neighbors $j \in \mathcal{N}_i^f$ never increase under intermittent feedback conditions. As a result, the formation neighbors $j \in \mathcal{N}_i^f$ remain inside the feedback region of agent i for all time. Specifically,

$$d_{ij} < R_s, \ j \in \mathcal{N}_i^f, \ i \in \mathcal{V}, \ \forall t \geq 0. \tag{3–13}$$

$\square$

3.4 Convergence Analysis

To prove convergence of the agents to the desired formation, an invariance principle for switched systems is applied to a common Lyapunov function candidate $V : \mathbb{R}^{2N} \to \mathbb{R}$ given by

$$V \triangleq \sum_{i=1}^{N} \varphi_i, \tag{3–14}$$

where V reaches its minimum value of 0 if the desired formation is achieved. Since the hybrid controller designed in (3–9) is discontinuous, the following theorem is introduced to facilitate the subsequent analysis.

Before proving the main theorem, the following lemma is developed to facilitate the subsequent analysis.

Lemma 3.2. *The inequality*

$$\sum_{i \in \mathcal{V}_f} \left(4\underline{\beta} \left\| \sum_{j \in \mathcal{N}_i^f} (q_i - q_j - c_{ij}) \right\|^2 - \rho_i \right) > 0 \tag{3–15}$$

52

is a sufficient condition for

$$\sum_{i \in \mathcal{V}_f} \left(\Gamma \left(\sum_{j=1}^{N} \nabla_{q_i} \varphi_j \right)^T \nabla_{q_i} \varphi_i \right) > 0, \tag{3–16}$$

where $\underline{\beta} \in \mathbb{R}_{>0}$ is a positive constant[2] defined as $\underline{\beta} \triangleq \min\limits_{j \in \mathcal{N}_i^f, i \in \mathcal{V}} \beta_i \beta_j$, and $\rho_i \in \mathbb{R}_{\geq 0}$ is a positive function defined as

$$\rho_i \triangleq \frac{\rho_{1,i}}{2k} + \frac{\rho_{2,i}}{2k^2},$$

where $\rho_{1,i}, \rho_{2,i} \in \mathbb{R}_{\geq 0}$ are functions defined as $\rho_{1,i} \triangleq c_{1,i}\gamma_i + c_{2,i}\gamma_i^2 + c_{3,i} \left(\sum_{k=1}^{N} \gamma_k \right)^2$ and $\rho_{2,i} \triangleq c_{4,i}\gamma_i^2 + c_{5,i} \left(\sum_{k=1}^{N} \gamma_k \right)^2$, where $c_{p,i} \in \mathbb{R}, \ p = 1, 2, \ldots 5$, are positive constants.

The proof for Lemma 3.2 is given in the Appendix A. The variables $\rho_{1,i}$ and $\rho_{2,i}$ can be upper bounded by constants since γ_i can be bounded above by the constant

$$\gamma_i \leq \left| \mathcal{N}_i^f \right| (R_s + \bar{c}_i)^2, \tag{3–17}$$

where $\bar{c}_i = \max\limits_{j \in \mathcal{N}_i^f} \|c_{ij}\|$. The proof of (3–17) can be determined by using (3–13), which implies $\|q_i - q_j\| \leq R_s, \ j \in \mathcal{N}_i^f$. Using the triangle inequality yields $\|q_i - q_j - c_{ij}\| \leq \|q_i - q_j\| + \|c_{ij}\| \leq R_s + \|c_{ij}\|$, which implies $\gamma_i = \sum\limits_{j \in \mathcal{N}_i^f} \|q_i - q_j - c_{ij}\|^2 \leq \sum\limits_{j \in \mathcal{N}_i^f} (R_s + \|c_{ij}\|)^2$, which proves (3–17).

Based on Lemma 3.2, the main result of this chapter is provided as follows.

Theorem 3.1. *Given (3–9), the maximum relative position errors of any two formation neighbors of the network system in (3–1) converges to*

$$\max_{j \in \mathcal{N}_i^f} \|q_i - q_j - c_{ij}\| \leq \sqrt{\frac{c_{\max}}{N_{\min}}}, \ i \in \mathcal{V} \tag{3–18}$$

---

[2] $\beta_i, \beta_j \neq 0$ is due to the fact that no open set of initial solutions can be attracted to the maxima of φ_i (i.e., $\beta_i = 0$) along the negative gradient motion $-\frac{\partial \varphi_i}{\partial q_i}$ [97], so that $\underline{\beta} \neq 0$ holds.

provided that the adjustable gain k in (3–5) is selected sufficiently large, and for each agent i there exists a time interval $[t_{k_i}, t_{k_i+1}) \subset [t_k, t_{k+n})$ for which agent i receives feedback from all its formation neighbors, i.e. $\underset{t \in [t_k, t_{k+n})}{\cup} \mathcal{V}_f = \mathcal{V}$, where $N_{\min} \triangleq \underset{i \in \mathcal{V}}{\min} \left| \mathcal{N}_i^f \right|$, where $|\cdot|$ denotes set cardinality for a set argument, $c_{\max} \in \mathbb{R}_{>0}$ is defined as $c_{\max} \triangleq \sqrt{\frac{[(N+1)R_s]^2}{\underline{\beta}}} \rho_{\max}$, $\rho_{\max} \in \mathbb{R}_{\geq 0}$ is a positive constant defined as $\rho_{\max} \triangleq \underset{i \in \mathcal{V}}{\max} \rho_i$ and can be decreased by increasing the control gain k in (3–5), and $n \in \mathbb{N}$ is a finite positive integer.

Proof. Consider the common Lyapunov function candidate V defined in (3–14), where V can be minimized at the critical points as shown in [54], and V reaches its minimum value of 0 when the desired formation is achieved. The time-derivative of V exists almost everywhere (a.e.), i.e., $\dot{V} \overset{a.e.}{\in} \dot{\tilde{V}}$, where $\dot{\tilde{V}}$ is the generalized time derivative of V defined as [98]

$$\dot{\tilde{V}} \triangleq \underset{\xi \in \partial V}{\cap} \xi^T K[\dot{q}] \tag{3–19}$$

where $K[\cdot]$ is the Filippov set. The finite sums property of the generalized gradient defined in [99] gives

$$\partial V \subset \left[\partial_{q_1} V^T, \, \partial_{q_2} V^T, \, \ldots, \, \partial_{q_N} V^T \right]^T. \tag{3–20}$$

Using (3–19) and (3–20), the generalized time derivative of V in (3–19) can be expressed as

$$\dot{\tilde{V}} \subset \sum_{i \in \mathcal{V}} \left(\underset{\xi_i}{\cap} \xi_i^T K[\dot{q}_i] \right). \tag{3–21}$$

where $\xi_i \in \partial_{q_i} V$. To turn the generalized gradient into the gradient, the points at which V is not differentiable and Lebesgue measure zero need to be considered. From the inequality in (3–13), d_{ij} never takes on the value $d_{ij} = R_s$, $j \in \mathcal{N}_i^f$, $i \in \mathcal{V}$, at the nonsmooth point of b_{ij}, so b_{ij} is differentiable w.r.t. q_i along the solution of the closed-loop system. Since B_{ik} and γ_i are differentiable functions, V is differentiable w.r.t. q_i along the solution of the closed-loop system for $i \in \mathcal{V}$. Therefore, the generalized

gradient can be expressed as

$$\partial_{q_i} V = \{\nabla_{q_i} V\}, \, i \in \mathcal{V}. \tag{3–22}$$

Based on (3–22), (3–21) can be rewritten as

$$\dot{\tilde{V}} \subset \sum_{i \in \mathcal{V}} \left(\nabla_{q_i} V^T K \left[\dot{q}_i \right] \right). \tag{3–23}$$

By segregating $\mathcal{V}$ into the sets, $\mathcal{V}_f$ and $\mathcal{V}_u$, (3–23) can be rewritten as

$$\dot{\tilde{V}} \subset \sum_{i \in \mathcal{V}_f} \left(\nabla_{q_i} V^T K \left[\dot{q}_i \right] \right) + \sum_{i \in \mathcal{V}_u} \left(\nabla_{q_i} V^T K \left[\dot{q}_i \right] \right). \tag{3–24}$$

From Assumption 3.1, the switching graph G_σ is invariant for $t \in [t_k, \, t_{k+1})$, so the set $\mathcal{V}_f$ is also invariant during that time period. Based on the hybrid control scheme in (3–9), the second term on the RHS of (3–24) will be zero, therefore,

$$\dot{\tilde{V}} \subset \sum_{i \in \mathcal{V}_f} \left(\nabla_{q_i} V^T K \left[\dot{q}_i \right] \right), \, t \in [t_k, \, t_{k+1}). \tag{3–25}$$

In addition, by the definition of $K \left[\cdot \right]$ in [100], the hybrid controller in (3–9) can be expressed as

$$K \left[\dot{q}_i \right] \subset \overline{co} \left\{ -\Gamma \nabla_{q_i} \varphi_i, \begin{bmatrix} 0 \\ 0 \end{bmatrix} \right\}, \tag{3–26}$$

where $\overline{co}$ denotes convex closure. Also based on Assumption 3.1, the switching time instance is Lebesgue measure zero, so (3–26) can be further expressed as $K \left[\dot{q}_i \right] \subset \{-\Gamma \nabla_{q_i} \varphi_i\}$. Thus, by using the gradient of V, (3–19) and (3–25) can be used to conclude that

$$\dot{V} \overset{a.e.}{\leq} - \sum_{i \in \mathcal{V}_f} \left(\Gamma \left(\sum_{j=1}^{N} \nabla_{q_i} \varphi_j \right)^T \nabla_{q_i} \varphi_i \right), \tag{3–27}$$

where $t \in [t_n, t_{n+1})$, $n \in \mathbb{N}$. Based on Lemma 3.2, an equivalent way to prove $\dot{V} \overset{a.e.}{<} 0$ is to show

$$\sum_{i \in \mathcal{V}_f} \left(4\underline{\beta} \left\| \sum_{j \in \mathcal{N}_i^f} (q_i - q_j - c_{ij}) \right\|^2 - \rho_i \right) > 0. \tag{3–28}$$

To develop a further sufficient condition for (3–28), we exploit the facts from [101] that

$\nabla_{q_i} \gamma_i = 2 \sum\limits_{j \in \mathcal{N}_i^f} (q_i - q_j - c_{ij})$ and

$$\|\nabla_{q_i} \gamma_i\| \geq \frac{\gamma_i}{(N+1)R_s}. \tag{3–29}$$

Then, from (3–13) and (3–29), a sufficient condition for (3–28) can be developed as

$$\sum_{i \in \mathcal{V}_f} \left(\beta \frac{\gamma_i^2}{[(N+1)R_s]^2} - \rho_i \right) > 0. \tag{3–30}$$

By solving (3–30) for γ_i and using (3–6), a further sufficient condition for (3–28) is

$$\sum_{j \in \mathcal{N}_i^f} \|q_i - q_j - c_{ij}\|^2 > c_{\max}, \ i \in \mathcal{V}_f, \tag{3–31}$$

Recall that V in (3–14) is a common Lyapunov function provided that (3–31) holds. Additionally, (3–31) can be extended to global (i.e., $i \in \mathcal{V}$) formation configuration convergence if the switching signal σ switches so that

$$\bigcup_{t \in [t_k, t_{k+n})} \mathcal{V}_f = \mathcal{V}, \tag{3–32}$$

for a finite positive integer $n \in \mathbb{N}$. Based on (3–31), the ultimate maximum formation error for the entire hybrid system can be expressed as (3–18), which can be made arbitrarily small for an arbitrary larger k. □

3.5 Simulation

To illustrate the performance of the developed hybrid controller, a simulation was performed with six dynamic agents and three obstacles. Six quadrotor UAVs were simulated based on a high fidelity dynamic model of each quadrotor that was encoded in the

Robot Operating System (ROS) [102] using the Gazebo [103] simulation environment. Specifically, a full 6 degree of freedom (DOF) UAV model with gravity, friction, contact forces, aerodynamics, motor dynamics and GPS sensors was simulated. Details of the simulation model and implementation code are given in [104]. The feedback from neighboring agents are from GPS sensors that were used to sense relative position between agents. The sensing link was modeled by a Bernoulli distribution with success probability of 0.5. At a rate of 1 Hz, a new network topology was generated from the distribution for every pair of neighboring agents, to determine if the pair could sense each other. Simulation parameters were set as $R_s = 25$, $\delta_1 = 5$, $\delta_2 = 5$, $k = 0.1$, and $\Gamma = 500$. Initially the agents are randomly located within the sensing region of their formation neighbors as shown in Fig. 3-1, and the final formation configuration is shown in Fig. 3-2. Note that positions of the six agents in Fig. 3-2 represent the relative positions of the desired formation configuration and do not necessarily represent the absolute locations of the six agents when the formation is achieved.
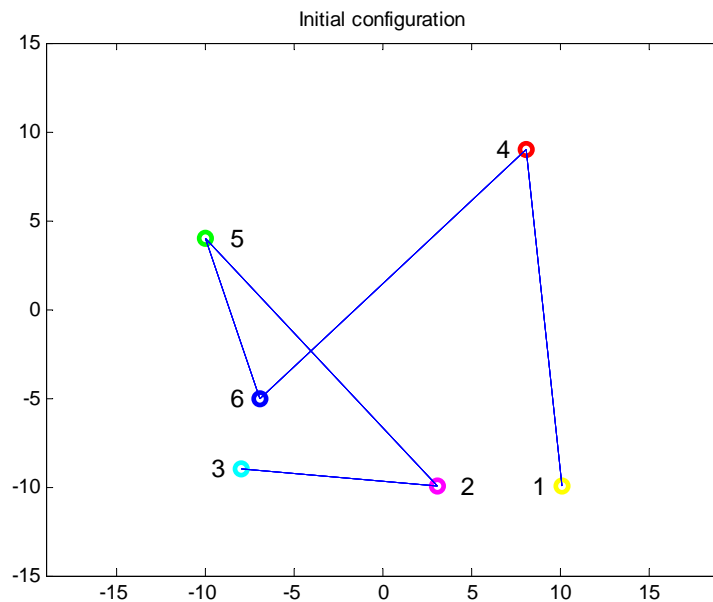
Figure 3-1. Initial configuration of six agents, which are connected (inside the feedback zones).
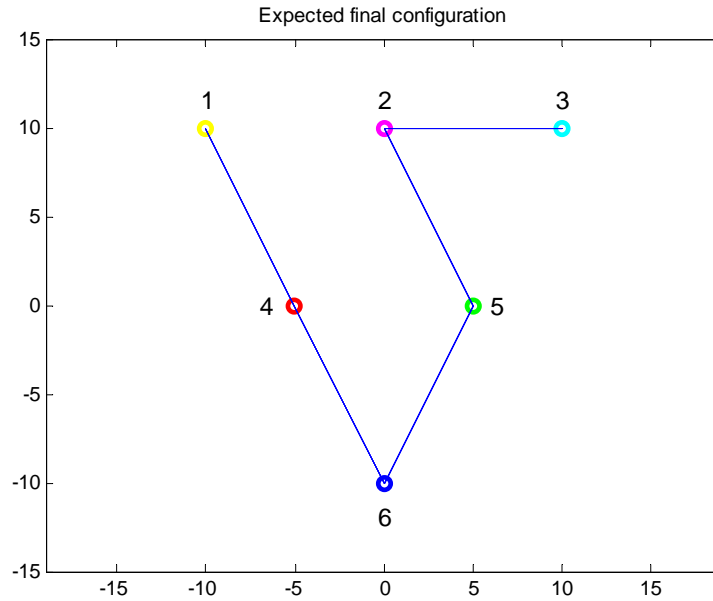
Figure 3-2. Desired formation configuration of six agents with network connectivity maintenance.

Fig. 3-3 depicts the trajectories of all six agents from the initial configuration to the final configuration denoted by circles, in the presence of three static obstacles denoted by squares. The figure also illustrates that the six agents can avoid collisions with other agents and the stationary obstacles as they move in the space. Moreover, they asymptotically achieve a goal formation under an switching graph that satisfies (3–32).
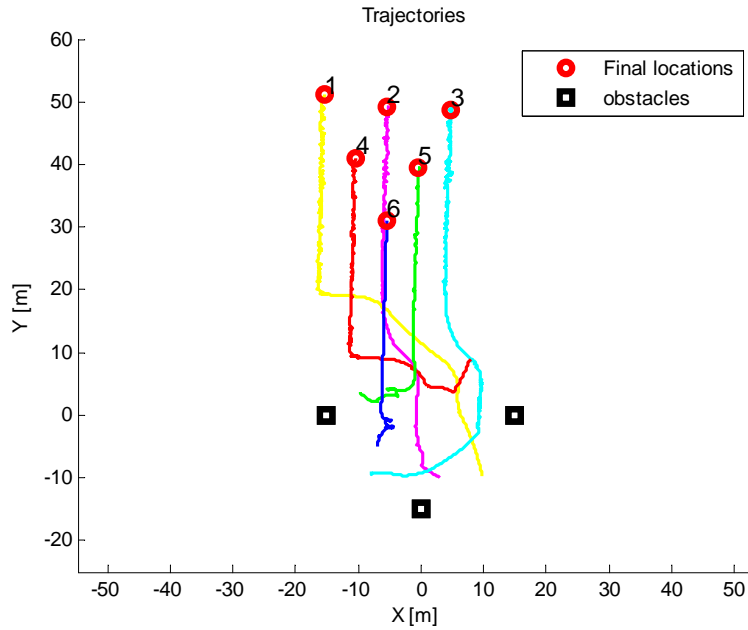
Figure 3-3. Trajectories of dynamic agents achieving formation configuration.

As indicated in Fig. 3-4, d_{ij} can increase as agents move. However, these distances always remain smaller than the feedback range R_s (i.e., remain connected). Recall that the relative distances in the goal formations are given by $\|c_{14}\| = \|c_{25}\| = \|c_{46}\| = \|c_{56}\| = 5\sqrt{5}$, and $\|c_{23}\| = 10$. Fig. 3-4 indicates that the final distances approximate these values, and the position errors remain sufficiently small.
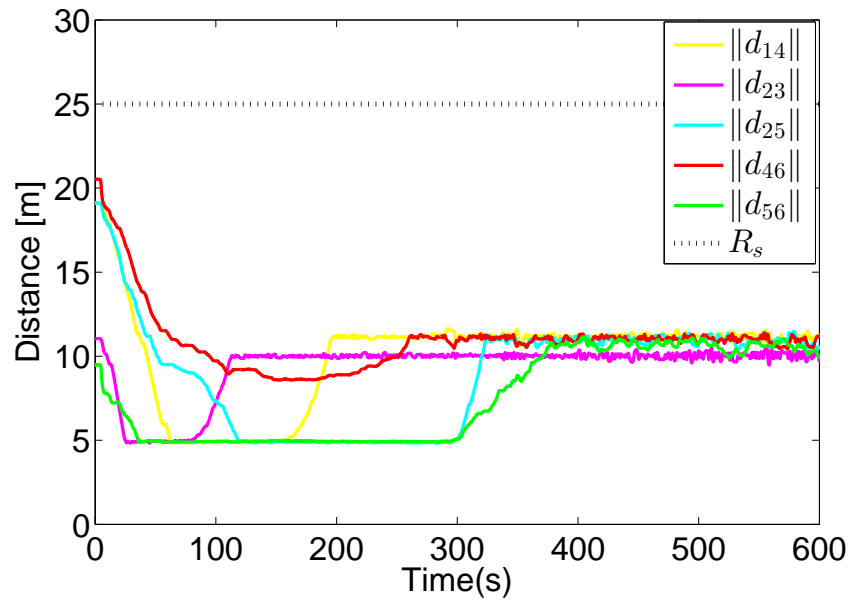
Figure 3-4. The inter-agent distances d_{ij} are always smaller than R_s

The intermittent switching signals of all links are depicted in Fig. 3-5, where the y-axes represent on-off signals. Each randomly generated signal is independent, and has an arbitrary switching sequence that satisfies Assumption 3.1.
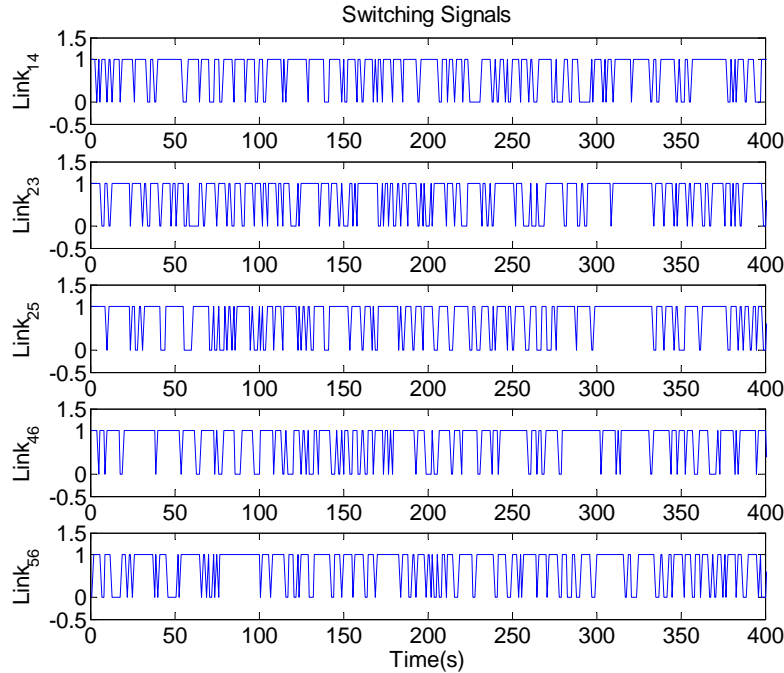
Figure 3-5. Statuses of sensing links between neighboring agents, where 1 represents sensing and 0 represents loss of sensing.

3.6   Conclusion

A hybrid controller is developed to achieve convergence of a network formation using only local intermittent feedback. At the same time, network connectivity is maintained and collisions between static and dynamic obstacles are avoided. A common Lyapunov function is used to prove convergence under an arbitrary switching sequence. Moreover, the entire formation configuration converges globally, if the switching signal satisfies a sufficient switching condition. The neighborhood of convergence can be made arbitrarily small with sufficiently large gains. Moreover, Zeno behavior is not allowed based on the developed switching conditions.

Effectiveness of the developed controller is verified by performing a simulation of six quadrotor UAVs in ROS and the Gazebo simulation environment. The UAVs achieve formation configuration with sufficient accuracy, and the formation neighbors remain within the feedback zone without obstacle collision.

61

Future efforts will focus on relaxing the assumption that the critical points introduced by the navigation function are isolated in the space of configurations.

CHAPTER 4
EVENT-TRIGGERED CONTROL OF MULTI-AGENT SYSTEMS UNDER TIME-VARYING NETWORK TOPOLOGIES

In this chapter, a decentralized controller that uses event-triggered scheduling is developed for the leader-follower consensus problem under fixed and switching communication topologies. To eliminate continuous inter-agent communication, state estimates of neighboring agents are designed for control feedback and are updated by scheduled communication to reset growing estimate errors. Since the estimate error is associated with a neighbor's control input, when the true state is unknown until the next communication, the state estimate is updated to avoid system instability. The communication event times are based on an event-triggered approach, which considers the interplay between system performance and minimal communication bandwidth and requires no communication for event detection. Since the control strategy produces switched dynamics, analysis is provided to show that Zeno behavior is avoided by developing a positive constant lower bound on the minimum inter-event interval. A Lyapunov-based convergence analysis is also provided to indicate asymptotic convergence of the developed control methodology. Simulation results are provided to demonstrate the effectiveness of the developed control strategy.

4.1 Preliminaries and Problem Statement

4.1.1 Algebraic Graph Theory Preliminaries

A directed graph $\bar{\mathcal{G}}$ consists of a finite node set $\mathcal{V}$ and an edge set $\mathcal{E}$, where $\mathcal{E} \subseteq (\mathcal{V} \times \mathcal{V})$ is a set of paired nodes. An edge, denoted as (j, i), implies that node i can obtain information from node j, but not vice versa. On the contrary, the graph $\mathcal{G}$ is undirected if $(i, j) \in \mathcal{E}$ implies $(j, i) \in \mathcal{E}$, and vice versa. The neighbor set of agent i is defined as $\mathcal{N}_i \triangleq \{j \in \mathcal{V} \mid (j, i) \in \mathcal{E}, j \neq i\}$.

A directed path is a sequence of edges in a graph. An undirected path of the undirected graph is defined analogously. An undirected graph is connected if there exists an undirected path between any two distinct nodes in the graph. An adjacency

matrix $\mathcal{A} = [a_{ij}] \in \mathbb{R}^{N \times N}$ of the directed graph is given by $a_{ij} = 1$ if $(j,\, i) \in \mathcal{E}$, and $a_{ij} = 0$ otherwise. For the undirected graph, $a_{ij} = a_{ji}$. For both the directed and undirected graph, $a_{ii} = 0$ holds, and furthermore, it is assumed that $a_{ij} = 1$ if $(j,\, i) \in \mathcal{E}$. The Laplacian matrix of the graph $\mathcal{G}$ is defined as $L = [l_{ij}] \in \mathbb{R}^{N \times N}$, where $l_{ii} = \sum_{j \neq i} a_{ij}$ and $l_{ij} = -a_{ij}$, where $i \neq j$.

4.1.2 Dynamics

Consider N follower agents, defined as $\mathcal{V} \triangleq \{1,\, 2, \cdots,\, N\}$, with a network topology modeled by an undirected graph $\mathcal{G} = (\mathcal{V},\, \mathcal{E})$. Let $\bar{\mathcal{G}}$ denote a directed graph with the node set $\mathcal{V} \cup \{0\}$ and the edge set that contains all edges in $\mathcal{E}$ and the edges connecting leader agent 0 and follower agent $j \in \mathcal{V}$. The dynamics of the followers and the leader are described by

$$\dot{x}_0 = A x_0, \tag{4–1}$$

$$\dot{x}_i = A x_i + B u_i, \tag{4–2}$$

where $x_i \in \mathbb{R}^n$ and $u_i \in \mathbb{R}^m$ denote the state and control input of follower agent $i \in \mathcal{V}$, respectively, $x_0 \in \mathbb{R}^n$ denotes the leader's state, $A \in \mathbb{R}^{n \times n}$ is a state matrix, and $B \in \mathbb{R}^{n \times m}$ is a full column rank matrix.

Assumption 4.1. The dynamics of the follower agents are controllable, i.e., the pair $(A,\, B)$ is stabilizable.

Definition 4.1. A directed graph is connected if each follower has a directed path from the leader.

4.1.3 Conventional Approach and Control Objective

A decentralized controller for the system in (4–1) and (4–2) can be developed using conventional continuous feedback such as in [74], for example, as

$$u_i = K \sum_{j \in \mathcal{N}_i} (x_j - x_i) + K d_i (x_0 - x_i),\ i \in \mathcal{V}, \tag{4–3}$$

where $K \in \mathbb{R}^{m \times n}$ is the control gain matrix designed in the subsequent analysis, and $d_i = 1$ if agent $i \in \mathcal{V}$ is connected to the leader, $d_i = 0$ otherwise. Note that this control implementation requires continuous state feedback from the neighboring agents. To reduce inter-agent communication, a control approach which requires intermittent communication will be developed such that leader-follower consensus is still achieved. That is, the network system described in (4–1) and (4–2) satisfies

$$\|\varepsilon_i\| \to 0 \quad \text{as} \quad t \to \infty, \quad i \in \mathcal{V}, \tag{4–4}$$

where $\varepsilon_i \triangleq x_i - x_0 \in \mathbb{R}^n$ represents the leader-follower consensus error for agent i.

4.2 Leader-Follower Consensus under Fixed Topologies

Consider N follower agents with a fixed network topology that satisfies the following two assumptions.

Assumption 4.2. The graph $\bar{\mathcal{G}}$ is connected.

Assumption 4.3. The followers that are connected to the leader can continuously receive information from the leader.

Based on Assumption 4.2, the matrix $H \in \mathbb{R}^{N \times N}$ defined as $H = L + D$ is positive definite [105], where $D \in \mathbb{R}^{N \times N}$ is defined as $D \triangleq \operatorname{diag}(d_1, d_2, \ldots, d_N)$. Based on Assumption 4.1, there exists a symmetric positive definite matrix $P \in \mathbb{R}^{n \times n}$ that satisfies the following Riccati inequality

$$PA + A^T P - 2\delta_{\min} PBB^T P + \delta_{\min} I_n < 0, \tag{4–5}$$

so the control gain in (4–3) can be designed as

$$K = B^T P, \tag{4–6}$$

where $\delta_{\min} \in \mathbb{R}_{>0}$ denotes the minimum eigenvalue of H and is a positive constant based on Assumption 4.2 and [105], and I is an identity matrix with denoted dimension.

To eliminate the need for continuous communication while achieving the control objective, an event-triggered based decentralized control approach is developed.

4.2.1 Controller Design

Based on the continuous controller in (4–3) and subsequent convergence analysis, a decentralized event-triggered controller for agent $i \in \mathcal{V}$ is designed as

$$u_i = K\hat{z}_i, \tag{4–7}$$

$$\hat{z}_i = \sum_{j \in \mathcal{N}_i} (\hat{x}_j - \hat{x}_i) + d_i(x_0 - \hat{x}_i) \tag{4–8}$$

where K is the control gain defined in (4–6). In (4–8), the computation of $\hat{z}_i$ only requires the estimates of agent i and its neighboring followers' state estimate (i.e., $\hat{x}_{j \in \mathcal{N}_i}$), instead of using their true states $x_{j \in \mathcal{N}_i}$ via continuous communication. When the leader is a neighbor, the true state x_0 is used since the leader state is available according to Assumption 4.3. The estimate $\hat{x}_j$ in (4–8) evolves according to the dynamics

$$\dot{\hat{x}}_j(t) = A\hat{x}_j(t), \, j \in \mathcal{N}_i, \, t \in \left[t_k^j, \, t_{k+1}^j\right), \tag{4–9}$$

$$\hat{x}_j\left(t_k^j\right) = x_j\left(t_k^j\right), \tag{4–10}$$

for $k = 0, 1, 2\ldots$, where $\hat{x}_j$ flows along the leader dynamics during $t \in \left[t_k^j, \, t_{k+1}^j\right)$ and is updated via x_j communicated from neighboring agent j at its discrete times t_k^j, for $j \in \mathcal{N}_i$, where t_k^j is the event-triggered time described in Section 4.2.3. Although agent i does not communicate the estimate $\hat{x}_i$, agent i maintains $\hat{x}_i$ for implementation in (4–8). The estimate $\hat{x}_i$ is updated continuously with the dynamics in (4–9) and discretely at time instances described in (4–10). Therefore, u_i is a piecewise continuous signal, where communication is required when state information is transmitted to, or received from, neighboring agents for estimate updates; otherwise, u_i flows continuously during the inter-event intervals.

4.2.2 Dynamics of Estimate Error

Since x_i follows different dynamics from the estimate $\hat{x}_i$ computed by its neighbors, an estimate error $e_i \in \mathbb{R}^n$ characterizing this mismatch is defined as

$$e_i \triangleq \hat{x}_i - x_i, \ i \in \mathcal{V}, t \in \left[t_k^i, t_{k+1}^i\right), \tag{4–11}$$

where e_i is reset to 0 at the event time t_k^i, $k = 0, 1, \ldots$, due to the estimate updates. Although x_i and $\hat{x}_i$ are both known for agent i; using $\hat{x}_i$ enables agent i to judge how farther signal $\hat{x}_i$, used by neighbors, is away from its true state x_i. Using (4–2), (4–7), and (4–9), the stack form of the time-derivative of (4–11) can be expressed as

$$\dot{e} = (I_N \otimes A)\, e + (H \otimes BK)\, \varepsilon + (H \otimes BK)\, e, \tag{4–12}$$

where $e \in \mathbb{R}^{nN}$ denotes $e \triangleq \left[e_1^T, e_2^T, \ldots, e_N^T\right]^T$, $\otimes$ denotes the Kronecker product, and $\varepsilon \in \mathbb{R}^{nN}$, defined as $\varepsilon \triangleq \left[\varepsilon_1^T, \varepsilon_2^T, \ldots, \varepsilon_N^T\right]^T$, is a stack form of ε_i.

4.2.3 Event-triggered Communication Mechanism

Fig. 4-1 depicts how the communication between neighboring agents proceeds during triggered events.
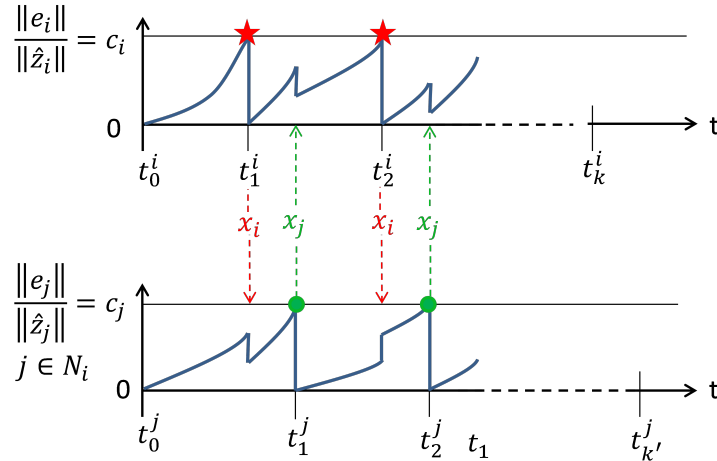
Figure 4-1. Inter-agent communication mechanism under an event-triggered approach. The stars and dots represent instances when decentralized triggering conditions are satisfied, and the triggered agents communicate their states over the network to update neighbors' estimates.

In Fig. 4-1, $\frac{\|e_i\|}{\|\hat{z}_i\|}$ is a decentralized, non-negative, and piecewise continuous signal used to verify the triggering condition. The detailed design of the trigger condition is shown in Section 4.2.5. The dots represent the event-triggered time t_k^i when $\frac{\|e_i\|}{\|\hat{z}_i\|}$ reaches a constant c_i, designed in the subsequent analysis. At t_k^i, x_i is communicated over the network to update the estimate $\hat{x}_i$, used by each neighboring agent $j \in \mathcal{N}_i$. Additionally, $\frac{\|e_i\|}{\|\hat{z}_i\|}$ is reset to zero at t_k^i since the updated estimate has no estimate error. Similarly, at neighbor agent j's event time t_k^j, x_j is communicated over the network to update the estimate $\hat{x}_j$. Since $\|\hat{z}_i\|$ is a decentralized and estimate-based function, verification of the triggering conditions requires no neighbor state information, and hence no communication is required during any inter-event interval (e.g., $[t_1^i, t_1^j)$, $[t_1^j, t_2^i)$, $[t_2^i, t_2^j)$, as in Fig. 4-1).

4.2.4 Closed-Loop Error System

Using (4–11), a non-implementable form (to facilitate the subsequent analysis) of (4–7) can be expressed as

$$u_i = K \sum_{j \in \mathcal{N}_i} [(x_j - x_i) + (e_j - e_i)] + K d_i (x_0 - x_i) - K d_i e_i. \tag{4–13}$$

Substituting (4–13) into the open-loop dynamics in (4–2) and using the definition in (4–4) yields a stack form of the closed-loop error system

$$\dot{\varepsilon} = (I_N \otimes A) \varepsilon - (H \otimes BK) \varepsilon - (H \otimes BK) e. \tag{4–14}$$

To facilitate the subsequent analysis, a relation between ε and $\hat{z}$ is developed, where $\hat{z} \triangleq [\hat{z}_1, \hat{z}_2, \ldots, \hat{z}_N]^T \in \mathbb{R}^{nN}$ represents the stack form of $\hat{z}_i$

$$\hat{z} \triangleq (H \otimes I_n) [(1_N \otimes x_0) - \hat{x}], \tag{4–15}$$

where $\hat{x} \triangleq [\hat{x}_1, \hat{x}_2, \ldots, \hat{x}_N]^T \in \mathbb{R}^{nN}$, and 1_N is the ones vector with denoted dimension. Using the relation

$$\varepsilon_i = x_i - x_0 = (\hat{x}_i - e_i) - x_0,$$

the useful expression

$$\hat{x} - (1_N \otimes x_0) = \varepsilon + e \tag{4–16}$$

can be obtained. Combining (4–15) and (4–16) yields

$$\varepsilon = - \left(H^{-1} \otimes I_n \right) \hat{z} - e, \tag{4–17}$$

where $\hat{z}$ is governed by the dynamics

$$\dot{\hat{z}} = (I_N \otimes A) \hat{z}, \tag{4–18}$$

where (4–1) and (4–9) were used.

4.2.5 Convergence Analysis

In this section, leader-follower consensus with the event-triggered controller designed in (4–7) is examined using Lyapunov-based analysis. To facilitate the subsequent convergence analysis, the event time t_k^i is explicitly defined as below.

Definition 4.2. An event time t_k^i for the follower agent is defined as

$$t_k^i \triangleq \inf \left\{ t > t_{k-1}^i \mid f_i(t) = 0 \right\}, \ i \in \mathcal{V} \tag{4–19}$$

for $k = 0, 1, 2 \ldots$, where $f_i(\cdot)$, denoted as $f_i(e_i(\cdot), \hat{z}_i(\cdot))$, is a decentralized trigger function

$$f_i(e_i, \hat{z}_i) \triangleq \|e_i\| - \sqrt{\frac{\sigma_i \left(k_1 - \frac{k_3}{\beta} \right)}{k_2 + k_3 \beta}} \|\hat{z}_i\|, \tag{4–20}$$

where $\sigma_i \in \mathbb{R}_{>0}$ satisfying $0 < \sigma_i < 1$ provides flexibility in real-time scheduling, and $\beta \in \mathbb{R}_{>0}$ satisfies

$$\beta > \frac{k_3}{k_1}, \tag{4–21}$$

where k_i, $i = 1,\, 2,\, 3$, are positive constants defined as

$$k_1 \triangleq \delta_1 S_{\min}\left(H^{-2}\right)$$

$$k_2 \triangleq S_{\min}\left(H \otimes \left(2PBB^T P\right)\right) - \delta_1$$

$$k_3 \triangleq S_{\min}\left(I_N \otimes \left(2PBB^T P\right) - H^{-1} \otimes 2\delta_1 I_n\right),$$

where $k_2 \neq 0$ and $k_3 \neq 0$, $\delta_1 \in \mathbb{R}_{>0}$ satisfies $0 < \delta_1 < \delta_{\min}$, and $S_{\min}\left(\cdot\right)$ denotes the minimum singular value of a matrix argument.

Theorem 4.1. *The controller designed in (4–7) ensures that the network system achieves asymptotic leader-follower consensus in the sense that*

$$x_i - x_0 \to 0 \quad \text{as} \quad t \to \infty, \quad i \in \mathcal{V} \tag{4–22}$$

provided that the estimate $\hat{x}_i$ in (4–7) is updated at t_k^i defined in Definition 4.2.

Proof. Consider a Lyapunov function candidate $V : \mathbb{R}^{nN} \to \mathbb{R}$ as

$$V \triangleq \varepsilon^T \left(I_N \otimes P\right) \varepsilon, \tag{4–23}$$

where P is a symmetric positive definite matrix satisfying (4–5). Using (4–6) and (4–14), the time derivative of (4–14) can be expressed as

$$\dot{V} = \varepsilon^T \left[I_N \otimes \left(PA + A^T P\right) - H \otimes \left(2PBB^T P\right)\right] \varepsilon - e^T \left[H \otimes \left(2PBB^T P\right)\right] \varepsilon. \tag{4–24}$$

Since H is symmetric and positive definite, (4–5) can be used to upper bound (4–24) as

$$\dot{V} \leq -\delta_{\min} \varepsilon^T \varepsilon - e^T \left[H \otimes \left(2PBB^T P\right)\right] \varepsilon. \tag{4–25}$$

Using (4–17), (4–25) can be upper bounded by

$$\dot{V} \leq - \delta_1 \hat{z}^T \left(H^{-2} \otimes I_n\right) \hat{z} - \delta_1 e^T e + 2\delta_1 e^T \left(H^{-1} \otimes I_n\right) \hat{z} - e^T \left[I_N \otimes \left(2PBB^T P\right)\right] \hat{z}$$
$$+ e^T \left[H \otimes \left(2PBB^T P\right)\right] e - \delta_2 \varepsilon^T \varepsilon, \tag{4–26}$$

where $\delta_2 \in \mathbb{R}_{>0}$ satisfies $\delta_{\min} = \delta_1 + \delta_2$. By using the inequality $x^T y \leq \frac{\beta}{2} \|x\|^2 + \frac{1}{2\beta} \|y\|^2$,
(4–26) can be upper bounded by

$$
\begin{aligned}
\dot{V} \leq & - k_1 \|\hat{z}\|^2 + 2k_3 \left(\frac{\beta}{2} \|e\|^2 + \frac{1}{2\beta} \|\hat{z}\|^2 \right) + k_2 \|e\|^2 - \delta_2 \varepsilon^T \varepsilon \\
\leq & - \sum_{i \in \mathcal{V}} \left[\left(k_1 - \frac{k_3}{\beta} \right) \|\hat{z}_i\|^2 - (k_2 + k_3 \beta) \|e_i\|^2 \right] - \delta_2 \varepsilon^T \varepsilon.
\end{aligned}
\tag{4–27}
$$

In (4–27), the necessary conditions for $\dot{V}$ to be negative definite are (4–19)-(4–21).
Using (4–19)-(4–21), (4–27) can be rewritten as

$$
\dot{V} \leq - \sum_{i \in \mathcal{V}} (1 - \sigma_i) \left(k_1 - \frac{k_3}{\beta} \right) \|\hat{z}_i\|^2 - \delta_2 \varepsilon^T \varepsilon,
\tag{4–28}
$$

which is strictly negative definite as

$$
\dot{V} \leq - \delta_2 \varepsilon^T \varepsilon.
\tag{4–29}
$$

Given (4–23) and (4–29),

$$
\|\varepsilon(t)\| \leq \|\varepsilon(0)\| \exp(-\gamma t),
$$

where $\gamma \in \mathbb{R}_{>0}$ is a positive constant. Based on (4–4), the exponential convergence of
$\|\varepsilon\|$ implies (4–22). $\qquad\square$

Remark 4.1. Based on (4–20), the constant c_i in Fig. 4-1 can be designed as $c_i = \sqrt{\frac{\eta_i \left(k_1 - \frac{k_3}{\beta} \right)}{k_2 + k_3 \beta}}$. At t_k^i, e_i will be reset to zero as agent i communicates its state x_i to all its neighboring agents to update $\hat{x}_i$, and hence $\frac{\|e_i\|}{\|\hat{z}_i\|} = 0$ (i.e., $f_i < 0$). After the update, $\|e_i\|$ grows in time until meeting the next trigger condition $\frac{\|e_i\|}{\|\hat{z}_i\|} = c_i$ (i.e., $f_i = 0$). Then, the cycle repeats.

4.2.6 Minimal Inter-Event Interval

To show the proposed trigger functions in Theorem 4.1 do not lead to Zeno behavior, it is sufficient to find a positive lower bound for the inter-event interval. To facilitate

subsequent analysis, two constants $\bar{c}_0$, $\bar{c}_1 \in \mathbb{R}_{>0}$ are defined as

$$\bar{c}_0 \triangleq S_{\max}(A) \tag{4–30}$$

$$\bar{c}_1 \triangleq S_{\max}((I_N \otimes A) + (H \otimes BK)) + S_{\max}(H \otimes BK) + S_{\max}(A), \tag{4–31}$$

where $S_{\max}(\cdot)$ denotes the maximum singular value of a matrix argument

Theorem 4.2. *The event time defined in (4–19) ensures that there exists at least one agent $h \in \mathcal{V}$ such that its minimum inter-event interval $\tau \in \mathbb{R}_{>0}$ is lower bounded by*

$$\tau \geq \frac{1}{c} \ln \left(\frac{1}{N} \sqrt{ \frac{\sigma_h \left(k_1 - \frac{k_3}{\beta} \right)}{k_2 + k_3 \beta} + 1 } \right), \tag{4–32}$$

where $h \in \mathcal{V}$ is defined in the subsequent analysis, and $c \in \mathbb{R}_{>0}$ is a positive constant defined as

$$c \triangleq \max \{ \bar{c}_0, \bar{c}_1 \}. \tag{4–33}$$

Proof. Inspired by the proof in [79], we consider an agent $h \in \mathcal{V}$ that satisfies

$$h \triangleq \arg\max_{i \in \mathcal{V}} \| \hat{z}_i \| .$$

Since $\| e_h \| \leq \| e \|$, the following inequality holds

$$\frac{\| e_h \|}{N \| \hat{z}_h \|} \leq \frac{\| e \|}{N \| \hat{z}_h \|} \leq \frac{\| e \|}{\| \hat{z} \|},$$

which is equivalent to

$$\frac{\| e_h \|}{\| \hat{z}_h \|} \leq N \frac{\| e \|}{\| \hat{z} \|}. \tag{4–34}$$

For any interval $t \in \left[t_k^h, t_{k+1}^h \right)$, $\frac{\| e \|}{\| \hat{z} \|}$ is continuous. To show the inter-event interval is lower bounded as in [77], one can investigate the time derivative of $\frac{\| e \|}{\| \hat{z} \|}$ over the interval $t \in \left[t_k^h, t_{k+1}^h \right)$ as

$$\frac{d}{dt} \left(\frac{\| e \|}{\| \hat{z} \|} \right) = \frac{d}{dt} \left[\frac{(e^T e)^{\frac{1}{2}}}{(\hat{z}^T \hat{z})^{\frac{1}{2}}} \right] \leq \frac{\| \dot{e} \|}{\| \hat{z} \|} + \frac{\| e \| \left\| \dot{\hat{z}} \right\|}{\| \hat{z} \|^2}. \tag{4–35}$$

Using (4–12), (4–17), (4–18), and applying the inequality $x^T y \leq \|x\| \|y\|$ yields

$$\frac{d}{dt}\left(\frac{\|e\|}{\|\hat{z}\|}\right) \leq \|(I_N \otimes A) + (H \otimes BK)\| \frac{\|e\|}{\|\hat{z}\|} + \|(I_N \otimes BK)\| + \|(H \otimes BK)\| \frac{\|e\|}{\|\hat{z}\|}$$
$$+ \|(I_N \otimes A)\| \frac{\|e\|}{\|\hat{z}\|},$$

which can be further expressed as

$$\dot{y} \leq \bar{c}_0 + \bar{c}_1 y, \tag{4–36}$$

where $\bar{c}_0$ and $\bar{c}_1$ are defined in (4–30) and (4–31), and $y : [0, \infty) \to \mathbb{R}_{\geq 0}$ is a non-negative, piecewise continuous function, which is differentiable in the inter-event interval and is defined as

$$y\left(t - t_k^h\right) \triangleq \frac{\|e(t)\|}{\|\hat{z}(t)\|}, \text{ for } t \in \left[t_k^h, t_{k+1}^h\right) \tag{4–37}$$

for $k = 0, 1, 2 \ldots$. The inequality in (4–36) can be simply upper bounded by

$$\dot{y} \leq c(1 + y), \tag{4–38}$$

where c is defined in (4–33). Based on (4–38), a non-negative function $\phi : [0, \infty) \to \mathbb{R}_{\geq 0}$, satisfying

$$\dot{\phi} = c(1 + \phi), \quad \phi(0) = y_0, \tag{4–39}$$

can be lower bounded by y as

$$y \leq \phi, \text{ for } t \in [0, \tau), \tag{4–40}$$

where $\tau \triangleq t_{k+1}^h - t_k^h \in \mathbb{R}_{>0}$ is the minimum inter-event interval, and $y_0 \in \mathbb{R}_{\geq 0}$ is the initial condition of y, which is 0 since $e\left(t_k^h\right) = 0$ for $k = 0, 1, 2 \ldots$. An analytical solution to (4–39) with initial condition $\phi(0) = 0$ can be solved as

$$\phi(t) = \exp(ct) - 1. \tag{4–41}$$

Using (4–40) and (4–41) with $t \to \tau$ yields

$$\lim_{\varphi \to 0} y \left(\tau - \varphi\right) \leq \exp\left(c\tau\right) - 1. \tag{4–42}$$

Using (4–20) where $f_h \left(t_{k+1}^h\right) = 0$, (4–34), and $y\left(\tau\right)$ in (4–37) yields

$$\frac{1}{N} \sqrt{\frac{\sigma_h \left(k_1 - \frac{k_3}{\beta}\right)}{k_2 + k_3 \beta}} \leq \exp\left(c\tau\right) - 1,$$

which can be solved to yield (4–32). □

Remark 4.2. This lower bound implies that Zeno behaviors can be excluded. However, there is a trade-off between the minimum inter-event interval and the error convergence rate. The lower bound in (4–32) can be increased by selecting a higher σ_h, but this increase results in a slower convergence due to the fact that $\dot{V}$ in (4–28) becomes less negative.

4.3 Leader-Follower Consensus under Switching Topologies

In this section, an event-triggered based decentralized control approach is developed to extend the results developed in Section 4.2 to achieve leader-follower consensus under switching network topologies. To address the switching topologies, the following definition and assumptions are made.

4.3.1 Definitions and Assumptions

The time-varying interaction topology of the N followers described in (4–2) can be modeled by a switched undirected graph $\mathcal{G}_\sigma$, where the piecewise constant switching signal $\sigma : [0, \infty) \to \mathcal{P}$ indicates an underlying graph from a finite set $\mathcal{P} \triangleq \{1, 2, \ldots, M\}$ at time t, such that $\{\mathcal{G}_p : p \in \mathcal{P}\}$ includes all graphs in $\left\{\bigcup_{t \geq 0} \mathcal{G}\right\}$.

Similarly, the time-varying interaction topology of the leader-follower system described in (4–1)-(4–2) is modeled by a directed switching graph denoted as $\bar{\mathcal{G}}_\sigma$, which consists of the node set $\mathcal{V} \cup \{0\}$ and the edge set that contains all edges in $\mathcal{G}_\sigma$ and the edges connecting node 0 and the followers that have a directed edge from the leader.

Assumption 4.4. $\bar{\mathcal{G}}_p$ is connected for each $p \in \mathcal{P}$.

Assumption 4.5. The switching signal σ has a finite number of switches in a finite time interval. Specifically, σ switches at t_q and is invariant during a non-vanishing interval $[t_q, t_{q+1})$, $q = 0, 1, \ldots$, with $t_0 = 0$, $0 < \mu < t_{q+1} - t_q < T$, where μ, $T \in \mathbb{R}$ are positive constants, and μ is a non-vanishing dwell-time. Additionally, the switching sequence of σ is arbitrary.

4.3.2 Controller Design

Instead of continuous state feedback, the developed decentralized controller is a piecewise continuous input signal, where inter-agent communication is required only at discrete events. These events include topology switches and triggered events when the decentralized trigger condition is met, and the design of this trigger condition is based on insights from the Lyapunov-based state convergence analysis.

Motivated by conventional continuous feedback controller as in (4–3) and based on the subsequent convergence analysis, a decentralized event-triggered controller for agent $i \in \mathcal{V}$ is designed as

$$u_i = K\hat{z}_i, \tag{4–43}$$

$$\hat{z}_i = \sum_{j \in \mathcal{N}_i} (\hat{x}_j - \hat{x}_i) + d_i(x_0 - \hat{x}_i), \tag{4–44}$$

where $\mathcal{N}_i$ is a time-varying neighbor set, and the followers that are connected to the leader can continuously receive x_0 from the leader. In contrast to the controller in (4–3), the computation of $\hat{z}_i$ for the controller in (4–43) only requires the estimates of agent i and its neighboring followers' state estimate (i.e., $\hat{x}_{j \in \mathcal{N}_i}$), instead of using their true states $x_{j \in \mathcal{N}_i}$ via continuous communication. The estimate $\hat{x}_j$ in (4–44) evolves according to the dynamics

$$\hat{x}_j \left(t_E^j \right) = x_j \left(t_E^j \right) \tag{4–45}$$

$$\dot{\hat{x}}_j = A\hat{x}_j, \; t \in \left[t_E^j, t_{E+1}^j \right), \; j \in \{i\} \cup \mathcal{N}_i \tag{4–46}$$

$$
t_E^j = \begin{cases} t_q, & \text{if } j \text{ is a new neighbor} \\[2ex] t_k^j, & \text{otherwise} \end{cases}, \tag{4–47}
$$

for E, $k = 0, 1, 2 \ldots$, where $\hat{x}_j$ is updated via x_j communicated from neighboring agent j at its discrete times t_E^j and flows along the leader dynamics during $t \in \left[t_E^j, t_{E+1}^j \right)$, for $j \in \mathcal{N}_i$. In (4–47), t_q is the time when $\bar{\mathcal{G}}_\sigma$ switches, and t_k^j is the event-triggered time of the follower agent j. Although agent i does not communicate the estimate $\hat{x}_i$, agent i maintains $\hat{x}_i$ for implementation in (4–44). The estimate $\hat{x}_i$ is updated continuously with the dynamics in (4–46) and discretely at time instances described in (4–45). Therefore, u_i is a piecewise continuous signal, where communication is required when any new one-hop neighbor is connected or when state information is transmitted to, or received from, neighboring agents for estimate updates; otherwise, u_i flows continuously during the inter-event intervals.

Remark 4.3. In (4–47), since the link between two follower neighbors is undirected, $j \in \mathcal{N}_i$ implies $i \in \mathcal{N}_j$. That is, mutual communication is conducted at t_q if $j \in \mathcal{N}_i$ is a new neighbor.

4.3.3 Dynamics of Estimate Error

Since x_i follows different dynamics from the estimate $\hat{x}_i$ computed by its neighbors, the estimate error e_i characterizing this mismatch as

$$
e_i \triangleq \hat{x}_i - x_i, \ i \in \mathcal{V}, \ t \in \left[t_E^i, t_{E+1}^i \right), \tag{4–48}
$$

where e_i is reset to 0 at t_E^i due to the estimate updates. Although x_i and $\hat{x}_i$ are both known for agent i: using $\hat{x}_i$ enables agent i to judge how far a neighbor's estimate of x_i is from its actual state. Using (4–2), (4–43), and (4–46), the time-derivative of (4–48) can be expressed as

$$
\dot{e}_i = A \left(\hat{x}_i - x_i \right) - BK \sum_{j \in \mathcal{N}_i} \left(\hat{x}_j - \hat{x}_i \right) - BKd_i \left(x_0 - \hat{x}_i \right),
$$

which can be written in stack form as

$$\dot{e} = (I_N \otimes A)\, e + (H_\sigma \otimes BK)\, \varepsilon + (H_\sigma \otimes BK)\, e, \tag{4–49}$$

where e denotes $e \triangleq \left[e_1^T,\, e_2^T, \ldots,\, e_N^T\right]^T$, ε defined as $\varepsilon \triangleq \left[\varepsilon_1^T,\, \varepsilon_2^T,\, \ldots,\, \varepsilon_N^T\right]^T$ is a stack form of ε_i introduced in (4–4), and the matrix $H_{\sigma(t)} \in \mathbb{R}^{N \times N}$ is defined as $H_{\sigma(t)} \triangleq L_{\sigma(t)} + D_{\sigma(t)}$, where $D_{\sigma(t)} \in \mathbb{R}^{N \times N}$ is defined as $D_{\sigma(t)} \triangleq \operatorname{diag}\left(d_1\left(t\right),\, d_2\left(t\right),\, \ldots,\, d_N\left(t\right)\right)$, and $L_{\sigma(t)} \triangleq L\left(t\right)$. Based on Assumption 4.4, there exists a symmetric positive definite matrix P that satisfies the following Riccati inequality

$$PA + A^T P - 2\delta_p PBB^T P + \delta_p I_n < 0, \tag{4–50}$$

where $\delta_p \in \mathbb{R}_{>0}$ denotes the minimum eigenvalue of H_p and is a positive constant based on Assumption 4.4 and [105], and the control gain in (4–3) can be designed as

$$K = B^T P. \tag{4–51}$$

To facilitate the subsequent analysis, a minimum value of a finite set composed of δ_p, $\delta_{\min} \in \mathbb{R}_{>0}$, is defined as

$$\delta_{\min} \triangleq \min\left\{\delta_p \mid p \in \mathcal{P}\right\}. \tag{4–52}$$

4.3.4 Closed-Loop Error System

Using (4–48), a non-implementable form (to facilitate the subsequent analysis) of (4–43) can be expressed as (4–13). Substituting (4–13) into the open-loop dynamics in (4–2) and using the definition in (4–4) yields the closed-loop error system

$$\dot{\varepsilon}_i = A\varepsilon_i + BK \sum_{j \in \mathcal{N}_i} \left(x_j - x_i\right) + BK d_i \left(x_0 - x_i\right) + BK \sum_{j \in \mathcal{N}_i} \left(e_j - e_i\right) - BK d_i e_i,$$

where the stack form can be expressed as

$$\dot{\varepsilon} = (I_N \otimes A)\, \varepsilon - (H_\sigma \otimes BK)\, \varepsilon - (H_\sigma \otimes BK)\, e. \tag{4–53}$$

To facilitate the subsequent analysis, a relation between ε and $\hat{z}$ is developed, where $\hat{z}$ can be expressed as

$$\hat{z} \triangleq (H_\sigma \otimes I_n)[1_N \otimes x_0 - \hat{x}].\tag{4–54}$$

Combining (4–16) and (4–54) yields

$$\varepsilon = -\left(H_\sigma^{-1} \otimes I_n\right)\hat{z} - e,\tag{4–55}$$

where $\hat{z}$ is governed by the dynamics defined in (4–18).

4.3.5 Convergence Analysis

In this section, convergence of leader-follower consensus with the event-triggered controller designed in (4–43) is examined using a Lyapunov-based analysis. In addition to proving the convergence of the error signal ε, the analysis also establishes a trigger condition associated with a trigger function that establishes when agents communicate state information.

To facilitate the subsequent convergence analysis, the event time t_k^i is explicitly defined.

Definition 4.3. An event-triggered time t_k^i is defined as

$$t_k^i \triangleq \inf\left\{t > t_{k-1}^i \mid f_i(t) = 0\right\}, \, i \in \mathcal{V},\tag{4–56}$$

for $k = 1, 2, \ldots$, where $t_0^i = 0$, and $f_i(\cdot)$, denoted as $f_i(e_i(\cdot), \hat{z}_i(\cdot))$, is a decentralized trigger function defined as

$$f_i(e_i, \hat{z}_i) \triangleq \|e_i\| - \sqrt{\frac{\eta_i\left(k_1 - \frac{k_3}{\beta}\right)}{k_2 + k_3\beta}}\,\|\hat{z}_i\|,\tag{4–57}$$

where $\eta_i \in \mathbb{R}_{>0}$ satisfying $0 < \eta_i < 1$ provides flexibility in real-time scheduling, and β is a positive constant satisfying

$$\beta > \frac{k_3}{k_1},\tag{4–58}$$

78

where k_i, $i = 1, 2, 3$, are positive constants defined as

$$k_1 \triangleq \min_{p \in \mathcal{P}} \left\{ \delta_{m1} S_{\min} \left(H_p^{-2} \right) \right\}$$

$$k_2 \triangleq \max_{p \in \mathcal{P}} \left\{ S_{\max} \left(H_p \otimes \left(2PBB^T P \right) \right) - \delta_{m1} \right\}$$

$$k_3 \triangleq \max_{p \in \mathcal{P}} \left\{ S_{\max} \left(I_N \otimes \left(2PBB^T P \right) - H_p^{-1} \otimes 2\delta_{m1} I_n \right) \right\},$$

where $\delta_{m1} \in \mathbb{R}_{>0}$ satisfies $0 < \delta_{m1} < \delta_{\min}$ such that $k_2 > 0$ and $k_3 > 0$, and $S_{\max}(\cdot)$ denotes the maximum singular value of the matrix argument.

Theorem 4.3. *The controller designed in (4–43) ensures that the network system in (4–1) and (4–2) modeled by the switching graph $\bar{\mathcal{G}}_\sigma$ achieves asymptotic leader-follower consensus defined in (4–4) provided that the estimate $\hat{x}_i$ in (4–45) is updated at t_E^i, defined in Definition 4.3.*

Proof. Consider a Lyapunov function candidate V defined as

$$V \triangleq \varepsilon^T \left(I_N \otimes P \right) \varepsilon, \tag{4–59}$$

where P is a symmetric positive definite matrix satisfying (4–50). Using (4–51) and (4–53), the time derivative of (4–59) can be expressed as

$$\dot{V} = -e^T \left[H_\sigma \otimes \left(2PBB^T P \right) \right] \varepsilon . \varepsilon^T \left[I_N \otimes \left(PA + A^T P \right) - H_\sigma \otimes \left(2PBB^T P \right) \right] \varepsilon \tag{4–60}$$

Since $H_{\sigma \in \mathcal{P}}$ is symmetric and positive definite, (4–50) and (4–52) can be used to upper bound (4–60) as

$$\dot{V} \leq -\delta_{\min} \varepsilon^T \varepsilon - e^T \left[H_\sigma \otimes \left(2PBB^T P \right) \right] \varepsilon. \tag{4–61}$$

Using (4–55), (4–61) can be expressed as

$$\dot{V} \leq - \delta_{m1} \hat{z}^T \left(H_\sigma^{-2} \otimes I_n \right) \hat{z} - \delta_{m1} e^T e + 2\delta_{m1} e^T \left(H_\sigma^{-1} \otimes I_n \right) \hat{z} - e^T \left[I_N \otimes \left(2PBB^T P \right) \right] \hat{z}$$

$$+ e^T \left[H_\sigma \otimes \left(2PBB^T P \right) \right] e - \delta_{m2} \varepsilon^T \varepsilon, \tag{4–62}$$

where $\delta_{m2} \in \mathbb{R}_{>0}$ satisfies $\delta_{\min} = \delta_{m1} + \delta_{m2}$. By using the inequality $x^T y \leq \|x\| \|y\|$, (4–62) can be upper bounded as

$$\dot{V} \leq -k_1 \|\hat{z}\|^2 + k_2 \|e\|^2 + 2k_3 \|e\| \|\hat{z}\| - \delta_{m2}\varepsilon^T\varepsilon. \qquad (4\text{–}63)$$

Using the inequality $\|x\| \|y\| \leq \frac{\beta}{2} \|x\|^2 + \frac{1}{2\beta} \|y\|^2$, (4–63) can be upper bounded as

$$\begin{aligned}
\dot{V} \leq & -k_1 \|\hat{z}\|^2 + 2k_3 \left(\frac{\beta}{2} \|e\|^2 + \frac{1}{2\beta} \|\hat{z}\|^2 \right) + k_2 \|e\|^2 - \delta_{m2}\varepsilon^T\varepsilon \\
\leq & -\left(k_1 - \frac{k_3}{\beta} \right) \|\hat{z}\|^2 + (k_2 + k_3\beta) \|e\|^2 - \delta_{m2}\varepsilon^T\varepsilon \\
\leq & -\sum_{i \in \mathcal{V}} \left[\left(k_1 - \frac{k_3}{\beta} \right) \|\hat{z}_i\|^2 - (k_2 + k_3\beta) \|e_i\|^2 \right] - \delta_{m2}\varepsilon^T\varepsilon. \qquad (4\text{–}64)
\end{aligned}$$

In (4–64), two necessary conditions for $\dot{V}$ to be negative definite are

$$0 < k_1 - \frac{k_3}{\beta}$$

$$\|e_i\|^2 \leq \frac{\eta_i \left(k_1 - \frac{k_3}{\beta} \right)}{k_2 + k_3\beta} \|\hat{z}_i\|^2, \qquad (4\text{–}65)$$

which are satisfied provided that (4–56)-(4–58) are satisfied. Provided (4–58) and (4–65) are satisfied, then (4–64) can be rewritten as

$$\dot{V} \leq -\sum_{i \in \mathcal{V}} (1 - \eta_i) \left(k_1 - \frac{k_3}{\beta} \right) \|\hat{z}_i\|^2 - \delta_{m2}\varepsilon^T\varepsilon, \qquad (4\text{–}66)$$

$$\leq -\delta_{m2}\varepsilon^T\varepsilon, \qquad (4\text{–}67)$$

which implies V is a common Lyapunov function. The linear differential inequality resulting from (4–59) and (4–67) can be solved to conclude that

$$\|\varepsilon\| \leq \|\varepsilon(0)\| \exp(-\gamma t),$$

where γ is a positive constant. The exponential convergence of $\|\varepsilon\|$ implies (4–4). $\qquad \square$

Remark 4.4. Based on (4–57), the constant c_i in Fig. 4-1 can be designed as $c_i = \sqrt{\frac{\eta_i \left(k_1 - \frac{k_3}{\beta} \right)}{k_2 + k_3\beta}}$. At t_k^i, e_i will be reset to zero as agent i communicates its state x_i to all its

neighboring agents to update $\hat{x}_i$, and hence $\frac{\|e_i\|}{\|\hat{z}_i\|} = 0$ (i.e., $f_i < 0$). After the update, $\|e_i\|$ grows in time until meeting the next trigger condition $\frac{\|e_i\|}{\|\hat{z}_i\|} = c_i$ (i.e., $f_i = 0$). Then, the cycle repeats.

4.3.6 Minimal Inter-Event Interval

Zeno execution is defined as infinite switches in a finite interval. Exclusion of Zeno execution can be sufficiently proven by finding a positive lower bound between any two contiguous discrete events (i.e., $\left[t_E^j, t_{E+1}^j\right)$) [79]. Based on Assumption 4.5, graph switches never cause Zeno execution (i.e., $\mu < t_{q+1} - t_q$). Therefore, only the following three intervals smaller than μ are analyzed.

Case 1. Consider any inter-event interval $\left[t_k^j, t_{k+1}^j\right)$, where $0 < t_{k+1}^j - t_k^j < \mu$. This interval is proven to be lower bounded by a positive constant in Theorem 4.4.

Case 2. Consider any inter-event interval $\left[t_q, t_{k+1}^j\right)$, for $0 < t_{k+1}^j - t_q < \mu$. By (4–47), a new neighbor agent $j \in \mathcal{N}_i$ has a mutual communication at t_q, at which time e_j is reset to zero. Therefore, t_q can be considered as the instant t_k^j, which implies *Case 1* and *Case 2* are equivalent.

Case 3. Consider any inter-event interval $\left[t_k^j, t_q\right)$, for $0 < t_q - t_k^j < \mu$. Then, the next cycle must be $\left[t_q, t_{k+1}^j\right)$ since t_{k+1}^j comes earlier than t_{q+1}. Therefore, proving a positive lower bound of the interval $\left[t_q, t_{k+1}^j\right)$ implies no Zeno execution since infinite switches can not happen in the finite interval. Moreover, finding the lower bound of $\left[t_q, t_{k+1}^j\right)$ is equivalent to proving *Case 2*.

Based on the three cases above, Zeno execution can be excluded provided that Theorem 4.4 is proven. To facilitate the subsequent analysis, two constants $\bar{c}_0, \bar{c}_1$ are defined as

$$\bar{c}_0 \triangleq \max_{p \in \mathcal{P}} \left\{ S_{\max}\left(A\right) \right\} \tag{4–68}$$

$$\bar{c}_1 \triangleq \max_{p \in \mathcal{P}} \left\{ S_{\max}\left(\left(I_N \otimes A\right) + \left(H_p \otimes BK\right)\right) + S_{\max}\left(H_p \otimes BK\right) + S_{\max}\left(A\right) \right\} \tag{4–69}$$

Theorem 4.4. *The event-triggered time defined in ([4–56](#)) ensures that there exists an agent $h \in \mathcal{V}$ such that the interval $\left[t_k^h, \, t_{k+1}^h\right)$ is lower bounded by*

$$\tau \geq \frac{1}{\max\left\{\bar{c}_0, \, \bar{c}_1\right\}} \ln \left(\frac{1}{N} \sqrt{\frac{\eta_h \left(k_1 - \frac{k_3}{\beta}\right)}{(k_2 + k_3 \beta)}} + 1 \right),$$

where $\tau \triangleq t_{k+1}^h - t_k^h$ is the minimum interval, h is an agent that satisfies

$$h = \arg \max_{i \in \mathcal{V}} \sup_{t \in \mathbb{R}_{\geq 0}} \|\hat{z}_i\|.$$

Proof. The proof is similar to the proof of Theorem [4.2](#) and is thus omitted. □

4.4 Simulation

In this section, two simulations are performed to demonstrate the control effectiveness of the event-triggered approaches. In the first simulation, the consensus control under fixed network topology is conducted, and the problem for switching network topologies is investigated in the second simulation. Each simulation consists of 4 followers and 1 leader, whose initial condition are assigned with arbitrary finite constants.

4.4.1 Fixed Network Topology

A leader-follower network system with a fixed network topology is depicted in Fig. [4-2](#).
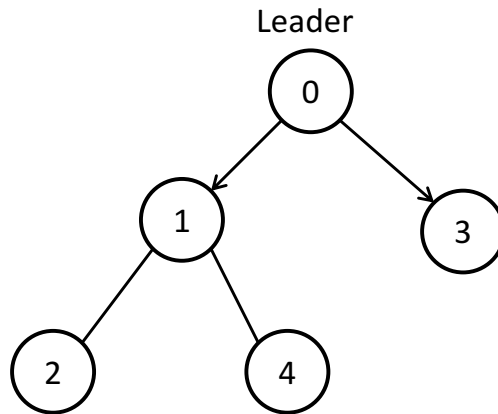

Figure 4-2. Network topology of the graph $\bar{\mathcal{G}}$, where the agent indexed by 0 is the leader and other agents are the followers.

The dynamics of the leader and the followers and the Laplacian matrix of the graph $\bar{\mathcal{G}}$ are

$$A = \begin{bmatrix} 1 & 1 \\ 0 & 1 \end{bmatrix}, B = \begin{bmatrix} 0 \\ 1 \end{bmatrix}, L = \begin{bmatrix} 2 & -1 & 0 & -1 \\ -1 & 1 & 0 & 0 \\ 0 & 0 & 0 & 0 \\ -1 & 0 & 0 & 1 \end{bmatrix}.$$

Based on the network topology in Fig. 4-2, the smallest nonzero eigenvalue of H is $\delta_{\min} = 0.2679$, and the solution P of (4–5) and the control gain $K = B^T P$ are

$$P = \begin{bmatrix} 24.82 & 10.58 \\ 10.58 & 9.13 \end{bmatrix}, K = \begin{bmatrix} 10.58 & 9.13 \end{bmatrix}.$$

The initial conditions of each agent for the simulation are $x_0 = [1, 1]^T$, $x_1 = [10, 2]^T$, $x_2 = [3, 7]^T$, $x_3 = [9, -4]^T$, and $x_4 = [6, 5]^T$. The consensus errors of each follower agent are shown in Fig. 4-3 and Fig. 4-4, where both plots show the leader-follower asymptotic consensus.
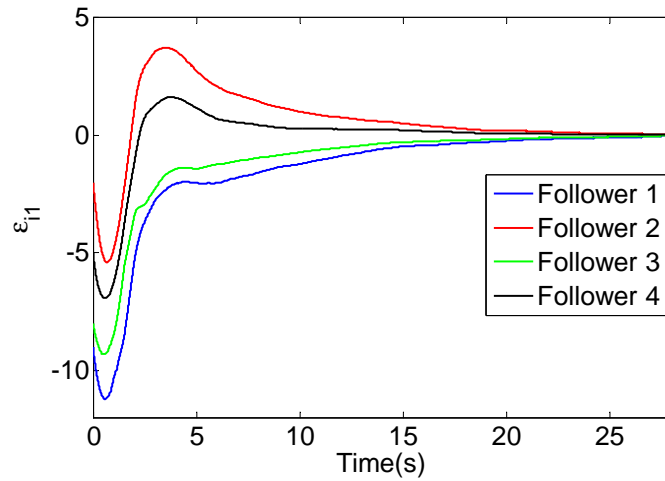
Figure 4-3. Consensus error ε_{i1} of follower agents.
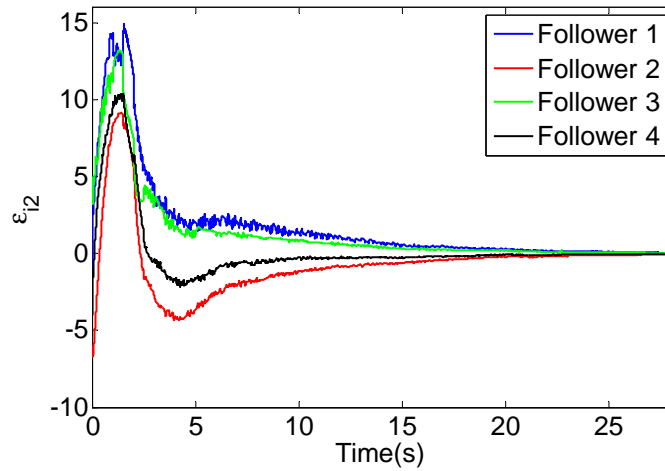
Figure 4-4. Consensus error ε_{i2} of follower agents.

For ε_{i2}, the sawtooth waves reflect the jumps of the control input whenever events are triggered. Fig. 4-5 shows triggered events individually. The average intervals between two contiguous events within follower agents 1-4 are 44 ms, 24 ms, 80 ms, and 17 ms, respectively. These intervals imply that Zeno behavior did not occur.
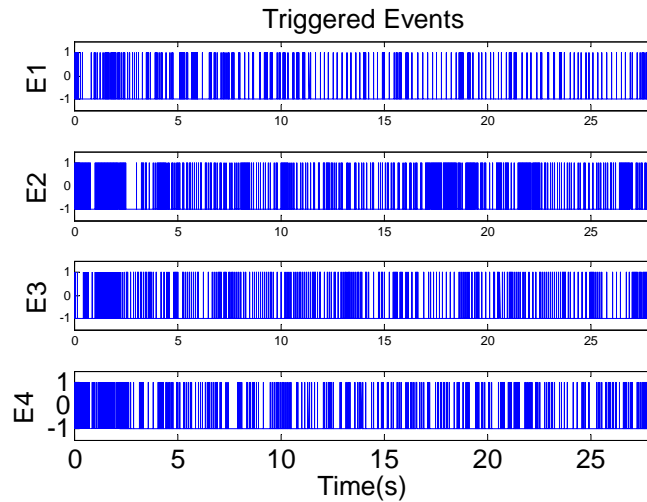
Figure 4-5. $E1$-$E4$ represent the occurrences of the events for all follower agents (1: triggered, -1: not triggered).
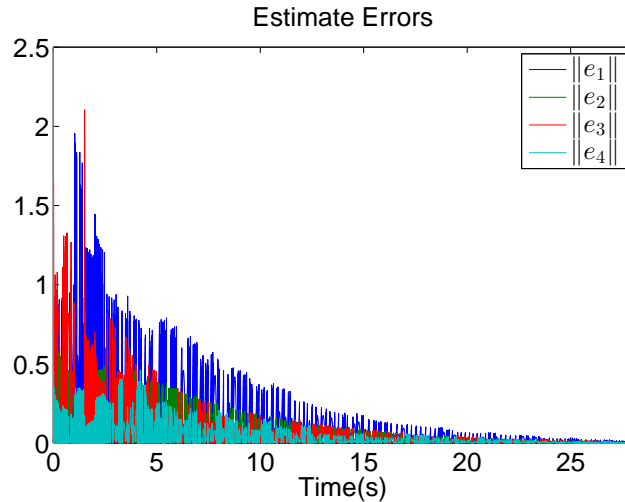
Figure 4-6. Norm of the estimate errors of the follower agents.

Fig. 4-6 shows asymptotic convergences of the estimate errors for follower agent 1-4, which implies the estimate asymptotically converges to the true states.

4.4.2 Switching Network Topologies

The time-varying interaction topology switches between three graphs $\bar{\mathcal{G}}_1$, $\bar{\mathcal{G}}_2$, and $\bar{\mathcal{G}}_3$, described in Fig. 4-7, where the arbitrary switching signal is depicted in Fig. 4-8. The effectiveness of the event-triggered strategy is visualized through on-off signals, and the average inter-event interval.
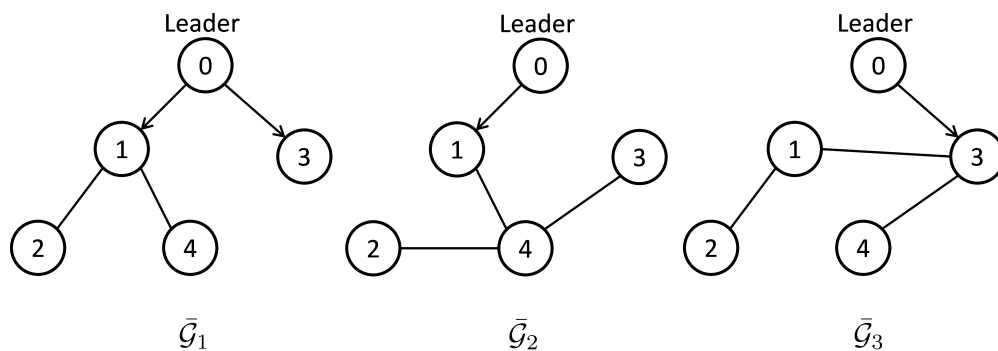
Figure 4-7. The interaction graphs $\bar{\mathcal{G}}_1$, $\bar{\mathcal{G}}_2$, and $\bar{\mathcal{G}}_3$, where the leader is indexed by 0.
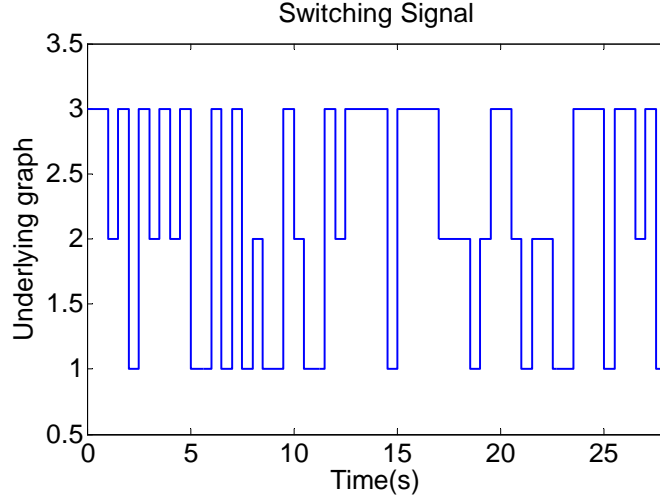
Figure 4-8. An arbitrary switching signal that indicates the sequence of the three underlying graphs.

The dynamics of the leader and the followers described by (4–1) and (4–2) are

$$A = \begin{bmatrix} 1 & 1 \\ 0 & 1 \end{bmatrix}, \qquad B = \begin{bmatrix} 0 \\ 1 \end{bmatrix},$$

and the corresponding $H_{p \in \{1,2,3\}}$ matrix of the three graphs are

$$H_1 = \begin{bmatrix} 3 & -1 & 0 & -1 \\ -1 & 1 & 0 & 0 \\ 0 & 0 & 1 & 0 \\ -1 & 0 & 0 & 1 \end{bmatrix}, \quad H_2 = \begin{bmatrix} 2 & 0 & 0 & -1 \\ 0 & 1 & 0 & -1 \\ 0 & 0 & 1 & -1 \\ -1 & -1 & -1 & 3 \end{bmatrix},$$

$$H_3 = \begin{bmatrix} 2 & -1 & -1 & 0 \\ -1 & 1 & 0 & 0 \\ -1 & 0 & 3 & -1 \\ 0 & 0 & -1 & 1 \end{bmatrix}.$$

Based on the network topology in Fig. 4-7, the smallest nonzero eigenvalues of H_1, H_2, and H_3 are $\delta_1 = 0.2679$, $\delta_2 = 0.1392$, and $\delta_3 = 0.1729$, respectively, which implies $\delta_{\min} = \delta_2$, and the solution P to the Riccati inequality in (4–50) and the control gain

86

$K = B^T P$ are

$$P = \begin{bmatrix} 38.7868 & 17.5485 \\ 10.58 & 9.13 \end{bmatrix},$$

$$K = \begin{bmatrix} 17.5485 & 15.708 \end{bmatrix}.$$

The initial conditions of each agent for the simulation are $x_0 = [1, \ 1]^T$, $x_1 = [10, \ 2]^T$, $x_2 = [3, \ 7]^T$, $x_3 = [9, \ -4]^T$, and $x_4 = [6, \ 5]^T$. The consensus errors of each follower agent are shown in Fig. 4-9 and Fig. 4-10, and both plots show asymptotic convergences for the leader-follower consensus.
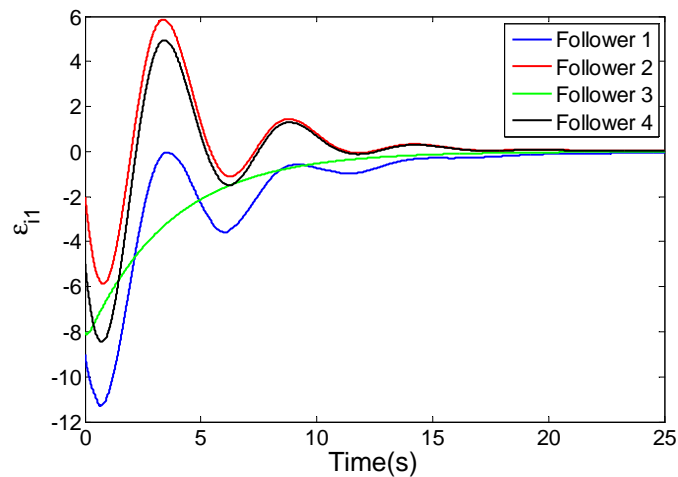
Figure 4-9. Consensus errors ε_{i1} by the follower agents.

Compared to Fig. 4-10, the trajectory in Fig. 4-9 is smooth since the discontinuous control input is acting on the second element of the system state. In Fig. 4-10, the sawtooth waves reflect the jumps of the control input when discrete events happen.
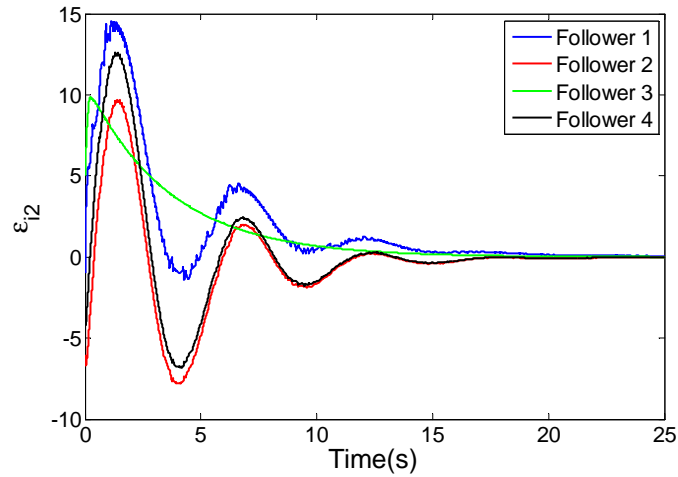
Figure 4-10. Consensus errors ε_{i2} by the follower agents.

Fig. 4-11 shows triggered events individually, where 1 represents the event when the state is sent to its neighbors, and -1 represents the interval with no communication. The average intervals between two contiguous triggered events within follower agents 1-4 are 52 ms, 20 ms, 58 ms, and 18 ms, respectively. These intervals not only mean that Zeno behavior can be excluded from this simulation, but also implies that the developed decentralized controller can stabilize the networked system with only intermittent communication.
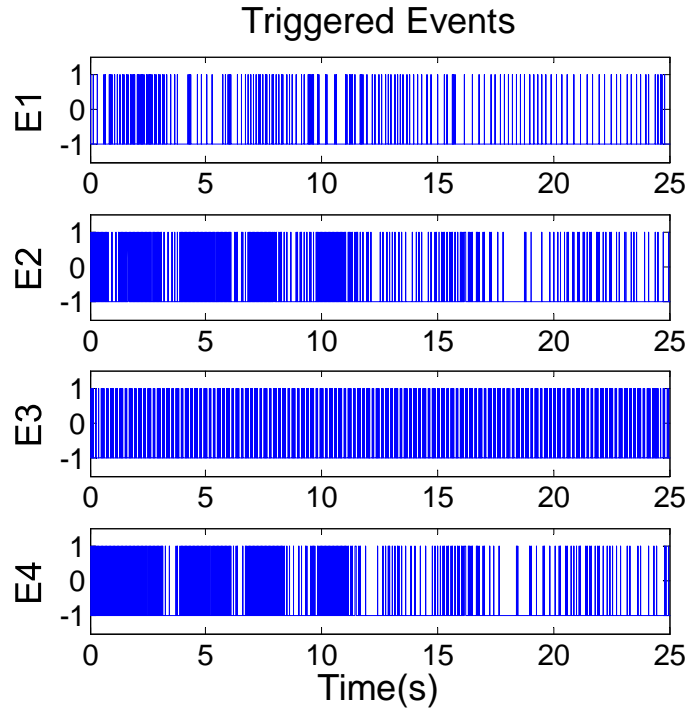
Figure 4-11. $E1$-$E4$ represent the occurrences of the events for all follower agents (1: triggered, -1: not triggered).
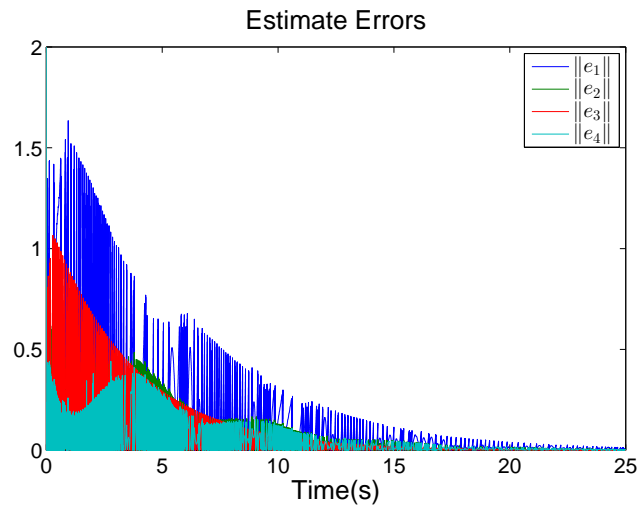
Figure 4-12. Norm of estimate errors of the follower agents.

Fig. 4-12 shows asymptotic convergences of the estimate errors for follower agents 1-4, which implies the estimates asymptotically converge to the true states.

4.5 Discussion

A decentralized event-triggered control scheme for the leader-follower network consensus under time-varying network topologies is developed to reduce communication with neighboring agents while ensuring the stability of the system. The estimate-based decentralized controller along with the decentralized trigger function reduces the number of inter-agent communications and prevents potential communication channel overload. A Lyapunov-based stability analysis indicates that the network system achieves asymptotic leader-follower consensus under this event-triggered control scheme. Moreover, the trigger function is proven to never exhibit Zeno behavior. Numerical simulation results illustrate favorable convergence with event-triggered communications.

CHAPTER 5
DECENTRALIZED EVENT-TRIGGERED CONTAINMENT CONTROL OF NETWORKED SYSTEMS

In Chapter 5, a decentralized event-triggered control scheme is developed for the containment control problem. An estimate-based decentralized controller is designed for each agent so that it is only required to communicate with neighboring agents at discrete event times. These events are determined by a decentralized trigger function that only requires local information. Different from conventional strategies, the developed control approach does not require continuous communication with local neighboring follower agents for state feedback, reducing communication bandwidth. The event-triggered approach is facilitated by developing a positive constant lower bound on the inter-event interval, which indicates Zeno behavior is avoided. A Lyapunov-based convergence analysis is provided to indicate asymptotic convergence of the developed strategy. Simulation results are provided to demonstrate the effectiveness of the developed control strategy.

5.1 Preliminaries

5.1.1 Preliminaries

To describe the interaction between follower nodes, an undirected graph $\mathcal{G}_{\mathcal{F}} = (\mathcal{V}_{\mathcal{F}}, \mathcal{E}_{\mathcal{F}})$ is defined, where $\mathcal{V}_{\mathcal{F}} \triangleq \{1, \ldots, F\}$ is the index set of the F follower nodes, and $\mathcal{E}_{\mathcal{F}} \subseteq \mathcal{V}_{\mathcal{F}} \times \mathcal{V}_{\mathcal{F}}$ is the corresponding edge set. An undirected edge (i, j) is an element of $\mathcal{E}_{\mathcal{F}}$ if $i, j \in \mathcal{V}_{\mathcal{F}}$ can exchange information mutually. Without loss of generality, the undirected graph is assumed to be simple (i.e., $(i, i) \notin \mathcal{E}, \forall i \in \mathcal{V}_{\mathcal{F}}$). The follower neighbor set $\mathcal{N}_{\mathcal{F}i} \triangleq \{j \in \mathcal{V}_{\mathcal{F}} \mid (j, i) \in \mathcal{E}_{\mathcal{F}}\}$ is a set of follower nodes that can deliver information to agent i. To describe the interaction topology of all nodes, a directed graph $\mathcal{G} = (\mathcal{V}_{\mathcal{F}} \cup \mathcal{V}_{\mathcal{L}}, \mathcal{E}_{\mathcal{F}} \cup \mathcal{E}_{\mathcal{L}})$ is defined as a supergraph of $\mathcal{G}_{\mathcal{F}}$ formed by connecting an additional edge $(k, i) \in \mathcal{E}_{\mathcal{L}}$ to $\mathcal{G}_{\mathcal{F}}$ if the leader $k \in \mathcal{V}_{\mathcal{L}}$ communicates information to the follower $i \in \mathcal{V}_{\mathcal{F}}$, where $\mathcal{V}_{\mathcal{L}} \triangleq \{F + 1, \ldots, F + L\}$ is the indexed set of the leader nodes, and $\mathcal{E}_{\mathcal{L}} \subseteq \mathcal{V}_{\mathcal{L}} \times \mathcal{V}_{\mathcal{F}}$ is a leader-follower edge set. The leader neighbor set

$\mathcal{N}_{\mathcal{L}i} \triangleq \{j \in \mathcal{V}_{\mathcal{L}} \mid (j, i) \in \mathcal{E}_{\mathcal{L}}\}$ is a set of leaders that can deliver information to follower i. The adjacency matrix $\mathcal{A} = [a_{ij}] \in \mathbb{R}^{(F+L) \times (F+L)}$ of graph $\mathcal{G}$ is also defined such that $a_{ii} = 0$, $a_{ij} = 1$ if $(j, i) \in \mathcal{E}_{\mathcal{F}} \cup \mathcal{E}_{\mathcal{L}}$, and $a_{ij} = 0$ otherwise. Similar to $\mathcal{L}_1$, the Laplacian matrix of graph $\mathcal{G}$ can be expressed as $\mathcal{L} = \begin{bmatrix} \mathcal{L}_{\mathcal{F}} & \mathcal{L}_{\mathcal{L}} \\ 0_{L \times F} & 0_{L \times L} \end{bmatrix}$, where $\mathcal{L}_{\mathcal{L}} \in \mathbb{R}^{F \times L}$, 0 is the zero matrix of defined dimensions, and $\mathcal{L}_{\mathcal{F}} \triangleq \mathcal{L}_1 + D \in \mathbb{R}^{F \times F}$ is a symmetric matrix, where $D = [d_{ij}] \in \mathbb{R}^{F \times F}$ is a diagonal matrix defined such that $d_{ii} = \sum_{l \in \mathcal{V}_{\mathcal{L}}} a_{il}$ and $d_{ij} = 0$ for $i \neq j$.

To facilitate the subsequent analysis, the following lemma from [88] is provided.

Lemma 5.1. *[88] If graph $\mathcal{G}$ is connected, then the symmetric matrix $\mathcal{L}_{\mathcal{F}}$ is positive definite.*

5.1.2 Dynamics

Consider a network system composed of F follower agents and L leader agents, with dynamics

$$\dot{x}_i = A x_i, \qquad i \in \mathcal{V}_{\mathcal{L}} \tag{5–1}$$

$$\dot{x}_i = A x_i + B u_i, \ i \in \mathcal{V}_{\mathcal{F}} \tag{5–2}$$

where $x_i \in \mathbb{R}^n$ and $u_i \in \mathbb{R}^m$ denote the state and control input of agent i, respectively, $B \in \mathbb{R}^{n \times m}$ is a full column rank matrix, and $A \in \mathbb{R}^{n \times n}$ is a state matrix.

Assumption 5.1. The dynamics of the agents are controllable, or the pair (A, B) is stabilizable.

Assumption 5.2. Each follower has directed paths from at least one leader.

5.2 Development of the Event-Triggered Decentralized Controller

The containment control objective is to ensure the states of all the followers converge to the convex hull spanned by the leaders' states, such as [73]

$$\left\| x_{\mathcal{F}} + \left(\mathcal{L}_{\mathcal{F}}^{-1} \mathcal{L}_{\mathcal{L}} \otimes I_n \right) x_{\mathcal{L}} \right\| \to 0 \text{ as } t \to \infty. \tag{5–3}$$

In this section, an event-triggered based decentralized controller is developed to minimize the inter-agent communication while achieving the containment control objective defined in (5–3). Different from conventional approaches, event-triggered control methods generate a piecewise continuous control signal, where the discontinuities are due to the state estimate updates. The discrete events are generated from the satisfaction of a triggering condition. The triggering condition is designed based on insights from the Lyapunov-based state convergence analysis.

5.2.1 Controller Design

Based on the subsequent convergence analysis, the decentralized event-triggered controller for agent $i \in \mathcal{V}_{\mathcal{F}}$ is designed as

$$u_i = K \hat{z}_i \tag{5–4}$$

$$\hat{z}_i = \sum_{j \in \mathcal{N}_{\mathcal{F}i}} (\hat{x}_j - \hat{x}_i) + \sum_{j \in \mathcal{N}_{\mathcal{L}i}} (x_j - \hat{x}_i), \ i \in \mathcal{V}_{\mathcal{F}}, \tag{5–5}$$

where K is the control gain designed as

$$K = B^T P. \tag{5–6}$$

Based on Assumption 5.1, $P \in \mathbb{R}^{n \times n}$ is a symmetric positive definite matrix that satisfies the following Riccati inequality

$$PA + A^T P - 2\delta_{\min} PBB^T P + \delta_{\min} I_n < 0, \tag{5–7}$$

where I is an identity matrix with denoted dimension, and $\delta_{\min} \in \mathbb{R}^+$ denotes the minimum eigenvalue of $\mathcal{L}_{\mathcal{F}}$, where $\mathcal{L}_{\mathcal{F}}$ is positive definite based on Assumption 5.2 and Lemma 5.1.

In (5–5), the followers that are connected to the leader can continuously receive information from the leader, and the computation of $\hat{z}_i$ in (5–5) only requires the estimates of agent i and its neighboring followers' state (i.e., $\hat{x}_{j \in \mathcal{N}_{\mathcal{F}i}}$), instead of using their true states $x_{j \in \mathcal{N}_{\mathcal{F}i}}$ via continuous communication. The estimate $\hat{x}_j$ in (5–5) evolves according

to the following dynamics

$$\dot{\hat{x}}_j(t) = A\hat{x}_j(t), \; j \in \mathcal{N}_{\mathcal{F}i} \cup \{i\}, \; t \in \left[t_k^j, t_{k+1}^j\right), \tag{5–8}$$

$$\hat{x}_j\left(t_k^j\right) = x_j\left(t_k^j\right), \tag{5–9}$$

for $k = 0, 1, 2 \ldots$, where $\hat{x}_j$ flows along the leader dynamics during $t \in \left[t_k^j, t_{k+1}^j\right)$ and is updated via x_j communicated from neighboring agent j at its discrete times t_k^j, for $j \in \mathcal{N}_{\mathcal{F}i}$. Although agent $i \in \mathcal{V}_{\mathcal{F}}$ does not communicate the estimate $\hat{x}_i$, agent i maintains $\hat{x}_i$ for implementation in (5–5). The estimate $\hat{x}_i$ is updated continuously with the dynamics in (5–5) and discretely at time instances described in (5–9). Therefore, u_i is a piecewise continuous signal, which has discontinuities when state information is transmitted to, or received from, neighboring agents for estimate updates; otherwise, u_i flows continuously during the inter-event intervals. The generation of the event times will be described in Section 5.2.3.

5.2.2 Dynamics of Estimate Errors

Since x_i follows different dynamics from the estimate $\hat{x}_i$ for $i \in \mathcal{V}_{\mathcal{F}}$, an estimate error $e_i \in \mathbb{R}^n$ characterizing the mismatch is defined as

$$e_i(t) \triangleq \hat{x}_i(t) - x_i(t), \; i \in \mathcal{V}_{\mathcal{F}}, \; t \in \left[t_k^i, t_{k+1}^i\right), \tag{5–10}$$

where e_i is reset to 0 at the event time t_k^i, $k = 0, 1, 2, \ldots$. Although x_i and $\hat{x}_i$ are both known for agent i, using $\hat{x}_i$ enables agent i to judge how far another $\hat{x}_i$ in its neighboring agent is away from its actual state x_i. Using (5–2), (5–4), and (5–8), the time-derivative of (5–10) can be expressed as

$$\dot{e}_i = A(\hat{x}_i - x_i) - BK \sum_{j \in \mathcal{N}_{\mathcal{F}i}} (\hat{x}_j - \hat{x}_i) - BK \sum_{j \in \mathcal{N}_{\mathcal{L}i}} (x_j - \hat{x}_i), \; t \in \left[t_k^i, t_{k+1}^i\right),$$

which has a stacked form of

$$\dot{e} = (I_F \otimes A) e + (I_F \otimes BK) \varepsilon + (\mathcal{L}_{\mathcal{F}} \otimes BK) e, \tag{5–11}$$

where $e \in \mathbb{R}^{nF}$ denotes $e \triangleq \left[e_1^T, e_2^T, \ldots, e_F^T \right]^T$, $\otimes$ denotes the Kronecker product, and

$\varepsilon \in \mathbb{R}^{nF}$ is a stacked form of ε_i defined as $\varepsilon \triangleq \left[\varepsilon_1^T, \ldots, \varepsilon_F^T \right]^T$, where $\varepsilon_i \in \mathbb{R}^n$ represents

the relative neighboring state tracking error as

$$\varepsilon_i \triangleq \sum_{j \in \mathcal{N}_{\mathcal{F}i} \cup \mathcal{N}_{\mathcal{L}i}} \left(x_i - x_j \right), \, i \in \mathcal{V}_{\mathcal{F}}, \tag{5–12}$$

which has a stacked form

$$\varepsilon = \left(\mathcal{L}_{\mathcal{F}} \otimes I_n \right) x_{\mathcal{F}} + \left(\mathcal{L}_{\mathcal{L}} \otimes I_n \right) x_{\mathcal{L}}. \tag{5–13}$$

5.2.3 Event-Triggered Communication Mechanism

A follower agent's state estimate is updated whenever communication is triggered

by a neighbor's trigger condition or its own trigger condition. Please see Figure 4-1 in

Chapter 4 for further details on the communication mechanism. The triggered condition

is defined in Section 5.3.

5.2.4 Closed-Loop Error System

Using (5–10), a non-implementable form (to facilitate the subsequent analysis) of

(5–4) can be written as

$$u_i \left(t \right) = K \sum_{j \in \mathcal{N}_{\mathcal{F}i} \cup \mathcal{N}_{\mathcal{L}i}} \left[\left(x_j \left(t \right) - x_i \left(t \right) \right) + \left(e_j \left(t \right) - e_i \left(t \right) \right) \right], \tag{5–14}$$

where $e_{j \in \mathcal{V}_{\mathcal{L}}} = 0$ due to continuous communication from leaders. Substituting (5–14) into

the open-loop dynamics in (5–2) yields

$$\dot{x}_i = A x_i + B K \sum_{j \in \mathcal{N}_{\mathcal{F}i} \cup \mathcal{N}_{\mathcal{L}i}} \left(x_j \left(t \right) - x_i \left(t \right) \right) + B K \sum_{j \in \mathcal{N}_{\mathcal{F}i} \cup \mathcal{N}_{\mathcal{L}i}} \left(e_j \left(t \right) - e_i \left(t \right) \right),$$

or equivalently

$$\dot{x}_{\mathcal{F}} = \left(I_F \otimes A \right) x_{\mathcal{F}} - \left(\mathcal{L}_{\mathcal{F}} \otimes B K \right) x_{\mathcal{F}} - \left(\mathcal{L}_{\mathcal{L}} \otimes B K \right) x_{\mathcal{L}} - \left(\mathcal{L}_{\mathcal{F}} \otimes B K \right) e \tag{5–15}$$

$$\dot{x}_{\mathcal{L}} = \left(I_F \otimes A \right) x_{\mathcal{L}}, \tag{5–16}$$

where $x_{\mathcal{F}} \triangleq \left[x_1^T, \ldots, x_F^T \right]^T \in \mathbb{R}^{nF}$, $x_{\mathcal{L}} \triangleq \left[x_1^T, \ldots, x_L^T \right]^T \in \mathbb{R}^{nL}$ are the stacked states of the follower and leader agents, respectively. Using (5–15) and (5–16), the closed-loop error system can be expressed as

$$
\begin{aligned}
\dot{\varepsilon} &= \left(\mathcal{L}_{\mathcal{F}} \otimes I_n \right) \dot{x}_{\mathcal{F}} + \left(\mathcal{L}_{\mathcal{L}} \otimes I_n \right) \dot{x}_{\mathcal{L}} \\
&= \left(\mathcal{L}_{\mathcal{F}} \otimes I_n \right) \left[\left(I_F \otimes A \right) x_{\mathcal{F}} - \left(\mathcal{L}_{\mathcal{F}} \otimes BK \right) x_{\mathcal{F}} - \left(\mathcal{L}_{\mathcal{L}} \otimes BK \right) x_{\mathcal{L}} - \left(\mathcal{L}_{\mathcal{F}} \otimes BK \right) e \right] \\
&\quad + \left(\mathcal{L}_{\mathcal{L}} \otimes I_n \right) \left(I_F \otimes A \right) x_{\mathcal{L}} \\
&= \left[\left(I_F \otimes A \right) - \left(\mathcal{L}_{\mathcal{F}} \otimes BK \right) \right] \varepsilon - \left(\mathcal{L}_{\mathcal{F}}^2 \otimes BK \right) e,
\end{aligned}
\tag{5–17}
$$

where (5–13) is used.

To facilitate the subsequent convergence analysis, an alternative form of (5–13) associated with an auxiliary function $\hat{z} \triangleq \left[\hat{z}_1^T, \ldots, \hat{z}_F^T \right]^T \in \mathbb{R}^{nF}$ is developed. Based on (5–10) and (5–12), the relative state tracking error can be expressed as

$$
\begin{aligned}
\varepsilon_i &= \sum_{j \in \mathcal{N}_{\mathcal{F}i}} \left[(\hat{x}_i - e_i) - (\hat{x}_j - e_j) \right] + \sum_{j \in \mathcal{N}_{\mathcal{L}i}} \left[(\hat{x}_i - e_i) - x_j \right] \\
&= -\hat{z}_i - \sum_{j \in \mathcal{N}_{\mathcal{F}i}} (e_i - e_j) - \sum_{j \in \mathcal{N}_{\mathcal{L}i}} e_i, \quad i \in \mathcal{V}_{\mathcal{F}},
\end{aligned}
\tag{5–18}
$$

where $\hat{z}_i$ is defined in (5–5). The stacked form of ε_i in (5–18) can be expressed as

$$
\varepsilon = -\hat{z} - \left(\mathcal{L}_{\mathcal{F}} \otimes I_n \right) e,
\tag{5–19}
$$

where $\hat{z}$ is governed by the dynamics

$$
\dot{\hat{z}} = \left(I_F \otimes A \right) \hat{z},
\tag{5–20}
$$

where (5–5), (5–8), (5–16), and the property of the Kronecker product $(A \otimes B)(C \otimes D) = (AC \otimes BD)$ were used.

5.3 Convergence Analysis

In this section, the event-triggered controller designed in (5–4) is examined using a Lyapunov-based analysis. In addition to proving convergence of the error signal ε,

the analysis also establishes a trigger condition associated with a trigger function that establishes when agents communicate state information.

To facilitate the subsequent convergence analysis, the event time t_k is explicitly defined below.

Definition 5.1. An event time t_k^i is defined as

$$t_k^i \triangleq \inf \left\{ t > t_{k-1}^i \mid f_i(t) = 0 \right\}, \; i \in \mathcal{V}_{\mathcal{F}} \tag{5–21}$$

for $k = 1, 2 \ldots$, where $t_0^i = 0$, and $f_i(\cdot)$, denoted as $f_i(e_i(\cdot), \hat{z}_i(\cdot))$, is a trigger function defined as

$$f_i(e_i(t), \hat{z}_i(t)) \triangleq \|e_i(t)\| - \sqrt{\frac{\eta_i \left(\delta_1 - \frac{k_2}{\beta} \right)}{(k_1 + k_2 \beta)}} \|\hat{z}_i(t)\|, \tag{5–22}$$

where $\eta_i \in \mathbb{R}_{>0}$ satisfying $0 < \eta_i \leq 1$ is a weighting term[1] , and $\beta \in \mathbb{R}_{>0}$ is a positive constant satisfying

$$\beta > \frac{k_2}{\delta_1}. \tag{5–23}$$

In (5–22), k_1, $k_2 \in \mathbb{R}$ are positive constants defined as

$$k_1 \triangleq S_{\max} \left(\mathcal{L}_{\mathcal{F}}^3 \otimes \left(2PBB^T P \right) - \mathcal{L}_{\mathcal{F}}^2 \otimes \delta_1 \right) \tag{5–24}$$

$$k_2 \triangleq \frac{1}{2} S_{\max} \left(\mathcal{L}_{\mathcal{F}} \otimes 2\delta_1 I_n - \mathcal{L}_{\mathcal{F}}^2 \otimes \left(2PBB^T P \right) \right), \tag{5–25}$$

where $\delta_1 \in \mathbb{R}_{>0}$ satisfies $0 < \delta_1 < \delta_{\min}$, and $S_{\max}(\cdot)$ denotes the maximum singular value of a matrix argument.

Theorem 5.1. *The controller designed in (5–4) ensures asymptotic containment control defined in (5–3) provided that the estimate $\hat{x}_i$ in (5–4) is updated at t_k^i defined in (5–21), for $i \in \mathcal{V}_{\mathcal{F}}$.*

---

[1] η_i is a weighting term that has a trade-off between convergence performance and the size of inter-event interval.. That is, moving η_i close to 1 can increase the inter-event interval, but the convergence performance is compromised, and vice versa.

Proof. Consider a candidate Lyapunov function $V : \mathbb{R}^{nF} \to \mathbb{R}$ defined as

$$V \triangleq \varepsilon^T \left(I_F \otimes P \right) \varepsilon, \tag{5–26}$$

where P is defined in (5–7). Using (5–6) and (5–17), the time derivative of (5–26) can be expressed as

$$\dot{V} = \varepsilon^T \left[I_F \otimes \left(PA + A^T P \right) - \mathcal{L}_\mathcal{F} \otimes \left(2PBB^T P \right) \right] \varepsilon - e^T \left[\mathcal{L}_\mathcal{F}^2 \otimes \left(2PBB^T P \right) \right] \varepsilon. \tag{5–27}$$

Using (5–7), (5–27) can be upper bounded by

$$\dot{V} \leq - \delta_{\min} \varepsilon^T \varepsilon - e^T \left[\mathcal{L}_\mathcal{F}^2 \otimes \left(2PBB^T P \right) \right] \varepsilon. \tag{5–28}$$

Using (5–19), (5–28) can be upper bounded by

$$\dot{V} \leq - \delta_1 \left[\hat{z}^T \hat{z} + 2e^T \left(\mathcal{L}_\mathcal{F} \otimes I_n \right) \hat{z} + e^T \left(\mathcal{L}_\mathcal{F}^2 \otimes I_n \right) e \right] - e^T \left[\mathcal{L}_\mathcal{F}^2 \otimes \left(2PBB^T P \right) \right]$$

$$\times \left[-\hat{z} - \left(\mathcal{L}_\mathcal{F} \otimes I_n \right) e \right] - \delta_2 \varepsilon^T \varepsilon \tag{5–29}$$

$$\leq - \delta_1 \hat{z}^T \hat{z} - \delta_2 \varepsilon^T \varepsilon + e^T \left[\mathcal{L}_\mathcal{F}^3 \otimes \left(2PBB^T P \right) - \left(\mathcal{L}_\mathcal{F}^2 \otimes \delta_1 \right) \right] e \tag{5–30}$$

$$- e^T \left[\left(\mathcal{L}_\mathcal{F} \otimes 2\delta_1 I_n \right) - \mathcal{L}_\mathcal{F}^2 \otimes \left(2PBB^T P \right) \right] \hat{z}, \tag{5–31}$$

where $\delta_2 \in \mathbb{R}_{>0}$ satisfies $\delta_1 + \delta_2 = \delta_{\min}$. By using the inequality $x^T y \leq \|x\| \|y\|$, (5–31) can be upper bounded as

$$\dot{V} \leq - \delta_1 \|\hat{z}\|^2 + k_1 \|e\|^2 + 2k_2 \|e\| \|\hat{z}\| - \delta_2 \varepsilon^T \varepsilon, \tag{5–32}$$

where k_1 and k_2 are defined in (5–24) and (5–25). Using the inequality $\|x\| \|y\| \leq \frac{\beta}{2} \|x\|^2 + \frac{1}{2\beta} \|y\|^2$, (5–32) can be upper bounded by

$$\dot{V} \leq - \delta_1 \|\hat{z}\|^2 + 2k_2 \left(\frac{\beta}{2} \|e\|^2 + \frac{1}{2\beta} \|\hat{z}\|^2 \right) + k_1 \|e\|^2 - \delta_2 \varepsilon^T \varepsilon$$

$$\leq - \left(\delta_1 - \frac{k_2}{\beta} \right) \|\hat{z}\|^2 + \left(k_1 + k_2 \beta \right) \|e\|^2 - \delta_2 \varepsilon^T \varepsilon$$

$$\leq - \sum_{i \in \mathcal{V}_\mathcal{F}} \left[\left(\delta_1 - \frac{k_2}{\beta} \right) \|\hat{z}_i\|^2 - \left(k_1 + k_2 \beta \right) \|e_i\|^2 \right] - \delta_2 \varepsilon^T \varepsilon. \tag{5–33}$$

In (5–33), two necessary conditions for $\dot{V}$ to be negative definite are to enforce $\delta_1 - \frac{k_2}{\beta} > 0$ and

$$\|e_i\|^2 \leq \frac{\eta_i \left(\delta_1 - \frac{k_2}{\beta} \right)}{(k_1 + k_2 \beta)} \|\hat{z}_i\|^2, \qquad (5\text{–}34)$$

which are satisfied provided the sufficient conditions in (5–21)-(5–23) are satisfied. Provided (5–34) is satisfied, then (5–33) can be rewritten as

$$\dot{V} \leq - \sum_{i \in \mathcal{V}_{\mathcal{F}}} (1 - \eta_i) \left(\delta_1 - \frac{k_2}{\beta} \right) \|\hat{z}_i\|^2 - \delta_2 \varepsilon^T \varepsilon, \qquad (5\text{–}35)$$

$$\leq - \delta_2 \varepsilon^T \varepsilon. \qquad (5\text{–}36)$$

The linear differential inequality resulting from (5–26) and (5–36) can be solved to conclude that

$$\|\varepsilon\| \leq \|\varepsilon(t_0)\| \, e^{-\gamma(t - t_0)},$$

where $\gamma \in \mathbb{R}_{>0}$ is a positive constant. Therefore, from (5–13) the convergence of ε implies (5–3). $\qquad \square$

Remark 5.1. The Riccati inequality defined in (5–7) and used in (5–28) is developed to facilitate the stability analysis.

5.4 Minimum Inter-Event Interval

To show the proposed trigger functions in Definition 5.1 do not lead to Zeno behavior, it is sufficient to find a positive lower bound for the inter-event interval. To facilitate subsequent analysis, two constants $\bar{c}_0, \bar{c}_1 \in \mathbb{R}_{>0}$ are defined as

$$\bar{c}_0 \triangleq S_{\max} \left(I_F \otimes BK \right) \qquad (5\text{–}37)$$

$$\bar{c}_1 \triangleq S_{\max} \left((I_F \otimes A) + (\mathcal{L}_{\mathcal{F}} \otimes BK) \right) + S_{\max} \left(\mathcal{L}_{\mathcal{F}} \otimes BK \right) + S_{\max} \left(I_F \otimes A \right). \qquad (5\text{–}38)$$

Theorem 5.2. *The event time defined in (5–21) ensures that there exists an agent*

$h \in \mathcal{V}_\mathcal{F}$ *such that its minimum inter-event interval* $\tau \in \mathbb{R}$ *is lower bounded by*

$$\tau \geq \frac{1}{\max\{\bar{c}_0,\, \bar{c}_1\}} \ln \left(\frac{1}{F} \sqrt{\frac{\eta_h \left(\delta_1 - \frac{k_2}{\beta} \right)}{(k_1 + k_2\beta)}} + 1 \right), \tag{5–39}$$

where h *is an agent that satisfies*

$$h = \arg\max_{i \in \mathcal{V}} \sup_{t \in \mathbb{R}_{\geq 0}} \|\hat{z}_i\|,$$

and F *is the number of follower agents defined in Section 5.1.1.*

Proof. See Theorem 2 in [92]. □

Remark 5.2. This lower bound implies that Zeno behaviors can be excluded. However, there is a trade-off between the minimum inter-event interval and the error convergence rate. The lower bound in (5–39) can be increased by selecting a higher η_h, but this increase results in a slower convergence due to the fact that $\dot{V}$ in (5–35) becomes less negative. Every agent has the freedom to adjust its η_h to make the minimum inter-event interval flexible.

5.5 Simulation

In this section, a network system consisting of 4 follower agents and 2 leader agents as depicted in Fig. 5-1 is simulated to illustrate the performance of the developed event-triggered control strategy. The effectiveness of the event-triggered strategy is visualized through on-off signals and the average inter-event interval.
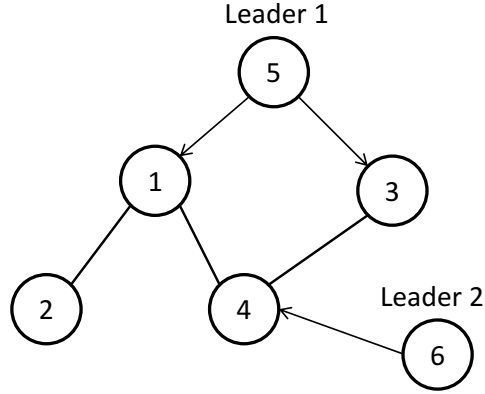
Figure 5-1. Network topology of graph $\mathcal{G}$, where agents 1-4 are followers and agents 5 and 6 are leaders.

The dynamics of the leader and the followers can be described by (5–1) and (5–2), where A, B are

$$A = \begin{bmatrix} 1 & 1 \\ 0 & 1 \end{bmatrix}, \qquad B = \begin{bmatrix} 0 \\ 1 \end{bmatrix}.$$

The network topology described in Fig. 5-1 yields $\mathcal{L}_\mathcal{F}$ as

$$\mathcal{L}_\mathcal{F} = \begin{bmatrix} 3 & -1 & 0 & -1 \\ -1 & 1 & 0 & 0 \\ 0 & 0 & 2 & -1 \\ -1 & 0 & -1 & 3 \end{bmatrix},$$

which has a smallest eigenvalue $\delta_{\min} = 0.4915$, and the solution P of (5–7) and the control gain $K = B^T P$ are

$$P = \begin{bmatrix} 15.897 & 5.969 \\ 5.969 & 5.266 \end{bmatrix},$$

$$K = \begin{bmatrix} 5.969 & 5.266 \end{bmatrix}.$$

The initial conditions of each agent for the simulation are $x_1 = (10, 2)^T$, $x_2 = (3, 7)^T$, $x_3 = (9, -4)^T$, $x_4 = (6, 5)^T$, $x_5 = (1, 1)^T$, $x_6 = (2, 2)^T$, and the state trajectories of each agent are shown in Fig. 5-2 and Fig. 5-3. The vertical scale in Fig. 5-2 and Fig.

5-3 are logarithmic due to the trajectory growth of the leaders. The system achieves containment control after 3 seconds. In Fig. 5-3, x_{i2} approaches zero during the transient response, and after 3 seconds they achieve containment control.
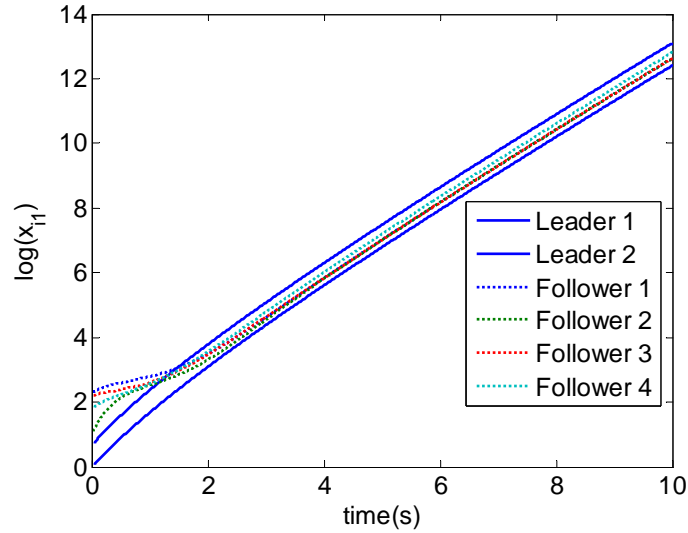

Figure 5-2. x_{i1} of leader and follower agents. (In logarithmic scale)
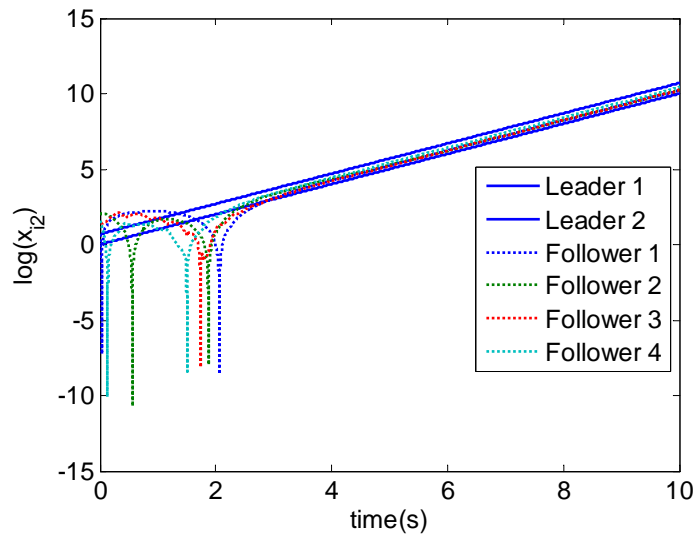
Figure 5-3. x_{i2} of leader and follower agents. (In logarithmic scale)

The triggered events are shown in Fig. 5-4, where 1 represents the event time when that agent sends its state to its neighboring agents for updating the estimate, and

-1 represents periods of time when there is no communication. The simulation results indicate that the average inter-event intervals for follower agent 1-4 are 29 ms, 10 ms, 78 ms, and 10 ms, respectively.
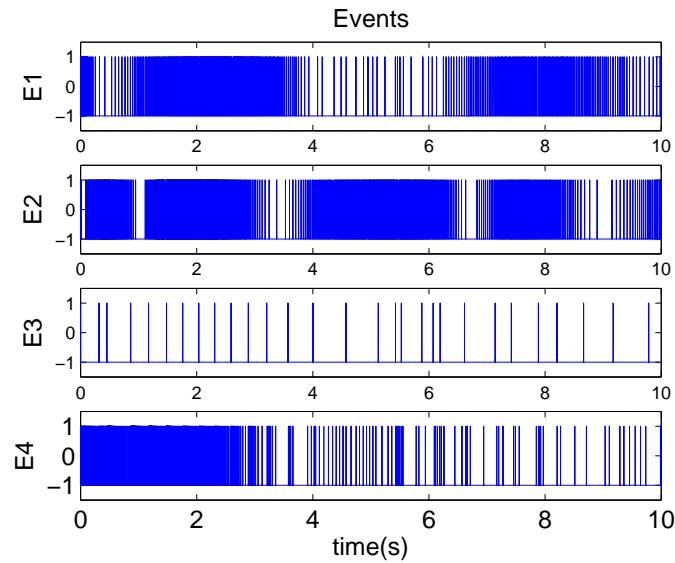
Figure 5-4. Plots $E1$ through $E4$ represent the occurrence of events in agent 1-4, respectively. (1: triggered , -1: not triggered)

Fig. 5-5 shows the norm of the estimate errors for Agents 1-4.
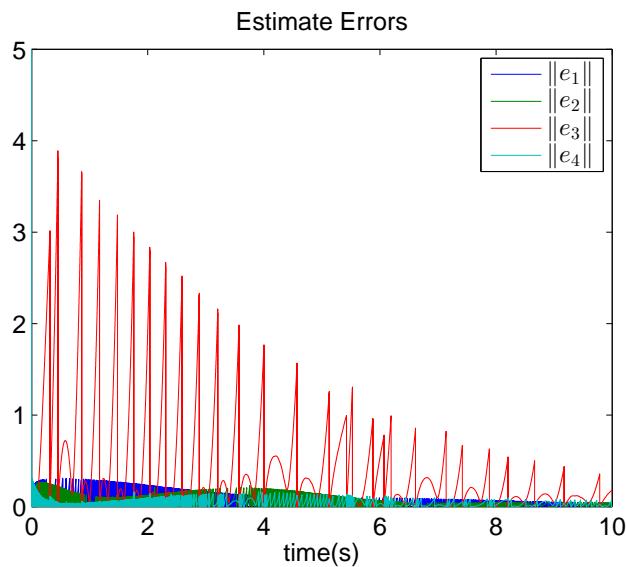
Figure 5-5. The norm of the estimate errors of the followers.

5.6   Discussion

A decentralized event-triggered control scheme for the containment control problem is developed to reduce communication frequencies between neighboring agents while ensuring stability of the system. The estimate-based controller along with the decentralized trigger function reduces the number of inter-agent communication events, during which no communication is required. A Lyapunov-based analysis indicates that the networked system achieves asymptotic containment control under this event-triggered control scheme where the trigger condition does not exhibit Zeno behavior. Numerical simulation results illustrate favorable convergence with event-triggered communications.

CHAPTER 6
CONCLUSIONS

Switched control theory provides a means to analyze systems with combined continuous and discontinuous dynamics; however, there are still challenges in the control system field that need to be solved using switched control tools. In this dissertation, switched systems theories are used to develop controllers and analyze the discontinuous closed-loop system, which results from events such as instant changes in the inertia of mechanical systems, intermittent communication, packet dropout, and failure of communication in the networked systems. Such discrete events can have dramatic impacts on the system stability. The switching sequences that represent the time instances when the discrete dynamics are introduced can also affect the stability, and therefore, several switched control theorems (i.e., that exploits a common Lyapunov function, or MLFs) are applied.

In Chapter 2, a robust OFB controller with a time-dependent switching signal is developed for a switched Euler-Lagrange system, which consists of subsystems with parametric uncertainties and additive bounded disturbances. Since switching between each subsystem introduces discontinuous dynamics and the switching sequence can be unpredictable in general cases, a stability analysis with arbitrary switching sequence is required. To this end, a design and analysis approach that uses MLFs is developed that results in semi-global UUB OFB tracking with arbitrary switching sequences provided that a minimum dwell-time condition is satisfied.

In Chapter 3, a switched controller is developed to achieve convergence of a formation of agents using only local feedback under both limited and intermittent sensing. At the same time, network connectivity is maintained and collisions between agents and obstacles are avoided. Since sensing topologies are time-varying, feedback signals can be interrupted and recovered in an unpredictable time sequence, and the resulting closed-loop systems require switched control methods to analyze stability. A

105

common Lyapunov function approach is used to ensure convergence under an arbitrary switching sequence. Moreover the entire formation configuration converges globally, if the switching signal satisfies a feasible condition in (3–32). The neighborhood of convergence can be made arbitrarily small with sufficiently large gains. Finally, the effectiveness of the proposed controller is verified by simulation results.

In Chapter 4, a decentralized event-triggered control scheme for the leader-follower network consensus problem is developed to reduce communication with neighboring agents without sacrificing the stability of the system. The estimate-based controller along with the decentralized trigger function is developed to reduce the number of inter-agent communications and prevent communication channel overload. Intermittent communication introduces discrete dynamics and requires a switched control approach for a Lyapunov-based stability analysis. The analysis indicates the network system achieves asymptotic leader-follower consensus under the developed event-triggered control scheme. Moreover, the trigger function is proven to never exhibit Zeno behavior.

In Chapter 5, discontinuous dynamics also appear due to intermittent communication between follower agents, but the decentralized event-triggered control scheme is designed for containment control problems, where more than one leader exists in the networked system. The control objective is to force the states of the followers to converge asymptotically to a region spanned by the states of the leaders. A Lyapunov-based analysis indicates that the networked system achieves asymptotic containment control under this event-triggered control scheme where the trigger condition does not exhibit Zeno behavior. Numerical simulation results illustrate favorable convergence with event-triggered communications.

In all the chapters of this dissertation, switched control algorithms are used to analyze the stability of systems with hybrid dynamics. Analysis methods that use a common Lyapunov function are favorable since they ensure the stability of the switched system under an arbitrary switching signal. However, finding the existence

of a common Lyapunov function is sometimes infeasible and MLFs may need to be used. Although MLFs can be applied to prove the stability of most control systems, such analysis methods impose a constraint on the switching signal. Investigation and development of new approaches to relax switching constraints is an area for future research. Furthermore, the event-triggered control approaches developed in Chapter 4 and 5 for networked systems require model knowledge and do not consider additive disturbance and packet dropout, which may exist in practical networked systems. Since these factors can dramatically change stability of the networked systems, development of new controllers and stability analyses along with new theories may be required to achieve the same control objectives.

PROOF THAT $\dot{V} < 0$

To facilitate the proof of Lemma 3.2, four properties are first introduced and proven.

Property A.1.

$$\|A\|^2 \leq 4\beta_i^2 \left| \mathcal{N}_i^f \right| \gamma_i. \tag{A-1}$$

Proof. By definition $A \triangleq \beta_i (\nabla_{q_i} \gamma_i) = \beta_i \left(2 \sum_{j \in \mathcal{N}_i^f} (q_i - q_j - c_{ij}) \right) = 2\beta_i \sum_{j \in \mathcal{N}_i^f} (q_i - q_j - c_{ij}),$

from which it follows that

$$\|A\|^2 = 4\beta_i^2 \left\| \sum_{j \in \mathcal{N}_i^f} (q_i - q_j - c_{ij}) \right\|^2$$

$$\leq 4\beta_i^2 \left(\sum_{j \in \mathcal{N}_i^f} \|q_i - q_j - c_{ij}\| \right)^2. \tag{A-2}$$

By applying the Cauchy-Schwarz inequality, (A–2) can be bounded by

$$\|A\|^2 \leq 4\beta_i^2 \left(\sum_{j \in \mathcal{N}_i^f} \|q_i - q_j - c_{ij}\|^2 \right) \left(\sum_{j \in \mathcal{N}_i^f} 1 \right)$$

$$\leq 4\beta_i^2 \left| \mathcal{N}_i^f \right| \sum_{j \in \mathcal{N}_i^f} \|q_i - q_j - c_{ij}\|^2. \tag{A-3}$$

Based on (A–3) and the definition of γ_i in (3–6), the inequality in (A–1) can be obtained.

$\square$

Property A.2.

$$\|B\| \leq \gamma_i \left(\left| \mathcal{N}_i^f \right| \frac{2}{\delta_2} + |\mathcal{N}_i \cup \mathcal{M}_i| \frac{2}{\delta_1} \right). \tag{A-4}$$

Proof. By definition: $B \triangleq \gamma_i (\nabla_{q_i} \beta_i) = \gamma_i \left(\sum_{j \in \mathcal{N}_i^f} (\nabla_{q_i} b_{ij}) \bar{b}_{ij} + \sum_{k \in \mathcal{N}_i \cup \mathcal{M}_i} (\nabla_{q_i} B_{ik}) \bar{B}_{ik} \right),$ where

$\bar{B}_{ik} \triangleq \prod_{j \in \mathcal{N}_i^f} b_{ij} \prod_{h \in \mathcal{N}_i \cup \mathcal{M}_i, h \neq k} B_{ih}$ and $\bar{b}_{ij} \triangleq \prod_{k \in \mathcal{N}_i \cup \mathcal{M}_i} B_{ik} \prod_{l \in \mathcal{N}_i^f, l \neq j} b_{il}.$ Since b_{ij} and $B_{ik} \in [0, 1],$
then $\bar{b}_{ij}, \bar{B}_{ik} \in [0, 1].$ Thus, $\|B\|$ can be upper bounded as

$$\|B\| \leq \gamma_i \left(\sum_{j \in \mathcal{N}_i^f} \|\nabla_{q_i} b_{ij}\| + \sum_{k \in \mathcal{N}_i \cup \mathcal{M}_i} \|\nabla_{q_i} B_{ik}\| \right). \tag{A-5}$$

By using (3–12), the inequality $0 \leq \|\nabla_{q_i} b_{ij}\| \leq \frac{2}{\delta_2}$ can be established. In a similar manner, $\|\nabla_{q_i} B_{ik}\| \leq \frac{2}{\delta_1}$. Then, (A–4) is proven by applying these inequalities term by term to (A–5). $\qquad\square$

Property A.3.

$$\|C\|^2 \leq 4 \left|\mathcal{N}_i^f\right| \gamma_i. \tag{A–6}$$

Proof. By definition $C \triangleq \sum\limits_{j \in \mathcal{V}} \beta_j \left(\nabla_{q_i} \gamma_j\right) = \sum\limits_{j \in \mathcal{N}_i^f} \beta_j \left(\nabla_{q_i} \gamma_j\right) + \sum\limits_{j \in \mathcal{V} \setminus \mathcal{N}_i^f} \beta_j \left(\nabla_{q_i} \gamma_j\right).$ Since the graph is undirected, whenever j in $\mathcal{N}_i^f$ implies i in $\mathcal{N}_j^f$. Therefore, for any agent i in $\mathcal{N}_j^f$, $\nabla_{q_i} \gamma_j$ can be simplified as

$$
\begin{aligned}
\nabla_{q_i} \gamma_j &= \nabla_{q_i} \left(\sum_{i \in \mathcal{N}_j^f} \|q_j - q_i - c_{ji}\|^2 \right) \\
&= \nabla_{q_i} \left(\|q_j - q_i - c_{ji}\|^2 \right) \\
&\qquad + \nabla_{q_i} \left(\sum_{h \in \mathcal{N}_j^f, h \neq i} \|q_j - q_h - c_{jh}\|^2 \right) \\
&= -2 \left(q_j - q_i - c_{ji}\right) = 2 \left(q_i - q_j - c_{ij}\right),
\end{aligned}
\tag{A–7}
$$

where $c_{ij} = -c_{ji}$ is used. Using the result in (A–7), $\sum\limits_{j \in \mathcal{N}_i^f} \beta_j \left(\nabla_{q_i} \gamma_j\right)$ yields

$$
\begin{aligned}
\sum_{j \in \mathcal{N}_i^f} \beta_j \left(\nabla_{q_i} \gamma_j\right) &= \sum_{j \in \mathcal{N}_i^f} \beta_j \left(2 \left(q_i - q_j - c_{ij}\right)\right) \\
&= 2 \sum_{j \in \mathcal{N}_i^f} \beta_j \left(q_i - q_j - c_{ij}\right).
\end{aligned}
\tag{A–8}
$$

On the other hand, if j is not in $\mathcal{N}_i^f$, then $\nabla_{q_i} \gamma_j = \nabla_{q_i} \left(\sum\limits_{i \in \mathcal{N}_j^f} \|q_j - q_i - c_{ji}\|^2 \right) = 0,$ which indicates that $\sum\limits_{j \in \mathcal{V} \setminus \mathcal{N}_i^f} \beta_j \left(\nabla_{q_i} \gamma_j\right) = 0.$ Finally, using (A–8), C can be expressed as

$$C = \sum_{j \in \mathcal{N}_i^f} \beta_j \left(\nabla_{q_i} \gamma_j\right) = \sum_{j \in \mathcal{N}_i^f} \beta_j \left(2 \left(q_i - q_j - c_{ij}\right)\right).$$

According to triangle inequality and $\beta_j \in [0,\ 1]$, $\forall j \in \mathcal{V}$, $\|C\|$ can be bounded by

$$\|C\| \leq 2 \sum_{j \in \mathcal{N}_i^f} |\beta_j| \, \|(q_i - q_j - c_{ij})\|,$$

$$\leq 2 \sum_{j \in \mathcal{N}_i^f} \|(q_i - q_j - c_{ij})\|,$$

or equivalently

$$\|C\|^2 \leq \left(2 \sum_{j \in \mathcal{N}_i^f} \|(q_i - q_j - c_{ij})\| \right)^2.$$

Using Cauchy-Schwarz inequality, $\|C\|^2$ can be further bounded as

$$\|C\|^2 \leq 4 \sum_{j \in \mathcal{N}_i^f} 1^2 \sum_{j \in \mathcal{N}_i^f} \|(q_i - q_j - c_{ij})\|^2$$

$$\leq 4 \left| \mathcal{N}_i^f \right| \sum_{j \in \mathcal{N}_i^f} \|(q_i - q_j - c_{ij})\|^2$$

$$= 4 \left| \mathcal{N}_i^f \right| \gamma_i,$$

which proves (A–6). $\qquad\qquad\qquad\qquad\qquad\qquad\qquad\qquad\qquad\qquad\qquad\qquad$ □

Property A.4.

$$\|D\| \leq \left(\frac{2}{\delta_2} + \frac{2}{\delta_1} \right) \sum_{j=1}^N \gamma_j. \tag{A–9}$$

Proof. By using the definition of $D = \sum_{j=1}^N \gamma_j \left(\nabla_{q_i} \beta_j \right)$ and applying the same inequalities used in the proof of Property A.2

$$\|D\| = \left\| \sum_{j=1}^N \gamma_j \left(\nabla_{q_i} \beta_j \right) \right\| \leq \sum_{j=1}^N \|\gamma_j\| \, \|(\nabla_{q_i} \beta_j)\|$$

$$\leq \sum_{j=1}^N \|\gamma_j\| \left(\frac{2}{\delta_2} + \frac{2}{\delta_1} \right). \tag{A–10}$$

Since $\gamma_j \in \mathbb{R}_{\geq 0}$ (i.e., $\gamma_j = \|\gamma_j\|$), the inequality in (A–10) can be upper bounded by (A–9).

Proof of Lemma 3.2:

Consider the equation $(\nabla_{q_i}\varphi_i)^T \left(\sum_{j=1}^N \nabla_{q_i}\varphi_j\right) =$

$\left(\frac{\beta_i(\nabla_{q_i}\gamma_i) - \frac{\gamma_i}{k}(\nabla_{q_i}\beta_i)}{(\gamma_i^k + \beta_i)^{\frac{1}{k}+1}}\right)^T \left(\sum_{j=1}^N \frac{\beta_j(\nabla_{q_i}\gamma_j) - \frac{\gamma_j}{k}(\nabla_{q_i}\beta_j)}{(\gamma_j^k + \beta_j)^{\frac{1}{k}+1}}\right)$, and decompose this into smaller

pieces. Using [54] as inspiration, the sufficient condition for $\Gamma (\nabla_{q_i}\varphi_i)^T \left(\sum_{j=1}^N \nabla_{q_i}\varphi_j\right) > 0$

is to ensure the term

$$A^T C - \left[\frac{(\|B\| \|C\| + \|A\| \|D\|)}{k} + \frac{\|B\| \|D\|}{k^2}\right] > 0, \tag{A–11}$$

where A, B, C, $D \in \mathbb{R}^2$ defined as $A \triangleq \beta_i (\nabla_{q_i}\gamma_i)$, $B \triangleq \gamma_i (\nabla_{q_i}\beta_i)$, $C \triangleq \sum_{j\in\mathcal{V}} \beta_j (\nabla_{q_i}\gamma_j)$,

and $D \triangleq \sum_{j=1}^N \gamma_j (\nabla_{q_i}\beta_j)$ are from the numerator terms of $(\nabla_{q_i}\varphi_i)^T \left(\sum_{j=1}^N \nabla_{q_i}\varphi_j\right)$. Upper

bounds for $\|A\|^2$, $\|B\|^2$, $\|C\|^2$, and $\|D\|^2$ are proven in Property A.1-A.4 so that the

condition

$$A^T C - \left[\frac{\|B\|^2 + \|C\|^2 + \|A\|^2 + \|D\|^2}{2k} + \frac{\|B\|^2 + \|D\|^2}{2k^2}\right]$$

$$> 0 \tag{A–12}$$

can be satisfied, where (A–12) is a lower bound for (A–11).

The lower bound in (A–12) follows from an application of Young's inequality to (A–11): $A^T C - \left[\frac{\|B\|^2 + \|C\|^2 + \|A\|^2 + \|D\|^2}{2k} + \frac{\|B\|^2 + \|D\|^2}{2k^2}\right] \leq A^T C - \left[\frac{(\|B\|\|C\| + \|A\|\|D\|)}{k} + \frac{\|B\|\|D\|}{k^2}\right]$, and given the upper bounds established in Property A.1-A.4 it can be further lower bounded as:

$$A^T C - \left[\frac{\|B\|^2 + \|C\|^2 + \|A\|^2 + \|D\|^2}{2k} + \frac{\|B\|^2 + \|D\|^2}{2k^2}\right]$$

$$\geq 4\underline{\beta} \left\|\sum_{j\in\mathcal{N}_i^f} (q_i - q_j - c_{ij})\right\|^2 - \frac{\rho_{1,i}}{2k} - \frac{\rho_{2,i}}{2k^2}, \tag{A–13}$$

where $\rho_{1,i}$ and $\rho_{2,i}$ are defined in Lemma 3.2. In other words, if the right hand side of

(A–13) is positive, then $A^T C - \frac{(\|B\|\|C\| + \|A\|\|D\|)}{k} - \frac{\|B\|\|D\|}{k^2} > 0$, which gives a sufficient

condition for $(\nabla_{q_i}\varphi_i)^T \left(\sum_{j=1}^N \nabla_{q_i}\varphi_j\right) > 0$. Thus by (A–13) it proves Lemma 3.2. □

REFERENCES

[1] D. Liberzon, *Switching in Systems and Control*. Birkhauser, 2003.

[2] N. Hogan, "Impedance control: An approach to manipulation: Parts I, II, III," *J. Dyn. Syst. Meas. Control*, vol. 107, pp. 1–24, 1985.

[3] R. J. Downey, T.-H. Cheng, and W. E. Dixon, "Tracking control of a human limb during asynchronous neuromuscular electrical stimulation," in *Proc. IEEE Conf. Decis. Control*, Florence, IT, Dec. 2013, pp. 139–144.

[4] M. J. Bellman, T.-H. Cheng, R. J. Downey, and W. E. Dixon, "Stationary cycling induced by switched functional electrical stimulation control," in *Proc. Am. Control Conf.*, 2014, pp. 4802–4809.

[5] A. Atassi and H. Khalil, "A separation principle for the stabilization of a class of nonlinear systems," *IEEE Trans. Autom. Control*, vol. 44, no. 9, pp. 1672–1687, 1999.

[6] S. Tong, C. Liu, and Y. Li, "Fuzzy-adaptive decentralized output-feedback control for large-scale nonlinear systems with dynamical uncertainties," *IEEE Trans. Fuzzy Syst.*, vol. 18, no. 5, pp. 845–861, October 2010.

[7] Q. Zhou, P. Shi, J. Lu, and S. Xu, "Adaptive output-feedback fuzzy tracking control for a class of nonlinear systems," *IEEE Trans. Fuzzy Syst.*, vol. 19, no. 5, pp. 972–982, October 2011.

[8] S. Tong, Y. Li, and P. Sh, "Observer-based adaptive fuzzy backstepping output feedback control of uncertain mimo pure-feedback nonlinear systems," *IEEE Trans. Fuzzy Syst.*, vol. 20, no. 4, pp. 771–785, August 2012.

[9] H. K. Khalil and L. Praly, "High-gain observers in nonlinear feedback control," *Int. J. Robust Nonlinear Control*, vol. 24, pp. 993–1015, 2014.

[10] V. Ojleska and T. Kolemishevska-Gugulovska, "A robust output feedback control design for uncertain switched fuzzy systems," in *IEEE Intl. Conf. Intell. Syst.*, Bulgaria, Sept. 2012, pp. 264 – 271.

[11] G. S. Deaecto, J. C. Geromela, and J. Daafouz, "Dynamic output feedback H_∞ control of switched linear systems," *Automatica*, vol. 47, pp. 1713–1720, 2011.

[12] L. Yu-zhong, L. Lu, and L. Yan, "H-infinity dynamical output feedback control of switched systems with delayed perturbations," in *Proc. Conf. Chinese. Control Decis.*, June 2009, pp. 264 – 271.

[13] F. Long, C. Li, and C. Cui, "Dynamic output feedback H_∞ control for a class of switchedlinear systemswithexponential uncertainty," *Intl. J. Innovative Computing, Information and Control*, vol. 6, no. 4, pp. 1727–1736, April 2010.

[14] J. Daafouz and J. Bernussou, "Robust dynamic output feedback control for switched systems," in *Proc. IEEE Conf. Decis. Control*, Las Vegas, Nevada, USA, Dec. 2002.

[15] A. Benzaouia, O. Benmessaouda, and Y. Shi, "Output feedback stabilization of uncertain saturated discrete-time switching systems," *Intl. J. Innovative Computing, Information and Control*, vol. 5, no. 6, pp. 1735–1745, 2009.

[16] G. I. Bara, "Robust switched static output feedback control for discrete-time switched linear systems," in *Proc. IEEE Conf. Decis. Control*, Dec. 2007, pp. 4986–4992.

[17] J. Daafouz, P. Riedinger, and C. Iung, "Static output feedback control for switched systems," in *Proc. IEEE Conf. Decis. Control*, 2001, pp. 2093–2094.

[18] J. C. Geromel, P. Colaneri, and P. Bolzern, "Dynamic output feedback control of switched linear systems," *IEEE Trans. Autom. Control*, vol. 53, no. 3, pp. 720–733, April 2008.

[19] J. Qiu, G. Feng, H. Gao, and Y. Fan, "Exponential H_∞ static output feedback control of switched systems with average dwell-time and time-varying uncertainties," in *Proc. Conf. Chinese Control Decis.*, 2009, pp. 6383–6388.

[20] J. Lian, G. M. Dimirovski, and J. Zhao, "Robust H_∞ control of uncertain switched delay systems using multiple lyapunov functions," in *Proc. Am. Control Conf.*, June 2008, pp. 1582–1587.

[21] H. Nie, Z. Song, P. Li, and J. Zhao, "Robust H_∞ dynamic output feedback control for uncertain discrete-time switched systems with time varying delays," in *Proc. Conf. Chinese. Control Decis.*, Shenyang, P.R. China, 2008, pp. 4381–4386.

[22] S. Seshagiri and H. Khalil, "Output feedback control of nonlinear systems using RBF neural networks," *IEEE Trans. Neural Netw.*, vol. 11, pp. 69–79, 2000.

[23] X. Zhang, A. Behal, D. M. Dawson, and B. Xian, "Output feedback control for a class of uncertain MIMO nonlinear systems with non-symmetric input gain matrix," in *Proc. IEEE Conf. Decis. Control Eur. Control Conf.*, Seville, Spain, Dec. 2005, pp. 7762–7767.

[24] W. Chen, L. Jiao, J. Li, and R. Li, "Adaptive nn backstepping output-feedback control for stochastic nonlinear strict-feedback systems with time-varying delays," *IEEE Trans. Syst. Man Cybern.*, vol. 40, no. 3, pp. 939–950, 2010.

[25] B. Mirkin and P.-O. Gutman, "Robust adaptive output-feedback tracking for a class of nonlinear time-delayed plants," *IEEE Trans. Autom. Control*, vol. 55, no. 10, pp. 2418–2424, 2010.

[26] J. P. Hespanha and A. S. Morse, "Stability of switched systems with average dwell-time," in *Proc. IEEE Conf. Decis. Control*, December 1999, pp. 2655–2660.

[27] C. D. Persis, R. D. Santis, and A. S. Morse, "Nonlinear switched systems with state dependent dwell-time," in *Proc. IEEE Conf. Decis. Control*, 2002, pp. 4419–4424.

[28] L. Yu, S. Fei, F. Long, M. Zhang, and J. Yu, "Multilayer neural networks-based direct adaptive control for switched nonlinear systems," *Neurocomputing*, vol. 74, pp. 481–486, 2010.

[29] N. H. El-Farra, P. Mhaskar, and P. D. Christofides, "Output feedback control of switched nonlinear systems using multiple Lyapunov functions," *Syst. Control Lett.*, vol. 54, pp. 1163–1182, 2005.

[30] G.-H. Yang and J. Dong, "Switching fuzzy dynamic output feedback H_∞ control for nonlinear systems," *IEEE Trans. Syst. Man Cybern.*, vol. 40, no. 2, pp. 505–516, 2010.

[31] M. Wang, J. Zhao, and G. M. Dimirovski, "Dynamic output feedback robust H_∞ control of uncertain switched nonlinear systems," *Intl. J. Control Autom. Syst.*, vol. 9, no. 1, pp. 1–8, 2011.

[32] W. E. Dixon, E. Zergeroglu, and D. M. Dawson, "Global robust output feedback tracking control of robot manipulators," *Robotica*, vol. 22, pp. 351–357, 2004.

[33] W. Ren, R. W. Beard, and E. M. Atkins, "Information consensus in multivehicle cooperative control," *IEEE Control Syst. Mag.*, vol. 27, pp. 71–82, April 2007.

[34] R. Olfati-Saber, J. A. Fax, and R. M. Murray, "Consensus and cooperation in networked multi-agent systems," *Proc. IEEE*, vol. 95, no. 1, pp. 215 – 233, Jan. 2007.

[35] J. Lin, A. Morse, and B. Anderson, "The multi-agent rendezvous problem. Part 1: The synchronous case," *SIAM J. Control Optim.*, vol. 46, no. 6, pp. 2096–2119, 2007.

[36] J. Lin, A. Morse, and B. Anderson, "The multi-agent rendezvous problem. Part 2: The asynchronous case," *SIAM J. Control Optim.*, vol. 46, no. 6, pp. 2120–2147, 2007.

[37] Q. Hui, "Finite-time rendezvous algorithms for mobile autonomous agents," *IEEE Trans. Autom. Control*, vol. 56, no. 1, pp. 207–211, 2011.

[38] W. Dong and J. Farrell, "Cooperative control of multiple nonholonomic mobile agents," *IEEE Trans. Autom. Control*, vol. 53, no. 6, pp. 1434–1448, 2008.

[39] A. Jadbabaie, J. Lin, and A. Morse, "Coordination of groups of mobile autonomous agents using nearest neighbor rules," *IEEE Trans. Autom. Control*, vol. 48, no. 6, pp. 988–1001, June 2003.

[40] Z. Lin, M. Broucke, and B. Francis, "Local control strategies for groups of mobile autonomous agents," *IEEE Trans. Autom. Control*, vol. 49, no. 4, pp. 622–629, 2004.

[41] J. Fax and R. Murray, "Information flow and cooperative control of vehicle formations," *IEEE Trans. Autom. Control*, vol. 49, no. 9, pp. 1465–1476, Sept. 2004.

[42] M. De Gennaro and A. Jadbabaie, "Formation control for a cooperative multi-agent system using decentralized navigation functions," in *Proc. Am. Control Conf.*, June 2006, pp. 1346–1351.

[43] H. G. Tanner, A. Jadbabaie, and G. J. Pappas, "Flocking in fixed and switching networks," *IEEE Trans. Autom. Control*, vol. 52, no. 5, pp. 863–868, May 2007.

[44] H. Tanner and A. Kumar, "Towards decentralization of multi-robot navigation functions," in *Proc. IEEE Int. Conf. Robot. Autom.*, April 2005, pp. 4132 – 4137.

[45] J. A. Gouvea, F. Lizarralde, and L. Hsu, "Formation control of dynamic nonholonomic mobile robots with curvature constraints via potential functions," in *Proc. Am. Control Conf.*, 2013, pp. 3045–3050.

[46] H. G. Tanner, A. Jadbabaie, and G. J. Pappas, "Stable flocking of mobile agents part ii: Dynamic topology," in *Proc. Conf. Chinese Control Decis.*, 2003, pp. 2016 –2021.

[47] G. Wen, G. Hu, and W. Yu, "Leader-following consensus control for linear multi-agents systems with switching directed topologies," in *IEEE Int. Conf. Control & Autom.*, Hangzhou, China, June 2013, pp. 111–116.

[48] G. Wen, W. Yu, J. Cao, G. Hu, and G. Chen, "Consensus control of switching directed networks with general linear node dynamics," in *Asia Control Conf. (ASCC)*, Istanbul, Turkey, June 2013, pp. 1–6.

[49] D. V. Dimarogonas and K. J. Kyriakopoulos, "On the rendezvous problem for multiple nonholonomic agents," *IEEE Trans. Autom. Control*, vol. 52, no. 5, pp. 916–922, May 2007.

[50] M. Zavlanos and G. Pappas, "Potential fields for maintaining connectivity of mobile networks," *IEEE Trans. Robot.*, vol. 23, no. 4, pp. 812–816, Aug. 2007.

[51] M. Ji and M. Egerstedt, "Connectedness preserving distributed coordination control over dynamic graphs," in *Proc. Am. Control Conf.*, 2005, pp. 93–98.

[52] M. Ji and M. Egerstedt, "Distributed coordination control of multiagent systems while preserving connectedness," *IEEE Trans. Robot.*, vol. 23, no. 4, pp. 693–703, Aug. 2007.

[53] D. Dimarogonas and K. Johansson, "Decentralized connectivity maintenance in mobile networks with bounded inputs," in *Proc. IEEE Int. Conf. Robot. Autom.*, May 2008, pp. 1507–1512.

[54] Z. Kan, A. Dani, J. M. Shea, and W. E. Dixon, "Network connectivity preserving formation stabilization and obstacle avoidance via a decentralized controller," *IEEE Trans. Autom. Control*, vol. 57, no. 7, pp. 1827–1832, 2012.

[55] G. Wen, Z. Duan, W. Ren, and G. Chen, "Distributed consensus of multi-agent systems with general linear node dynamics and intermittent communications," *Int. J. Robust Nonlinear Control*, 2013, dOI: 10.1002/rnc.3001.

[56] G. Wen, Z. Duan, W. Yu, and G. Chen, "Consensus in multi-agent systems with communication constraints," *Int. J. Robust Nonlinear Control*, 2011, oI: 10.1002/rnc.1687.

[57] Z. Zuo, C. Yang, and Y. Wang, "A unified framework of exponential synchronization for complex networks with time-varying delays," *Physics Letters A*, vol. 374, no. 19-20, pp. 1989–1999, April 2010.

[58] Y. Wang, J. Hao, and Z. Zuo, "A new method for exponential synchronization of chaotic delayed systems via intermittent control," *Physics Letters A*, vol. 374, pp. 2024–2029, 2010.

[59] G. Conte and P. Pennesi, "The rendezvous problem with discontinuous control policies," *IEEE Trans. Autom. Control*, vol. 55, no. 1, pp. 279–283, Jan. 2010.

[60] I. Suzuki and M. Yamashita, "Distributed anonymous mobile robots; formation of geometric patterns," *SIAM J. Comput.*, vol. 28, no. 4, pp. 1347–1363, 1999.

[61] H. Ando, Y. Oasa, I. Suzuki, and M. Yamashita, "Distributed memoryless point convergence algorithm for mobile robots with limited visibility," *IEEE Trans. Robot. Autom.*, vol. 15, no. 5, pp. 818–828, Oct 1999.

[62] Z. Lin, B. Francis, and M. Maggiore, "Necessary and sufficient graphical conditions for formation control of unicycles," *IEEE Trans. Autom. Control*, vol. 50, no. 1, pp. 121–127, Jan. 2005.

[63] Z. Qu, *Cooperative Control of Dynamical Systems: Applications to Autonomous Vehicles*.   New York: Springer-Verlag, 2009.

[64] J. Cortes, "Global and robust formation-shape stabilization of relative sensing networks," *Automatica*, vol. 45, pp. 2754–2762, Dec. 2009.

[65] Z. Lin, B. Francis, and M. Maggiore, "State agreement for continuous-time coupled nonlinear systems," *SIAM J. Control Optim.*, vol. 46, no. 1, pp. 288–307, 2007.

[66] S. Martínez, "Practical multiagent rendezvous through modified circumcenter algorithms," *Automatica*, vol. 45, no. 9, pp. 2010–2017, Sep. 2009.

[67] M. Ji, G. Ferrari-Trecate, M. Egerstedt, and A. Buffa, "Containment control in mobile networks," *IEEE Trans. Autom. Control*, vol. 53, no. 8, pp. 1972–1975, 2008.

[68] D. Dimarogonas and K. Kyriakopoulos, "Connectedness preserving distributed swarm aggregation for multiple kinematic robots," *IEEE Trans. Robot.*, vol. 24, no. 5, pp. 1213 –1223, 2008.

[69] F. Xiao, L. Wang, and T. Chen, "Connectivity preservation for multi-agent rendezvous with link failure," *Automatica*, vol. 48, pp. 25–35, Jan. 2012.

[70] T.-H. Cheng, Z. Kan, J. A. Rosenfeld, A. Parikh, and W. E. Dixon, "Decentralized formation control with connectivity maintenance and collision avoidance under limited and intermittent sensing," in *Proc. Am. Control Conf.*, Portland, Oregon, USA, June 2014, pp. 3201–3206.

[71] R. Olfati-Saber, J. A. Fax, and R. M. Murray, "Consensus problems in networks of agents with switching topology and time-delays," *IEEE Trans. Autom. Control*, vol. 49, no. 9, pp. 1520–1533, 2004.

[72] Z. Kan, J. Klotz, T. Cheng, and W. E. Dixon, "Ensuring network connectivity for nonholonomic robots during decentralized rendezvous," in *Proc. Am. Control Conf.*, Montreal, Canada, June 27-29 2012.

[73] Z. Li, W. Ren, X. Liu, and M. Fu, "Distributed containment control of multi-agent systems with general linear dynamics in the presence of multiple leaders," *Int. J. Robust Nonlinear Control*, vol. 23, pp. 534–547, March 2011.

[74] W. Ni and D. Cheng, "Leader-following consensus of multi-agent systems under fixed and switching topologies," *Syst. Control Lett.*, vol. 59, pp. 209–217, 2010.

[75] J. Klotz, Z. Kan, J. M. Shea, E. L. Pasiliao, and W. E. Dixon, "Asymptotic synchronization of leader-follower networks of uncertain Euler-Lagrange systems," in *Proc. IEEE Conf. Decis. Control*, Florence, IT, Dec. 2013, pp. 6536–6541.

[76] J. Hu, G. Chen, and H.-X. Li, "Distributed event-triggered tracking control of second-order leader-follower multi-agent systems," in *Proc. Chin. Control Conf.*, July 2011, pp. 4819–4824.

[77] P. Tabuada, "Event-triggered real-time scheduling of stabilizing control tasks," *IEEE Trans. Autom. Control*, vol. 52, no. 9, pp. 1680–1685, Sep. 2007.

[78] X. Wang and M. Lemmon, "Self-triggered feedback control systems with finite-gain $\mathcal{L}_2$ stability," *IEEE Trans. Autom. Control*, vol. 54, pp. 452 –467, March 2009.

[79] D. V. Dimarogonas and K. H. Johansson, "Event-triggered control for multi-agent systems," in *Proc. IEEE Conf. Decis. Control*, Dec. 2009, pp. 7131–7136.

[80] D. V. Dimarogonas and K. H. Johansson, "Event-triggered cooperative control," in *Proc. European Control Conf.*, Budapest, Hungary, August 2009, pp. 3015–3020.

[81] L. Zhongxin and C. Zengqiang, "Event-triggered average-consensus for multi-agent systems," in *Proc. Chin. Control Conf.*, Beijing, China, July 2010, pp. 4506–4511.

[82] Z. Liu, Z. Chen, and Z. Yuan, "Event-triggered average-consensus of multi-agent systems with weighted and direct topology," *J. Syst. Science Complex.*, vol. 25, pp. 845–855, October 2012.

[83] D. V. Dimarogonas, E. Frazzoli, and K. H. Johansson, "Distributed event-triggered control for multi-agent systems," *IEEE Trans. Autom. Control*, vol. 57, no. 5, pp. 1291–1297, May 2012.

[84] X. Meng and T. Chen, "Event based agreement protocols for multi-agent networks," *Automatica*, vol. 49, pp. 2125–2132, July 2013.

[85] G. S. Seybotha, D. V. Dimarogonas, and K. H. Johansson, "Event-based broadcasting for multi-agent average consensus," *Automatica*, vol. 49, pp. 245–252, Jan. 2013.

[86] G. Shi and K. H. Johansson, "Multi-agent robust consensus–part ii: Application to distributed event-triggered coordination," in *Proc. IEEE Conf. Decis. Control*, Orlando, FL, USA, Dec. 2011, pp. 5738–5743.

[87] D. Xie, D. Yuan, J. Lu, and Y. Zhang, "Consensus control of second-order leader-follower multi-agent systems with event-triggered strategy," *Trans. Inst. Meas. Control*, vol. 35, no. 4, pp. 426–436, June 2013.

[88] G. Notarstefano, M. Egerstedt, and M. Haque, "Containment in leader-follower networks with switching communication topologies," *Automatica*, vol. 47, no. 5, pp. 1035–1040, 2011.

[89] Y. Cao, W. Ren, and M. Egerstedt, "Distributed containment control with multiple stationary or dynamic leaders in fixed and switching directed networks," *Automatica*, vol. 48, pp. 1586–1597, 2012.

[90] Z. Kan, J. Klotz, E. L. Pasiliao, and W. E. Dixon, "Containment control for a directed social network with state-dependent connectivity," in *Proc. Am. Control Conf.*, Washington DC, June 2013, pp. 1953–1958.

[91] Z. Kan, S. Mehta, E. Pasiliao, J. W. Curtis, and W. E. Dixon, "Balanced containment control and cooperative timing of a multi-agent system," in *Proc. Am. Control Conf.*, 2014, pp. 281–286.

[92] T.-H. Cheng, Z. Kan, J. R. Klotz, J. M. Shea, and W. E. Dixon, "Part 1: Decentralized event-triggered control for leader-follower consensus under switching topologies," in *Proc. Am. Control Conf.*, 2015, to appear.

[93] A. Behal, W. E. Dixon, B. Xian, and D. M. Dawson, *Lyapunov-Based Control of Robotic Systems*. Taylor and Francis, 2009.

[94] D. Liberzon and A. Morse, "Basic problems in stability and design of switched systems," *IEEE Control Syst. Mag.*, vol. 19, no. 5, pp. 59–70, 1999.

[95] H. Lin and P. J. Antsaklis, "Asymptotic disturbance attenuation properties for uncertain switched linear systems," *Nonlin. Anal.: Hybrid Syst.*, vol. 4, pp. 279–290, 2010.

[96] E. Zergeroglu, W. E. Dixon, D. Haste, and D. M. Dawson, "Composite adaptive output feedback tracking control of robotic manipulators," *Robotica*, vol. 17, pp. 591–600, 1999.

[97] C. S. Karagoz, H. I. Bozma, and D. E. Koditschek, "On the coordinated navigation of multiple independent disk-shaped robots," Dept. Comp. Inform. Sci., Univ. of Pennsylvania, Tech. Rep. MS-CIS-07-16, 2003.

[98] D. Shevitz and B. Paden, "Lyapunov stability theory of nonsmooth systems," *IEEE Trans. Autom. Control*, vol. 39 no. 9, pp. 1910–1914, 1994.

[99] F. Clarke, *Optimization and Nonsmooth Analysis*. Reading, MA: Addison-Wesley, 1983.

[100] B. E. Paden and S. S. Sastry, "A calculus for computing Filippov's differential inclusion with application to the variable structure control of robot manipulators," *IEEE Trans. Circuits Syst.*, vol. 34, no. 1, pp. 73–82, January 1987.

[101] H. G. Tanner and A. Kumar, "Formation stabilization of multiple agents using decentralized navigation functions," in *Robotics: Science and systems*, vol. I, Cambridge, MA, 2005, pp. 49–56.

[102] "Robot operating system," http://www.ros.org/.

[103] "Gazebo," http://gazebosim.org/.

[104] J. Meyer, A. Sendobry, S. Kohlbrecher, U. Klingauf, and O. Stryk, "Comprehensive simulation of quadrotor UAVs using ROS and Gazebo," *Lecture Notes in Computer Science*, pp. 400–411, 2012.

[105] P. Barooah and J. Hespanha, "Graph effective resistance and distributed control: Spectral properties and applications," in *Proc. IEEE Conf. Decis. Control*, 2006, pp. 3479–3485.

BIOGRAPHICAL SKETCH

Teng-Hu Cheng received his Bachelor of Science and Master of Science degrees in mechanical engineering from National Taiwan University, Taiwan in 2007 and 2009, respectively. He joined the Nonlinear Controls and Robotics lab under the supervision of Dr. Warren Dixon in August 2011 and received Doctor of Philosophy degree from the Department of Mechanical and Aerospace Engineering at the University of Florida in August 2015. During the summers of 2013 and 2014, he worked as a research intern with Air Force Research Laboratory (AFRL) at Eglin AFB and University of Florida REEF, aiding in designing cooperative control for networked systems with time-varying network topologies and developing event-driven control for networked systems. His research interests include networked system control, switched control, event-driven control, and nonlinear control.